



University of Tennessee, Knoxville
Trace: Tennessee Research and Creative Exchange

Doctoral Dissertations

Graduate School

5-2014

Studies of Economics and Stability with Variable Generation and Controllable Load

Hao Huang

University of Tennessee - Knoxville, hhuang11@utk.edu

Recommended Citation

Huang, Hao, "Studies of Economics and Stability with Variable Generation and Controllable Load." PhD diss., University of Tennessee, 2014.

https://trace.tennessee.edu/utk_graddiss/2764

This Dissertation is brought to you for free and open access by the Graduate School at Trace: Tennessee Research and Creative Exchange. It has been accepted for inclusion in Doctoral Dissertations by an authorized administrator of Trace: Tennessee Research and Creative Exchange. For more information, please contact trace@utk.edu.

To the Graduate Council:

I am submitting herewith a dissertation written by Hao Huang entitled "Studies of Economics and Stability with Variable Generation and Controllable Load." I have examined the final electronic copy of this dissertation for form and content and recommend that it be accepted in partial fulfillment of the requirements for the degree of Doctor of Philosophy, with a major in Electrical Engineering.

Fangxing Li, Major Professor

We have read this dissertation and recommend its acceptance:

Kevin Tomsovic, Yilu Liu, James Ostrowski

Accepted for the Council:

Dixie L. Thompson

Vice Provost and Dean of the Graduate School

(Original signatures are on file with official student records.)

Studies of Economics and Stability with Variable
Generation and Controllable Load

A Dissertation Presented for the
Doctor of Philosophy
Degree
The University of Tennessee, Knoxville

Hao Huang
May 2014

DEDICATION

This dissertation is dedicated to my dear family: my parents who are always support me
with all their endless love.

ACKNOWLEDGEMENTS

At this time, I would like to thank my advisor, Dr. Fangxing (Fran) Li, for his direction and encouragement during the four years Ph.D. study. He sets an excellent example on how to integrate the three characters: a good researcher, a popular teacher and an easy-going to communicate mentor together.

I would also appreciate my committee members: Dr. Kevin Tomsovic, Dr. Yilu Liu, and Dr. James Ostrowski for their precious time and valuable comments on my work. In addition, I want to thank all students in UT CURENT Lab, including the former alumni from the UT Power Lab. Their efforts and help make my research life colorful here.

At last, I want to give my love to my dear parents for their unconditional support and patience, which help me overcome all hardships over the years.

ABSTRACT

This work probes several aspects of the renewable resources and controllable loads. The investigation includes the impact of wind power in bidding process in a deregulated power market, the effect of load damping elements on power system frequency stability and security, and impact of controllable load on system operation from the viewpoint of economic volatility and physical security.

In the first part, new bidding models are developed under two schemes for wind generation to analyze the competition among generation companies (GENCOs) with transmission constraints considered. The proposed method employs the supply function equilibrium (SFE) to model a GENCO's bidding strategy. The bidding process is solved as a bi-level optimization problem. An intelligent search based on Genetic Algorithm (GA) and Monte Carlo simulation (MCS) is applied to obtain the solution. This model also considers the probabilistic variability of wind output.

In the second part, the effect of frequency-sensitive load on system frequency using typical system frequency response (SFR) model is investigated. Theoretic analysis based on transfer functions shows that the frequency deviation under a variable load-damping coefficient is relatively small and bounded when the power system is essentially stable; while the frequency deviation can be accelerated when the power system is unstable after disturbance. For the stable case, the largest frequency dip under a perturbation and the corresponding critical time can be derived by inverse Laplace transformation using a full model considering effect of load-damping coefficient. Further, the error in evaluating the load-damping coefficient gives the largest impact on frequency deviation right at the time when the largest frequency dip occurs.

In the last part, a new demand response model is presented. It models system economic dispatch as a feedback control process and introduces a flexible and adjustable load cost as a controlled signal to adjust load response. Compared to the conventional “one time use” static load dispatch model, this dynamic feedback demand response model can adjust load to desired level in finite discrete time steps. In addition, MCS and interval mathematics are applied to describing uncertainty of an individual end-user’s response to an ISO’s expected dispatch.

TABLE OF CONTENTS

| | |
|---|----|
| CHAPTER I Introduction and General Information..... | 1 |
| 1.1 Background..... | 1 |
| 1.1.1 Renewable Energy | 1 |
| 1.1.2 Generation Strategic Bidding Application in Pool-Based Energy Market | 2 |
| 1.1.3 Frequency Stability Issues | 5 |
| 1.1.4 Demand Response..... | 7 |
| 1.1.5 Critical Load Level (CLL)..... | 9 |
| 1.1.6 Dynamic Pricing | 10 |
| 1.1.7 Energy Storage Application in Power Grids..... | 11 |
| 1.2 Motivations | 13 |
| 1.3 Dissertation Outlines..... | 15 |
| 1.4 Scope and Contribution of This work..... | 17 |
| 1.4.1 On the Wind Bidding Strategy..... | 17 |
| 1.4.2 On the Sensitivity Study of Load-Damping Characteristic | 18 |
| 1.4.3 On the Controllable Load Model | 18 |
| CHAPTER II Literature Review..... | 20 |
| 2.1 Bidding in Power Market: Issue, Models and Algorithms | 20 |
| 2.2 Frequency Response Issue, Model and Research | 22 |
| 2.3 Economic Dispatch Review and New Model under Smart Grid | 25 |
| CHAPTER III Bidding Strategy for Wind Generation..... | 29 |
| 3.1 Background and Challenge of Wind Power Integration. | 29 |
| 3.2 Problem Formulation. | 29 |
| 3.2.1 GENCO's Bidding Strategy Model | 30 |
| 3.2.2 Market Clearance Model..... | 32 |
| 3.2.3 Probabilistic Model of Wind Generation Output..... | 33 |
| 3.2.4 Wind Generation Bidding Schemes..... | 34 |
| 3.3 Monte Carlo Simulation and Genetic Algorithm..... | 41 |
| 3.3.1 Monte Carlo Simulation..... | 41 |
| 3.3.2 Genetic Algorithm | 43 |
| 3.4 Numerical Examples..... | 50 |
| 3.4.1 PJM Five-Bus System..... | 50 |
| 3.4.2 IEEE 118 Bus System..... | 55 |
| 3.5 Conclusions..... | 58 |
| CHAPTER IV Sensitivity Analysis of Load-Damping Characteristic | 60 |
| 4.1 Background of Different Load Categories..... | 60 |
| 4.2 Sensitivity Function Derivation | 60 |
| 4.2.1 Single Machine (SISO) System | 60 |
| 4.2.2 Multi-machines System | 63 |
| 4.3 Stability Analysis using Total Differential Equation..... | 64 |
| 4.3.1 Total Differential Equation for Frequency Deviation..... | 64 |
| 4.3.2 Stability Analysis | 66 |
| 4.4 Largest Dip of Frequency Change $\Delta f_{max}(t)$ | 69 |
| 4.5 Proof of Alignment of the Maximum Sensitivity and the Largest Frequency Dip. | 70 |

| | |
|---|-----|
| 4.6 Numerical Simulations..... | 73 |
| 4.6.1 Single Machine (SISO) System | 73 |
| 4.6.2 Multi-machines System | 78 |
| 4.7 Conclusions..... | 82 |
| CHAPTER V Modeling Dynamic Demand Response using Monte Carlo simulation and Interval Mathematics for Boundary Estimation..... | 84 |
| 5.1 Background of Flat Load Level | 84 |
| 5.2 Load Dispatch Formulation | 84 |
| 5.2.1 Conventional Economic Dispatch..... | 85 |
| 5.2.2 LSE's Load Response Formulation | 87 |
| 5.2.3 Monte Carlo Simulation of LSE's Response Uncertainty | 92 |
| 5.2.4 Boundary Calculation with LSE's Response Uncertainty | 95 |
| 5.3 Simulation Results | 99 |
| 5.3.1 Controllable Load Response Result..... | 101 |
| 5.3.2 Output Variables Boundary Determination | 104 |
| 5.4 Conclusions..... | 105 |
| CHAPTER VI Conclusions and Recommendations..... | 107 |
| 6.1 Summary of Contributions..... | 107 |
| 6.2 Future Works | 110 |
| LIST OF REFERENCES | 111 |
| APPENDICES | 122 |
| APPENDIX A..... | 123 |
| A.1 Alternative Proof of the Alignment of the Maximum Sensitivity and the Largest Frequency Dip..... | 123 |
| APPENDIX B | 126 |
| B.1 Sensitivity Analysis Extension to Generator Inertia Coefficient H and Governor Speed Coefficient R in Power System Analysis | 126 |
| B.2 Sensitivity Function Derivation | 126 |
| B.2.1 Single Machine (SISO) System..... | 126 |
| B.2.2 Multi-machines System..... | 128 |
| B.3 Stability Analysis Using Total Differential Equation | 129 |
| B.3.1 Total Differential Equation for Frequency Deviation | 129 |
| B.3.2 Stability Analysis | 133 |
| B.4 Numerical Simulation Results..... | 137 |
| B.4.1 Single Machine (SISO) System..... | 137 |
| B.4.2 Multi-machines System..... | 142 |
| B.5 Conclusions | 147 |
| APPENDIX C | 149 |
| VITA..... | 150 |

LIST OF TABLES

| | |
|--|-----|
| Table 3.1 Line Impedance and Flow Limit..... | 51 |
| Table 3.2 Generator Data..... | 51 |
| Table 3.3 Profit Expectation for Each Generator in PJM Five-Bus System Scheme I..... | 51 |
| Table 3.4 Profit Expectation for Each Generator in PJM Five-Bus System Scheme II ... | 52 |
| Table 3.5 Profit Expectation for Each Generator in IEEE 118 Bus System Scheme I..... | 56 |
| Table 3.6 Profit Expectation for Each Generator in IEEE 118 Bus System Scheme II ... | 57 |
| Table 5.1 Line Impedance and Flow Limit Data | 100 |
| Table 5.2 Load Data..... | 100 |
| Table 5.3 Generation Data | 101 |
| Table 5.4 Load Cost Boundary by Monte Carlo Simulation | 104 |
| Table 5.5 Load Cost Boundary by Inerval Mathematics | 104 |

LIST OF FIGURES

| | |
|--|-----|
| Figure 1.1 LMP at all buses w.r.t. different system load levels for the PJM Five-Bus system | 10 |
| Figure 1.2 Critical Load Level (CLL) illustration graph | 10 |
| Figure 2.1 Relationship of various participants in energy market. | 26 |
| Figure 2.2 Feedback control model for load response | 28 |
| Figure 3.1 Framework of the proposed bi-level GA optimization process..... | 44 |
| Figure 3.2 Flowchart of the proposed GA and MCS for wind generation bidding scheme I48 | 48 |
| Figure 3.3 Flowchart of the proposed GA and MCS for wind generation bidding scheme II | 49 |
| Figure 3.4 Modified PJM Five-Bus Example | 50 |
| Figure 3.5 Comparison of Wind Generator Alta's Profit | 54 |
| Figure 3.6 Comparison of System Total Cost..... | 54 |
| Figure 4.1 Load frequency control diagram with input $\Delta P_L(s)$ and output $\Delta\Omega(s)$ | 60 |
| Figure 4.2 LFC block diagram of multiple generation machines case with input $\Delta P_L(s)$ and output $\Delta\Omega(s)$ | 63 |
| Figure 4.3 LFC equivalent block diagram of multiple generation machines case..... | 63 |
| Figure 4.4 SISO LFC block diagram with input $\Delta P_L(s)$ and output $\Delta\Omega(s)$ and varied load-damping coefficient D | 65 |
| Figure 4.5 Simulink diagram of a SISO system | 73 |
| Figure 4.6 $\Delta f(t)$ curves of a SISO system | 75 |
| Figure 4.7 $\partial\Delta f(t)/\partial t$ curve with critical time of a SISO system | 75 |
| Figure 4.8 $\partial\Delta f(t)/\partial D$ curve of a SISO system indicating that the max $\partial\Delta f(t)/\partial D$ occurs when the largest $\Delta f(t)$ occurs | 76 |
| Figure 4.9 Simulink diagram with a right half s -plane pole of a SISO system | 77 |
| Figure 4.10 $\Delta f(t)$ curves of a SISO system in Case A2..... | 77 |
| Figure 4.11 $\partial\Delta f(t)/\partial D$ curve of a SISO system in Case A2 | 78 |
| Figure 4.12 Simulink diagram of multi-machines system | 78 |
| Figure 4.13 $\Delta f(t)$ curves of multi-machines system..... | 79 |
| Figure 4.14 $\partial\Delta f(t)/\partial t$ curve with critical time of multi-machines system | 80 |
| Figure 4.15 $\partial\Delta f(t)/\partial D$ curve of multi-machines system indicating the max $\partial\Delta f(t)/\partial D$ occurs when the largest $\Delta f(t)$ occurs | 80 |
| Figure 4.16 Simulink diagram with a right half s -plane pole of multi-machines system.. | 81 |
| Figure 4.17 $\Delta f(t)$ curves of multi-machines system in Case B2 | 81 |
| Figure 4.18 $\partial\Delta f(t)/\partial D$ curve of multi-machines system in Case B2..... | 82 |
| Figure 5.1 Flowchart of controllable demand response process..... | 92 |
| Figure 5.2 Demand elasticity change to adjust load level | 92 |
| Figure 5.3 Flow chart of output boundary calculation by Monte Carlo simulation | 94 |
| Figure 5.4 Flow chart of output boundary calculation by interval mathematics | 99 |
| Figure 5.5 Modified PJM Five-Bus system | 100 |
| Figure 5.6 Total load level adjustment of the modified PJM Five-Bus system..... | 101 |
| Figure 5.7 Load cost adjustment at Bus B | 102 |
| Figure 5.8 Load cost adjustment at Bus C | 102 |
| Figure 5.9 Load cost adjustment at Bus D | 103 |

| | |
|--|-----|
| Figure B.1 SISO LFC block diagram with input $\Delta P_L(s)$ and output $\Delta\Omega(s)$ and varied generator inertia coefficient H or governor speed coefficient R | 130 |
| Figure B.2 $\Delta f(t)$ curves with H change of a SISO system..... | 138 |
| Figure B.3 $\Delta f(t)$ curves with R change of a SISO system | 139 |
| Figure B.4 $\partial\Delta f(t)/\partial H$ curve of a SISO system | 139 |
| Figure B.5 $\partial\Delta f(t)/\partial R$ curve of a SISO system..... | 140 |
| Figure B.6 $\Delta f(t)$ curves with H change of a SISO system in Case B.4.1.2..... | 141 |
| Figure B.7 $\Delta f(t)$ curves with R change of a SISO system in Case B.4.1.2..... | 141 |
| Figure B.8 $\partial\Delta f(t)/\partial H$ curve of a SISO system in Case B.4.1.2..... | 142 |
| Figure B.9 $\partial\Delta f(t)/\partial R$ curve of a SISO system in Case B.4.1.2 | 142 |
| Figure B.10 $\Delta f(t)$ curves with H change of multi-machines system..... | 143 |
| Figure B.11 $\Delta f(t)$ curves with R change of multi-machines system | 144 |
| Figure B.12 $\partial\Delta f(t)/\partial H$ curve of multi-machines system..... | 144 |
| Figure B.13 Aggregated $\partial\Delta f(t)/\partial R$ curve of multi-machines system..... | 145 |
| Figure B.14 $\Delta f(t)$ curves with H change of multi-machines system in Case B.4.2.2 | 146 |
| Figure B.15 $\Delta f(t)$ curves with R change of multi-machines system in Case B.4.2.2..... | 146 |
| Figure B.16 $\partial\Delta f(t)/\partial H$ curve of multi-machines system in Case B.4.2.2 | 147 |
| Figure B.17 Aggregated $\partial\Delta f(t)/\partial R$ curve of multi-machines system in Case B.4.2.2 | 147 |

CHAPTER I

INTRODUCTION AND GENERAL INFORMATION

1.1. Background

1.1.1. Renewable Energy

Different from other energy sources like fossil fuels, renewable energy cannot be depleted in the foreseeable future. It mainly comes from the natural sources such as biomass, waves, wind, solar, tides and geothermal. Long time ago, the renewable energy sources were already employed as windmills and watermills for agricultural production. In recent decades, under the challenge of conventional energy crisis, people realized that renewable energy could be a good alternative choice if compared with conventional energy sources. The renewable portfolio standard (RPS) issued by the US federal government requires more than 20 percent renewable energy penetration into the electricity grid. With the advance of new technologies in recent years, it is possible and necessary to integrate the renewable energy in a large scale into the electricity grid for industrial production, residential use and commercial application. Currently, wind and solar are two main renewable sources widely applied for utility use.

The advantage of renewable energy is that there is no “fuel” cost to produce them. Though it could be replenished, renewable energy also has some characteristics that present some challenges in practice. Since renewable energy comes from natural sources like wind and solar, it is prone to the impact from natural conditions such as weather, seasonal change, climate change, and geographic limitation. Usually, renewable energy is not evenly distributed in various places in a certain time period. Even worse, the places with plenty of renewable energy sources are usually not aligned with the places of huge

populations in most areas. That means that the renewable energy center is often far away from the population center (or load center). Hence, it always brings a financial challenge to integrate the renewable energy into the grid due to high cost of long distance transmission constructions. In addition, the natural sources often suffer from intermittency and uncertainty for accurate prediction. Thus, it is difficult to control renewable energy as opposed to its conventional counterparts.

The researches concerning with renewable energy mainly lie in the following areas: renewable energy forecasting, apparatus development such as flexible AC transmission system (FACTS), doubly fed induction generator (DFIG) in power electronics to receive and transfer renewable energy in electric grid and relevant control strategies and market rules to integrate renewable energy into the grid robustly while overcoming the impact from its intermittency and uncertainty.

1.1.2. Generation Strategic Bidding Application in Pool-Based Energy Market

Before electric power system deregulation, the old structure for a typical utility company in the grid is vertically integrated. Typically, from generation through transmission to distribution networks, all essential elements are combined together as a single utility company to serve the end load users in a particular area. The whole grid is comprised of several TRUST utility companies which spread out around its whole footprint territory. The utility companies could unite and cooperate together to set a self-favorable electricity price (often higher than its real cost) by their monopolized roles. Although it may be easier for system operation and management, it sacrifices its economic efficiency due to insufficient competition in the regulated market. Obviously,

there is no existing “soil ground” for generation to exert bidding strategies to earn more profits in this stage.

Since the conventional structure of power system suffers from economic inefficiency at the cost of vertical monopoly and regulation of utility companies, many researchers argue that the benefits of deregulating the old vertical structure of power industry as unbundling sectors of generation, transmission and distribution into a fully open and free market would naturally introduce more competitions within each sector in the whole grid that will not only help reduce the total cost for customers but also realize optimal distribution of resources for utility companies. However, the power and energy society realized that the transmission and distribution networks need to keep monopoly to maintain uniform operation of the power system due to their natural monopoly characteristics. Therefore, only monopoly of the generation sector is broken out and competition is introduced into this sector, but the transmission and distribution networks have to be open accessed for all GENCOs and loads fairly and equally to carry out electricity trades in that area.

Then in year 2000, to ensure non-discriminatory transmission open access service to GENCOs and bilateral transactions, the Federal Energy Regulatory Commission (FERC) decided to issue an order to create several non-profit organizations, called independent system operators (ISO) and regional transmission operators (RTO) such as New York ISO (NYISO), Electric Regulatory Council of Texas (ERCOT), ISO-New England (ISO-NE), Southern Power Pool (SPP), Midwest ISO (MISO), California ISO (CAISO), Pennsylvania, Jersey and Maryland Power Pool (PJM), to help organize regional power system for better planning and operations reliably and efficiently in each

particular area based on well-defined market rules and proper monitoring and regulation and timely response to system faults and accidents.

After the deregulation, generation, transmission and distribution are three independent sectors and no longer belong to any single utility company as in decades ago. This directly resulted in the pool-based wholesale power system market which consists of GENCOs, distribution companies (DISCOs) and load serving entities (LSEs) as major market players. Market players in the wholesale market may buy or sell electricity by submitting offers and bids (quantities and prices) to the ISO. The ISO collects all valid bids and offers from the pool to run the security constrained unit commitment (SCUC) and security constrained economic dispatch (SCED) to clear the market, generate and post the locational marginal pricing (LMP) for each bus of the whole system. The LMP is posted and refreshed by the ISO for every 5 minutes to 1 hour. The transactions of players on particular buses in a real-time power market are based on direction of the LMPs on those buses. And other economical specifications such as revenues and profits are calculated based on the LMPs and the true energy value. The ISO is also responsible for transactions feasibility check [1].

Thus, this pool-based wholesale power market structure makes the strategic bidding process of GENCOs a possible way for better participating in power system market. Note, GENCOs are mainly studied, as opposed to DISCOs and LSEs, for bidding issues in this area. For each independent power producers (IPPs), it will rely on the system network topology, historical data, current system load position and operation status and future information (if possible it could be known before hand) like load and weather forecasting, special time and events such as game days or weekends or holidays,

other GENCOs behaviors and system coordinated outages to decide its corresponding strategic bids such as marking up its bid cost or lowering down its bid cost, as well as withholding or releasing the associated quantity of power supply. To find the optimal bids, GENCOs could try to simulate all possible cases and risks to determine the best strategic bids for each one of them online or offline. If no one could gain more at the cost of other's benefits, then the balance point (bidding solution) is found. In essence, the solution for this generation bidding strategy is to find the Nash Equilibrium based on Game Theory. It is always a challenge to solve a strategic bidding problem quickly and accurately for a power market model, sometimes for a large scale and complex system problem, no solution exists. Currently, there are various algorithms including analytical solutions [2-4] and intelligent searches [5-7] which attempt to find the global optimal point for solution of this issue for a given power system market. But until now it is still a hot research topic on power system strategic bidding issues, especially for solutions of large capacity power system market. After this bids determination process, GENCOs will re-submit their calculated strategic optimal bids to the power pool again. The ISO will collect all new bids and offers from the pool to run the SCUC and SCED to clear the market, then regenerate and republish the new LMP for each bus of the whole system. This mutually interactive process goes on among GENCOs and the ISO throughout the whole market timeline.

1.1.3. Frequency Stability Issues

The power system standard frequency is 60 Hz in North America. In normal cases, the system should operate not far away from this frequency to keep all its components intact, steady and synchronized in most times. Otherwise, the blades of

generators will be damaged due to unexpected oscillation caused by lower frequency and thus could result in generation tripped from the grid, and even worse, a cascading failure of the entire system. The worst case of frequency instability is a blackout. Though blackouts rarely happen and normal power systems have some protection devices to create some comfortable margin (frequency threshold) to prevent frequency fluctuation under disturbances.

Frequency variation could be an increase or decrease. Usually frequency decrease is harder to handle than frequency increase because speed governing is effective in reducing excessive generation so as to prevent frequency increasing, while load shedding is the only feasible way to stop frequency decreasing when there is generation shortage [8]. Currently, there are many feasible solutions to handle frequency increase. Thus, this work addresses frequency deviations as frequency drops.

The cause of frequency drop varies. Since the power system is a weakly coupled system, i.e. frequency change mainly depending on real power change while voltage profile mainly depending on reactive power, it could be unbundled as two different independent systems for control purpose: the frequency-real power subsystem and the voltage-reactive power subsystem. Hence, the main reason for frequency change is from real power unbalance. The factors of which are unpredicted load increase, bad weather conditions, short circuits issues, protective device misoperation, and unexpected generation and transmission failures. To overcome the potential uncertain factors for frequency drop, various devices and control designs are embedded into the existing power systems such as automatic generation control (AGC).

If the system frequency drops down under the threshold for more than a preset duration, the frequency regulation will be activated. At first, the sensor could detect the frequency drop and then send back the feedback signal to system controllers, and then the primary frequency regulation of the droop speed governor will take effect to stop frequency reduction. But it could not erase the frequency error between the real-time frequency and the standard frequency. Then the secondary frequency regulation will initiate to cover it. Currently, AGC is mainly carried out in practice as for the secondary frequency regulation. But in some emergency cases (generation gap is large), it is impossible to keep system frequency secure only relying on generation side. Then, load shedding is an alternative choice for operators to consider. The advantages of load shedding is that it could respond quickly while generation re-adjustment always needs some extra time for reserve generators to warm up and wait for necessary ramping time. In some cases, the quick response time could be decisive to save a system from blackout. But its drawback is also obvious, i.e. some customers have to withstand some time for no electricity in certain area. There are many load shedding designs in practice. In this work, it only considers two classes of load shedding: one stage load shedding and multi-stage load shedding. One stage load shedding usually could have better frequency response result, but it can lose some necessary load and thus result in some losses for customers. While multi-stage load shedding can avoid large load tripping at the price of longer frequency recovering time.

1.1.4. Demand Response

The concept of demand response is defined by Department of Energy (DOE) as follows: “Demand response is a tariff or program established to motivate changes in

electric use by end-use customers in response to changes in the price of electricity over time, or to give incentive payments designed to induce lower electricity use at times of high market prices or when grid reliability is jeopardized.” [9] Individual participants clearly benefit by translating their demand reductions into lower bills, and it could benefit to all customers eventually.

In the present smart grid environment, with high penetration of renewable energy access and large scale distributed generation application, demand response has been paid great attention again for peak load reduction and transmission pressure relief in recent years. Unlike re-building new generation or transmission system to reduce potential peak hours load and transmission congestion, reasonable demand response schemes can alleviate system pressure and also postpone new construction of the system to save funding for future investment.

Demand response, also known as responsive load, or controllable load is an active load control pattern based on external incentive signals such as dynamic pricing, penalty or rebate. Because it respects with the willingness of loads, it is different with the conventional direct load control (DLC). The DLC is a passive load control method which is used effectively for many years in utility practice. In a vertical regulated system, based on system operation situation, the control center of a utility company sends directions to loads regarding their load position, and each individual load has to obey with the directions, otherwise they may still get tripped compulsively and receive penalties as well. While in a de-regulated environment, the ISO spreads out the incentive price signals (rebate bonus or penalty) to the loads in the whole system, and the load could choose to respond autonomously to earn extra bonus or avoid paying penalties or refuse to respond.

Usually, there is no penalty to loads for not responding to the directions. However, the ISO still has the power to implement DLC to restore frequency for security purpose when the system is in an emergency case.

The demand response for an individual load is small, but there are huge amount of loads in a system, hence the aggregated effect of demand response in LSEs is overwhelming in a large scale. Since the response is based on individual customer, it is more like a subjective behavior rather than an objective behavior, i.e. it introduces stochasticity and uncertainty of human behaviors into the system such as the amount of load change is uncertain, the time of load response is stochastic and inconsistent among each other load. Therefore, unlike the deterministic conventional generation control, it is always a challenge to design a good control strategy from load side.

1.1.5. Critical Load Level (CLL)

LMP methodology is a widely employed mechanism in existing deregulated power markets operation and planning. It has a unique step change pattern which is caused from critical load level (CLL) as total load reaches to a certain load limit. In Figure 1.1, it shows this step characteristic clearly [10-13]. The CLL introduced in [10-14] provides an important indication description for utility operators about present system operation status. Each CLL corresponds with binding limit of an individual system element, and all CLLs could be calculated as long as the system parameters are known beforehand [10-11]. The LMP stays the same in between the CLLs in neighborhood if power loss is neglected. It is shown as in Figure 1.2. The existing operation point is D_1 , between D_0 and D_2 , the price is the same. But it will take a vertical step jump of price when the load level across D_0 or D_2 .

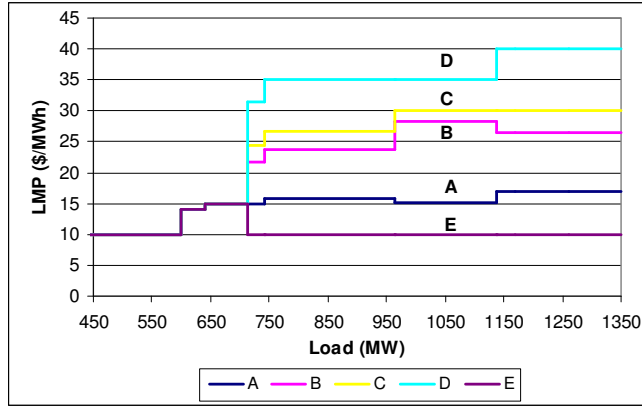


Figure 1.1 LMP at all buses w.r.t. different system load levels for the PJM five-bus system.

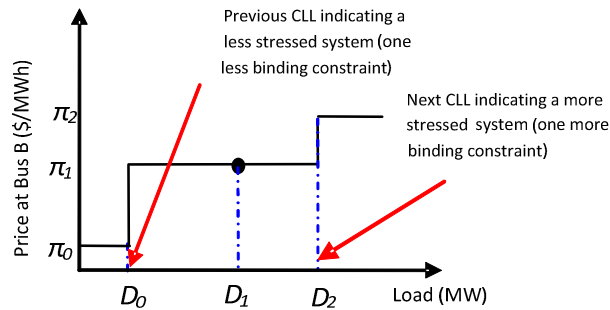


Figure 1.2 Critical Load Level (CLL) illustration graph

1.1.6. Dynamic Pricing

Dynamic pricing (also known as “time of price”), opposite to the static pricing, is cost reflective pricing varying by time of day. Though static rates, including time-invariant rates and Time of Use (TOU), are easy to implement in practice, it is inefficient and unfair because customers could not know when electricity is cheap or expensive to consume from it. In addition, the static rate also contains cost of utilities’ future risk, thus consumers have to overpay for this premium included [15-17].

Contrarily, dynamic rates render utilities the option to change prices on short term

in response to existing system status or wholesale pricing conditions. Dynamic pricing could be mainly classified as following types: Critical Peak Pricing (CPP), Peak Time Rebate (PTR) and Real-Time pricing (RTP) in power industry area. For a CPP or PTR rate, prices are lower on normal days, but much higher or rebate during peak hours on some event days, which may be caused by power supply shortage, harsh weather condition like extreme temperature or combination of them. RTP rates are updated frequently on an hourly or sub-hourly basis, to exactly reflect real spot prices in the wholesale market. These pricing patterns can be combined to yield hybrid patterns of dynamic pricing in practical use. For example, TOU and CPP, TOU and PTR are two most common combinations of dynamic pricing in practice. Also, end users' automating devices plus with dynamic pricing could produce better effect in many pilot experiments [15-18].

Dynamic pricing could bring many benefits to all participants in the energy market compared to the static pricing. For example, consumers could save money by avoiding electricity consumption during high price period according to the dynamic pricing signals. In particular, for low income customers, they gain instant saving when enrolled in dynamic pricing [15-17]. And it could benefit to all customers eventually. Power suppliers could avoid scheduling high production cost unit of peak hours to reduce cost as well. Also, intensity of transmission system and power loss could be mitigated if total load level is curtailed during peak hours.

1.1.7. Energy Storage Application in Power Grids

In practice, energy storage is already used as a backup solution to absorb mismatched power caused by renewable energy uncertain generation in short term or

power supply shortage during peak hours. With the vision of a high penetration of renewable energy in the future, it is apparently important to investigate new market structure design technology with energy storage strategies embedded to utilize high level renewable energy in smart grid environment.

Energy storage technologies attract increasing interest from researchers for its capability to mitigate risk of real power imbalance and frequency instability caused by shortage of power supply during peak hours or renewable energy uncertainty and intermittency. Further, it could also provide reactive power reserve support for voltage stability when penetration of renewable energy is high. In addition, it is also a good complementary to energy reserve to implicitly reduce needs for additional investment on unnecessary backup reserve. More important, with the energy storage cooperation, the owners of renewable energy sources could have more confidence to bid aggressively in energy market when they face renewable energy uncertainty and intermittency since the risk of failure to meet the power balance condition is reduced to a more acceptable lower level. It indicates that energy storage could act as a means of quality adjustment to improve the probability of availability of renewable energy sources in energy market. At last, energy storage, especially fitting for Plug-in Hybrid Electric Vehicle (PHEV) application, could work as a potential demand response source in energy market if combined with reasonable pricing systems such as RTP or TOU. This could boost the renewable energy development and integration in the whole power system to meet the DOE's national 20% wind penetration goal in the year 2030.

1.2. Motivations

It is always of significant importance to maintain the stability of a power system. In this regard, the related power system characteristic specifications such as system frequency response, bus voltage profile and current harmonic elements ratio are always concerns regarding power quality for system operators. Among those three items, system frequency response is one of the most important issues due to its global characteristic. For a stability analysis, a crucial task is to identify the frequency stability margin, i.e. the largest disturbance that the system frequency could resist to stay stable and the critical time (stable case) of the largest frequency dip when an external disturbance occurs or the critical time (unstable case) for frequency collapse if a fault occurs. In this work, the meaning of the critical time is the former one.

As in present smart grid environment, more and more renewable generations such as wind generations and solar generations are accessed into the grid to meet the Renewable Portfolio Standard (RPS) needs. Because the renewable sources especially the wind sources are subject to weather condition, it behaves obvious intermittency, uncertainty and sometimes unpredictability. Thus, the whole grid is also exposed to this intermittent effect transmitted from the renewable generations. With integration of renewable generations, the whole system is more stressed and vulnerable to potential interruptions. Besides, wind generations also reduce system voltage robustness by consuming lots of reactive power which is needed locally to support flat voltage profile. Further, switch of distributed induction motors into the grid could change the ratio between frequency sensitive load composition and the PQ constant load element, and this will affect the system frequency conversely. In fact, system load always fluctuates and is

very difficult to predict its future behaviors. On the other hand, even if the load is constant at least the load compositions ratio of non-frequency sensitive PQ constant load and frequency sensitive induction motor load may also change constantly. To discover the mutual effect of the frequency sensitive load or the load-damping characteristic on system frequency under operation of renewable generations, it is interesting to study with this relation from load side rather than the conventional generation side.

Renewable generations also need to participate into the power system market to gain necessarily enough profit for further development. But it rarely takes part into the power market due to its intermittent property under dispatch. Although there are various bidding strategies implemented for players of a pool-based power market, until now the existing market environments are mainly built for conventional generations to access the bidding process. In order to develop a suitable bidding scheme that is fit for renewable generations considering their essential intermittency and uncertainty, it is attempted to construct an initial draft scheme under smart grid operation environment to combine the renewable generations and the conventional generations into the power market bidding process and keep the market as fair and open as before for all participants in this work.

Conventionally, generation production is used to follow with load status changes for power balance purpose to keep system frequency stable around 60 Hz because generation is always centralized and easier to control and the amount of generation production could be scheduled before hand if no accident happens, while load is distributed among the whole system and hard to forecast and even control. In terms of this drawback of load characteristic, except the generation side control, the alternative control from the load side management has not been broadly studied in previous works.

In addition, flat load level profile is always a dream for system operators because this could easily realize the power balance between supply and demand. But in conventional ways, this flat load profile is not realistic because of load uncertainty and unpredictability in some degree. Also, the generation suffers from daily and seasonal load cyclical pattern and long-term load uncertainty for economical inefficiency of operation which could result in potential peak hours load and price spikes. If the generation-load balance is controlled from the load side rather than the generation side, this could be one possible direction to mitigate the load uncertainty and have a more robust and flatter load profile in practice. This also draws the need for a new economic dispatch framework model which could better adjust controllable load level autonomously from the load side to reach the desirable flat load level to meet power balance needed rather than the traditional and regular economic dispatch models.

1.3. Dissertation Outlines

The relevant literature review is briefly given in Chapter II.

In Chapter III, traditional bidding strategy optimization model considering from the generation side is reviewed and its solution methodology is also revisited at the beginning. In the current smart grid environment, especially with the wind power penetration cap limit in policy (RPS), new scheme needs to develop in order to meet the requirements due to the intermittency and uncertainty of wind power. In this chapter, two bidding schemes are proposed for wind power generation participating in the bidding process of a deregulated power market. Both schemes consider the wind power uncertainty in Monte Carlo (MC) description. The first scheme is to make the wind power as a negative load on the load side, while other kind of generation sources are used

to keep power balance; the other scheme is to let the wind power as a generation bidder to play in the market as well. Finally, the results of the two schemes are compared.

Chapter IV first revisits the classic system frequency response (SFR) model from which the system frequency response and the largest frequency dip with the associated critical time could be calculated. There are two kinds of descriptions of the SFR model - the Laplace transfer function model and the state space model [19-20]. Although the state space model may be a better tool for high order systems, the transfer function model is more widely used in practical power system studies. In fact, both the models have their own benefits, but in this work, the transfer function model is considered to conduct the research. Besides, most of existing studies have been carried out to discover the relation between the external interruption and the system frequency output. Many correlated results are derived based on the SFR model. However, very few studies are focused on the effect of system internal characteristic parameters on system frequency change. In this regard, first, the sensitivity function of the load damping characteristic parameter of all cases is obtained for system frequency stability analysis. Then, a proof about load damping characteristic variable on stability analysis is provided. In addition, the alignment of the occurring time of the max point of this sensitivity function and the largest frequency dip is discussed and proved. Finally a conclusion about the effect of system internal load damping characteristic parameters on system security and stability is stated.

Chapter V presents a closed-loop feedback control of controllable load dispatch model. It is developed for moving system operation status to the ideal load level position

in finite steps. This load response model is applied in flat load case and uncertainty of LSEs' response to ISO is considered as well.

Chapter VI gives a conclusion about all approaches and methodologies, as well as some guidelines for future works.

1.4. Scope and Contribution of This Work

The approach for motivating wind power to make full use of power market bidding process is studied. In addition, the issue of fast and accurate estimation of the effect of varying system load damping characteristic coefficient on system frequency response security and stability is also considered in this work. At last, an autonomous controllable load scheme which could lower down the peak load and its associated price spike is developed and tested.

1.4.1. On the Wind Bidding Strategy

In this part, a bidding strategy model with market rules for renewable energy (wind generation) to participate in a pool-based power market is built and solved. Two schemes are developed for wind power participating in power market bidding process under the lossless DCOPF model and the results of the two schemes are compared. Uncertainty of wind power is described in MCS. The proposed models are solved by Genetic Algorithms. The results show that with the wind power bidding strategic model, it could earn more in the smart grid environment and it could encourage more wind power generation integrate the grid operation. But the system needs to be restructured carefully.

1.4.2. On the Sensitivity Study of Load-Damping Characteristic

This part of the research work studies the system frequency stability and security from load side, especially from the frequency sensitive load. It gives a quantified mathematic description of the sensitivity function between system frequency and the load-damping coefficient. It proposes the classic SFR model to calculate the frequency sensitivity function of load damping characteristic coefficient D . This sensitivity function is then used for system frequency stability analysis based on the concept of the total differential equation of calculus. It indicates that the change of intrinsic element D could exert its effect on power system security and stability which is always omitted in previous studies. In addition, the alignment of the time of the max point of the sensitivity function occurs and the moment of the largest frequency dip is proved. It could provide an alternative way to calculate the critical time. At last, the conclusion could be drawn as this sensitivity function could provide indication for system frequency stability and security status. And the system security border needs to be reconsidered if the internal element of the system changes such as the change of load-damping coefficient due to the load control program. In addition, the critical time could be calculated from the frequency sensitivity function as well.

1.4.3. On the Autonomous Controllable Load Model

In this part, a new controllable load closed-loop feedback model is proposed and load response uncertainty is considered as well. The load response uncertainty is also described in MCS and interval mathematics. Based on this controllable load adjustment model, it could shave the peak hours load to avoid price spikes in order to reduce system pressure and keep system physical security indirectly. Compared with the conventional

DLC methodology, it gives more flexibility to load customers. Therefore, in the current deregulated power system, it is better to use market incentive as a control signal to induce load users to cut load usage at their will. The results show that the system high load level could be lowered down in finite steps under this controllable load feedback model. And it could be used either in practical power market operation online or for offline estimation.

CHAPTER II LITERATURE REVIEW

This chapter briefly reviews present studies related to this work of economic and security studies. These include wind power generators participating bidding, the sensitivity of the load-damping characteristic, and the closed loop feedback control of controllable load response model.

2.1. Bidding in Power Market: Issues, Models and Algorithms

Over the past decades, the old vertically structured power industry throughout the world has been de-regulated for market operations. The generation and transmission systems have been split into different entities to introduce competition into the power market. The purpose is to increase investment efficiency and reduce the cost of power supply [21].

A variety of market operation models have been proposed and practiced in various countries. Among all different models, the power pool market structure is the most popular one [2-6][22-24]. This power pool is managed by a market operator or an ISO to collect energy suppliers' bids from GENCOs and load consumers' offers from LSEs. Then, a market clearance price (MCP) is calculated as the bid price of the most expensive supplier that is needed to completely meet the demand [2]. This market structure is built to encourage suppliers to bid their energy price close to their marginal cost to ensure and improve economic efficiency. Further, to address the transmission constraints, an economic dispatch model is applied to minimize total generation supply cost while satisfying the system reliability and security requirements. Then, the LMP method [14] is usually employed to calculate the generation profit and load payment and

to manage the transmission constraints.

Therefore, to model the ISO's dispatch function and GENCO's individual behavior, it is naturally to split the bidding process into two parts [2-5][22]. The first part is the ISO market clearance process: the ISO collects all necessary information such as bids and offers from GENCOs and LSEs, and then performs SCED to set the market price. The second step is the GENCO's self-scheduling for their own payoff optimization such that they can present the best bidding strategy in the forthcoming market.

Modeling and solving bidding strategies problem has been a hot research topic for a long time. In [6], a probability based MC method is proposed to solve competitive generator game with imperfect information, but without transmission constraints. In [2], a mathematical analysis based on a Lagrangian Relaxation is proposed. In [25], a cooperative game is analyzed with potential coalitions and collusions of participants in electricity markets. A prime-dual interior point iteration based on sensitivity was developed to update bidding strategies for GENCOs in [3-4, 26]. Bidding with transmission constraint was solved in [4, 6, 23]. Also in [22], it is shown that the feasibility of Bender Decomposition to solve bidding strategy problems in two parts. In [3-5], an incomplete information case combined with transmission constraint was carried out. A bidding strategy problem was solved by MCS and GA in [27]. Intelligent heuristic search such as GA and Co-evaluation is also a good way to deal with bidding strategy problems in [5, 7, 27]. Further, for a multi-Nash Equilibria of multiplayer games in electricity markets, all Nash Equilibria, if exist, could be calculated based on solving polynomial equations in [28]. An analytical approach of transmission-constrained residual demand derivative is used for a power market bidding problem solution in [29-

31].

Strategies for wind power trading were studied in [32]. Two types of bid scenarios are proposed as linear bid and block bid trading for wind power generation, but the model did not consider transmission constraints and competition with other types of generators. In [33-34], a trading strategy is given for wind power producers to minimize their imbalance cost in short-term, but the transmission constraints as well as competition with other types of generators are not considered. In [35], the uncertainty of wind power generation was modeled in constraints of an optimization problem instead of in the objective function. However, it did not consider the wind power generation as a variable in the objective function of this optimization problem.

The goal of Chapter III is to develop a bidding strategy model for wind generation participating in the competition with conventional generators. Here, the difference between two types of generators is the high uncertainty of wind generation. Thus, probabilistic approach is taken for the bidding strategy model. Also, the transmission constraints are considered. To solve the overall problem, a bi-level optimization model is formulated where the upper-level sub-problem maximizes GENCOs' payoffs and the lower-level sub-problem solves the ISO's market clearance problem including economic dispatch and pricing. The MCS method is used to describe the wind generation statistical characteristic, linear programming (LP) is used to solve the lower-level sub-problem, and GA is used to solve the upper-level sub-problem.

2.2. Frequency Response Issue, Model and Research

The frequency of a power system is a very important performance signal to the system operator for stability and security considerations. The desired power system

frequency should stay within a very small, acceptable interval around its nominal value. Otherwise, the operator needs to take relevant actions immediately. In the past decades, there are many research works on power system frequency regulation [8, 19-20, 36]. Since the system frequency is essentially related to real power balance, it is natural to control real power output in the generation side such as using the AGC system. This is indeed one of very successful control applications in the power system operation in the past decades.

In recent years, the increasing stress in the transmission system may limit the effective power transfer from generation to load. Also, the penetration of intermittent renewable resources continues growing. Thus, the frequency and the related stability issue are being re-examined under this new paradigm [37]. Non-conventional means, such as DLC and dynamic pricing under the smart grid initiative, have attracted many research interests as an alternative solution for balancing service and frequency regulation [38-40], especially under a high penetration of load control.

Some early works on the load shedding or load control topic is to set up the well-known generation swing equation first, and then to employ classic tools in control theory, such as transfer function [8, 19-20, 36] and state space method [19], into the swing equation to find out the amount of load to shed. In [8, 36], a classic model, called the system frequency response (SFR), is introduced, and it is still accepted broadly. Also, in [8, 41], different implementations of adaptive under frequency load shedding (UFLS) are presented. In [42], a load shedding optimization scheme is presented. In [43], a classic closed-loop PID control strategy is implemented to regulate power system frequency. In [44], a general-order SFR model with load shedding scheme is proposed to produce a

closed-form expression of frequency response. In [45], a method to determine the frequency stability border for UFLS is presented. In [46], a SFR analysis approach suitable for normal and contingency operation conditions is proposed.

While many previous works were done to find the effect on the system frequency due to external disturbances, such as a large generator drop or a large load connection [8, 19-20, 36, 41], there is little work on the effect of the intrinsic load characteristics. With the increasingly large amount of frequency-sensitive load for frequency regulation [38-40, 47] and the increasing interests in load models [48], it is necessary to investigate the impact of load characteristics, namely, the load-damping coefficient D , on the system frequency regulation. However, the load-damping coefficient is still not fully understood and usually assumed as a constant from operational experience. Also, it may be highly variable under different operating points. In particular, under smart grid initiative with high-penetration controllable loads, the interrupted loads should consist of lots of motor loads which have a significantly different load-damping coefficient than the rest of the loads. Therefore, Chapter IV is aimed to study the impact of variation of such coefficient, namely, ΔD , on SFR. By intuition, one may always perform several dynamic case studies with various coefficient values; however, it is always desirable to have a fast and efficient model without repeated case studies.

With the above motivation, Chapter IV presents an efficient analytical method to study the impact of the load-damping coefficient as well as a mathematical approach to derive the lowest frequency dip. Therefore, the system operators may have a fast assessment of different scenarios of load-frequency characteristics to understand the potential frequency deviation under various emergencies, if the load-damping coefficient

is different from the estimated value. The study in Chapter IV indicates that the characteristic of frequency-sensitive load has an important effect on SFR when the system is unstable, which means the frequency protection devices may trip quicker than anticipated. Meanwhile, the study also shows that the external disturbance may dominate the load-frequency characteristics when the system is stable; hence, the load-frequency characteristic has much less impact on stability when the system is essentially stable.

2.3. Economic Dispatch Review and New Model under Smart Grid

With power system deregulation and, in recent decades, the forthcoming smart grid paradigm, controllable load, also referred to as demand response or responsive load, has emerged as a possible alternative solution for congestion mitigation, especially during peak hours. The participants in demand response includes the Independent System Operator (ISO), Individual Power Producers (IPP), Load Service Entities (LSE), and end-users as shown in Figure 2.1. Also, controllable demand response can help reduce generation production costs and increase a system's economic efficiency by curtailing system load level based on economic incentives and automatic smart devices [17-18].

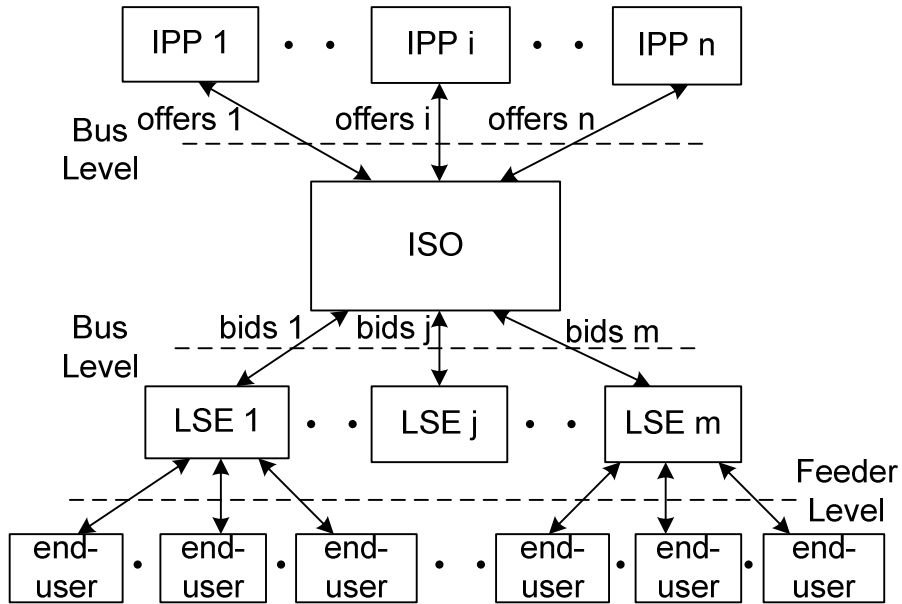


Figure 2.1 Relationship of various participants in power market

Traditionally, economic dispatch is implemented on the generation side based on a forecasted load level and is often considered a “static” process with rigid loads. This does not consider the dynamic feature of controllable load in response to dynamic prices. However, demand response in the present trading period should be related to the market signals in the previous trading periods, as seen in many other commodity markets. Therefore, it will be interesting to find an alternative dynamic and efficient model to address this problem.

There are only a few previous works focused on dynamic power market dispatch modeling. In [49-50], the entire power market was viewed as a dynamic system instead of a static system, and a multi-round cyclical and autonomous learning feedback control model is developed. It is assumed that each participant in a power market could learn another participant’s bidding strategy and, as a result, improve its own market behavior in

the following round. In the next round of bidding, the individual load will adjust its load bids in order to maximize its profits. After the repeated multi-round bidding process is applied, each individual participant will finally derive its maximum profit. When considering the load learning process and load variation, this load adjustment process should be modeled as a dynamic process. Some research works have studied the dynamics and stability of power market [51-52]. In [51], the stability of the power market was studied by checking system eigenvalues. In [52], oligopolistic double-sided auctions are modeled as a dynamic system and they are solved by feedback Nash-Cournot strategies. In [53], an analytical model was provided regarding the effects of market clearing time and price signal delay on power market stability. In [54-55], elastic load and price responsive load were considered. Also, the results of static economic dispatch, multi-temporal static dispatch, and centralized model predictive control (MPC) dispatch are compared.

In recent years, some ISOs and utilities use price incentives such as Time of Use (TOU) and dynamic pricing to encourage LSEs and end-users to decrease their load level, especially during peak hours, to avoid high generation production costs and transmission line congestion [56-61]. In addition, within the smart grid initiative, the uncertain effects of an overwhelming number of individual households' electricity consumption on load curtailment cannot be neglected. The effect of incentive for load curtailment varies and depends on many factors. Therefore, the real-time power market should be modeled as a dynamic feedback system considering the previous status effects and current system conditions [62]. The dynamic model can also provide more information about system stability that may not be obvious in static models. A controllable demand response

feedback control model is introduced as in Figure 2.2.

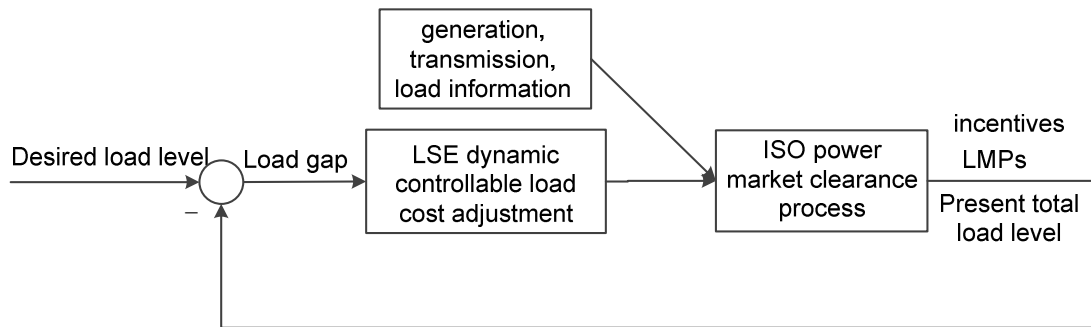


Figure 2.2 Feedback control model for load curtailment

In Figure 2.2, the ISO market clearance process gives out LMPs, economic incentives, and current total load level based on existing generation, transmission and load information to IPPs and LSEs. In this model, ISO could use incentives to affect the demand response of LSEs until a desired level is reached.

The work in Chapter V proposes formulation of a new closed-loop demand response feedback control model. It utilizes a flexible and adjustable load cost in an elastic economic dispatch model. It could be adjusted autonomously according to the gap between current and desired load level, and this process continues until the gap reaches zero. Boundary of load cost due to the uncertain nature of end-users' response is determined and calculated through MCS and interval mathematics. The effectiveness and validity of this load response model are verified through a numerical example based on PJM five-bus system in Chapter V.

CHAPTER III

BIDDING STRATEGY FOR WIND GENERATION CONSIDERING CONVENTIONAL GENERATION AND TRANSMISSION CONSTRAINTS

3.1 Background and Challenge of Wind Power Integration

Renewable sources such as wind sources are abundant in various places of the world. Also it is an environment friendly and clean energy with zero carbon emission. Thus, it is a good alternative energy to partially replace the conventional energy sources. In decades, plenty of wind farms with hundreds of wind turbine generators were built to utilize wind power. However, the wind power has not been fully integrated in the grid until now for several challenging reasons: essentially intermittent and uncertain behavior of wind, lack of necessary market rules for wind power integration into the grid and mismatch between wind generation and load operation styles, i.e. when the daily load is in a peak around 2 p.m., there may be no wind power available; while the wind power is spilled out to waste when less load is connected in the grid at the late night or before dawn. In this chapter, it proposes a market model to integrate wind power into the grid, and it also provides relevant market rules to cope with extra or less wind power generation cases. The study in this chapter can bring helpful indications for building reasonable power market with high renewable energy penetration.

3.2 Problem Formulation

In a complete information game, all players know other players' bidding strategy and their payoff functions. Equilibrium is reached when no player can increase its payoff by unilaterally changing its strategy.

Some assumptions commonly employed in bidding strategy study are listed as

follows:

- Each GENCO has only one generator candidate unit and bids a constant price for a single block for pure simplicity, while in practice a monotonically increasing multi-block bid model is commonly used.
- GENCO uses supply function equilibrium (SFE) model.
- Load is always inelastic and constant for simplicity because load's bids can be essentially modeled as negative generation if needed.
- The system is perfectly informed.
- Power losses on transmission lines are neglected. Note that the transmission limit is considered in this chapter.
- Unit commitment is already settled down and fixed, only the economic dispatch process is considered in this chapter.
- Wind power generation output follows normal distribution. Its mean value and variance are predicted by ISO beforehand. ISO could rely on this information for dispatch.
- The LMPs in day-ahead market are the same as those in the real-time market.

3.2.1 GENCO's Bidding Strategy Model

GENCOs cannot decide the price just by themselves. It is the ISO to clear the market and determine the price; however, GENCOs can affect the price via their bidding strategies. Hence, the whole bidding process is a bi-level optimization problem. The first level is that each GENCO maximizes its own profit, and the second level is a transmission constrained economic dispatch by ISO to minimize total production cost

under all security constraints.

Suppose all conventional GENCOs have a convex quadratic production cost function as (wind GENCOs have the same description with index j)

$$C_i = C(G_i) = a_i G_i^2 + c_i G_i + d_i \quad (3.1)$$

Its marginal cost is calculated as

$$\frac{dC_i}{dG_i} = 2a_i G_i + c_i \quad (3.2)$$

where a_i is the generation cost coefficients of conventional GENCO i (\$/MWh²), c_i is the marginal cost of conventional GENCO i , d_i is the generation cost coefficients of conventional GENCO i (\$), G_i is the scheduled generation of conventional GENCO i (MWh), C_i is the generation production cost function of conventional GENCO i (\$).

It is a linear function of its scheduled generation G_i . Obviously, GENCOs can prepare their strategic bids by changing a_i and c_i . For simplicity, in this chapter, only c_i will be changed with a multiplication with a bidding strategic coefficient variable b_i and also let a_i equals to zero based on assumption at the beginning of this section. Therefore, each GENCO will submit generator bids to the ISO according to the following linear supply function for Generator i .

$$f_i = b_i \cdot \frac{\partial C_i}{\partial G_i} = b_i \cdot c_i \quad (3.3)$$

where f_i is the bidding price of conventional GENCO i (\$/MWh) and b_i is the unknown bidding strategic coefficient variable of conventional GENCO i (it equals to 1 for non-strategic price takers).

Note: wind GENCO shares the same description as in (3.1), (3.2) and (3.3), the

only difference is that we use the subscript j for wind GENCOs, while other GENCOs use the subscript i .

3.2.2 Market Clearance Model

Suppose the ISO uses a transmission constrained economic dispatch to clear the market after collecting all bids and to calculate the market price based on the LMP model. If the wind power generation output is taken as a deterministic variable, the classic general DCOPF dispatch model is given as follows: [1, 63]

$$\min \sum_{i=1}^{M_C} b_i \cdot c_i \cdot G_i + \sum_{j=M_C+1}^T b_j \cdot c_j \cdot G_j \quad (3.4)$$

subject to

$$\sum_{l=1}^n G_l = \sum_{l=1}^n D_l \quad (3.5)$$

$$G_{i_{\min}} \leq G_i \leq G_{i_{\max}}, G_{j_{\min}} \leq G_j \leq G_{j_{\max}} \quad (3.6)$$

$$\sum_{l=1}^n GSF_{k-l} \cdot (G_l - D_l) \leq Limit_k \quad (3.7)$$

for $k=1,2,\dots,m$.

where GSF_{k-l} is the generation shift factor to line k from Bus l , $G_{i_{\min}}$, $G_{i_{\max}}$ is the min and max generation output of conventional GENCO i (MWh), G_j is the ISO generation dispatch of wind GENCO j (MWh), $G_{j_{\min}}$, $G_{j_{\max}}$ is the min and max generation output of wind GENCO j (MWh), G_l is the generation at Bus l (MWh), D_l is the load demand at Bus l (MWh), $Limit_k$ is the thermal limit of transmission line k , m is number of transmission lines, T is number of GENCOs, M_C is the number of conventional GENCOs, b_j is the unknown bidding strategic coefficient variable wind GENCO j (it equals to 1 for

non-strategic price takers), c_j is the marginal cost of conventional GENCO i or wind GENCO j (\$/MWh), n is the number of buses.

The control variables are b_i , b_j , G_i and G_j . The GENCO production cost is minimized in (3.4). Constraint (3.5) ensures the balance of supply and demand. Constraint (3.6) represents the generation capacity limit. Constraint (3.7) represents the transmission line constraints.

After the economic dispatch is solved, LMP at each bus l can be calculated as follows [14]:

$$LMP_l = \lambda + \left(\sum_{k=1}^m \mu_k \cdot GSF_{k-l} \right) \quad (3.8)$$

where $-\lambda$ is the Lagrange multiplier of (3.5), and $-\mu_k$ is the Lagrange multiplier of (3.7). Note that we take $-\lambda$ and $-\mu_k$ as the Lagrange multipliers such that we have positive signs when calculating LMP as shown in (3.8).

Once the energy market is cleared by ISO, each GENCO i will be paid according to its LMP and its dispatched generation. The payoff function for the conventional GENCO i and the wind GENCO j is given by

$$profit_i = LMP_i \cdot G_i - c_i \cdot G_i \quad (3.9)$$

$$profit_j = LMP_j \cdot G_j - c_j \cdot G_j \quad (3.10)$$

3.2.3 Probabilistic Model of Wind Generation Output

Wind generation output at a specific time spot is usually uncertain and cannot be described as a deterministic variable, so it is broadly accepted to use a random variable, subject to a statistical distribution, to represent it. However, it is difficult to determine the distribution type due to insufficient historical data. Since wind speed forecast error is

usually considered normally distributed and the wind speed w.r.t. wind power output can be considered linearly related in a small region, the wind power output is assumed to roughly follow normal distribution from the viewpoint of the day-ahead operation. Thus, the wind power output distribution is given by [12].

$$G_j(t) \sim N_D(\mu_j(t), \sigma_j(t)^2) \quad (3.11)$$

$$\varphi(x) = \frac{1}{\sigma_j \sqrt{2\pi}} e^{-\frac{(x-\mu_j)^2}{2\sigma_j^2}} \quad (3.12)$$

$$\Phi(x) = \int_{-\infty}^x \varphi(u) du \quad (3.13)$$

where $G_j(t)$ is the power generation output of wind GENCO j at time t (MWh), $\mu_j(t)$ is the mean value of $G_j(t)$, $\sigma_j(t)$ is the variance of $G_j(t)$, $\varphi(x)$ is the probability density function (PDF) of $G_j(t)$, and $\Phi(x)$ is the cumulative density function (CDF) of $G_j(t)$, N_D denotes normal distribution.

3.2.4 Wind Generation Bidding Schemes

From ISO's perspective, the increasing penetration of renewable power such as wind and solar presents great challenges because of the intermittency and uncertainty of renewables. This makes it harder than conventional generation to be controlled in practice. For example, in [35], the wind power generation is considered nondispatchable and sampled in different scenarios. For each scenario, it is taken as a deterministic negative load in the power balance constraint rather than in the objective function of the economic dispatch program. The ISO runs security constrained economic dispatch to find the output of conventional GENCOs. Finally, expectation will be taken to combine all scenarios' results together. As a matter of fact, it suffices to considering wind power

generation as a zero production cost source. It means that the wind power generation will always be dispatched first because it often has the lowest production cost in reality. And this also matches with current practical dispatch policy, i.e., to dispatch renewable energy in priority to meet the percentage of wind penetration in the Renewable Portfolio Standards (RPS). This is probably a legitimate model when the wind power generation penetration level in the grid is low and insignificant.

However, with an increasing penetration of wind power integrated into the grid, the above simple treatment of wind power generation as a negative load is likely neither feasible nor reasonable. Also, this treatment tends to discourage wind power suppliers producing more wind power or making more profits. Although the advantage of this dispatch scheme is its easy implementation in practice, this scheme also excludes wind generation as a bidder in electric power market. Therefore, in this chapter, two schemes are modeled to consider wind GENCOs as constraints (always dispatched first and being price takers) and as strategic bidders, respectively.

Scheme I: Wind Power as Constraint in Dispatch

Suppose the mean and variance values can be assessed beforehand. The ISO may use its mean value and its bidding price to carry out economic dispatch. When wind generation is considered into this bidding model, it should have some important adjustment. First, since wind source is intermittent, it is hard to use only one deterministic scenario to represent its performance. We have to consider its probabilistic characteristics, i.e., its expectation and variance.

In this chapter, a MCS model, elaborated in the next section, is employed to model the randomness. Suppose we take s samples for wind power generation output

$G_j(t)$, and each sampled scenario has a corresponding probability P_s and a corresponding wind power generation output G_{j_s} for wind GENCO j . Note that $\sum_s P_s = 1$ for probability and $\mu_j(t) = E(G_j(t)) = G_j$ based on the proposed assumption.

Based on the previous discussion, for each MC scenario s , the economic dispatch scheme from ISO's perspective can be described mathematically as follows:

$$\min \sum_{i=1}^{M_C} b_{i_s} \cdot c_i \cdot G_{i_s} \quad (3.14)$$

subject to

$$\sum_{l=1}^n G_l = \sum_{l=1}^n D_l \quad (3.15)$$

$$G_{i_{\min}} \leq G_{i_s} \leq G_{i_{\max}} \quad (3.16)$$

$$\sum_{l=1}^n GSF_{k-l} \cdot (G_l - D_l) \leq Limit_k \quad (3.17)$$

for $k=1,2,\dots,m$, and all s .

where b_{i_s} is the unknown bidding strategic coefficient variable of conventional GENCO i in scenario s (it equals to 1 for non-strategic price takers), G_{i_s} is the scheduled generation of conventional GENCO i in scenario s (MWh). The control variables are b_{i_s} and G_{i_s} .

The difference between (3.4) and (3.14) is that wind power generation variables are removed in (3.14). In fact, wind power generation cost could be viewed as zero cost in this case. In addition, the wind generation capacity constraint is removed in (3.16), while (3.15) and (3.17) remains the same as (3.5) and (3.7). Also, $\sum_{l=1}^n D_l$ in (3.15) and (3.17) is the total load subtract total wind power generation offset. Besides, the LMP

calculation still follows (3.8) and the payoff function for conventional GENCO i and wind GENCO j are the same as (3.9) and (3.10), respectively, after this transmission constrained economic dispatch process. For each scenario s , the profit of conventional GENCO i is as follows:

$$profit_{i-s} = LMP_{i-s} \cdot G_{i-s} - c_i \cdot G_{i-s} \quad (3.18)$$

Since the wind GENCO j is a price-taker in this case, its profit function at scenario s is calculated as follows:

$$profit_{j-s} = LMP_{j-s} \cdot G_{j-s} - c_j \cdot G_{j-s} \quad (3.19)$$

Therefore, the whole bidding process can be rewritten as a bi-level optimization problem as follows:

$$\max_{i,s} profit_{i-s} = \max_{i,s} (LMP_{i-s} \cdot G_{i-s} - c_i \cdot G_{i-s}) \quad (3.20)$$

subject to

$$b_{i\min} \leq b_{i-s} \leq b_{i\max} \quad (3.21)$$

$$\min \sum_{i=1}^M b_{i-s} \cdot c_i \cdot G_{i-s} \quad (3.22)$$

subject to

$$\sum_{l=1}^n G_l = \sum_{l=1}^n D_l \quad (3.23)$$

$$G_{i\min} \leq G_{i-s} \leq G_{i\max} \quad (3.24)$$

$$\sum_{l=1}^n GSF_{k-l} \cdot (G_l - D_l) \leq Limit_k \quad (3.25)$$

for $k=1, 2, \dots, m$ and all s .

The control variables are b_{i_s} and G_{i_s} . The objective function for a strategic bidder i at scenario s is given by (3.20). The first constraint (3.21) is to set a limitation with b_{i_s} selection to be realistic; otherwise, the bidder can have infinite market power in theory.

Thus, the total profit expectation of conventional GENCO i for all scenarios is calculated as follows:

$$profit_i = E[profit_{i_s}] = \sum_s P_s \cdot profit_{i_s} \quad (3.26)$$

And the total profit expectation of wind GENCO j for all scenarios is calculated as follows:

$$profit_j = E[profit_{j_s}] = \sum_s P_s \cdot profit_{j_s} \quad (3.27)$$

Scheme II: Wind Power as Strategic Bidder

In this scheme, the randomness of wind power is also modeled via MCS. This is the same as in Scheme I.

The difference is that wind GENCOs are taken as strategic bidders in this scheme. According to the proposed assumption in Subsection 3.2.4, since wind is not a constant power source, its payoff function needs to be modified for each sampled scenario s as follows:

a) $G_j > G_{j_s}$

$$profit_{j_s} = LMP_{j_s} \cdot G_{j_s} - c_j \cdot G_{j_s} + LMP_{j_s} (G_{j_s} - G_j) \quad (3.28a)$$

b) $G_j < G_{j_s}$

$$\begin{aligned}
profit_{j-s} &= LMP_{j-s} \cdot G_j - c_j \cdot G_{j-s} + LMP_{j-s} (G_{j-s} - G_j) \\
&= LMP_{j-s} \cdot G_{j-s} - c_j \cdot G_{j-s}
\end{aligned} \tag{3.28b}$$

Next, the objective function in (3.28a) and (3.28b) is explained. After sampling, it is a deterministic process for each scenario. At the end of the ISO's market clearance process, all LMPs and generation dispatches will be settled. The wind GENCO will get its revenue as shown by the first item on the left hand side of (3.28a) and (3.28b). The second item in (3.28a) and (3.28b) is its production cost.

The third item in (3.28a) is the obligation penalty cost if it cannot meet the dispatch requirement in day-ahead market subject to its output uncertainty, because it has to purchase the gap amount of power from the real-time spot market. If it has more generation than required in day-ahead market as in (3.28b), it is assumed to earn extra profits from selling it to the real-time spot market with the day-ahead price. Note, this approach represents the penalty or extra profit due to insufficient or overproduced output in real-time. Since the goal of this chapter is to compare the two schemes, as long as they are based on the same assumption (no price difference between day-ahead and real-time), the comparison is fair.

Therefore, the whole bidding process can be rewritten as a bi-level optimization problem shown below:

if it is a conventional GENCO

$$\max_{i,s} profit_{i-s} = \max_{i,s} (LMP_{i-s} \cdot G_{i-s} - c_i \cdot G_{i-s}) \tag{3.29}$$

or if it is a wind GENCO with $G_j > G_{j-s}$

$$\max_{j,s} profit_{j-s} = \max_{j,s} (LMP_{j-s} \cdot G_{j-s} - c_j \cdot G_{j-s} + LMP_{j-s} (G_{j-s} - G_j)) \tag{3.30a}$$

or if it is a wind GENCO with $G_j < G_{j_s}$

$$\max_{j,s} \text{profit}_{j_s} = \max_{j,s} (LMP_{j_s} \cdot G_{j_s} - c_j \cdot G_{j_s}) \quad (3.30b)$$

subject to

$$b_{i_{\min}} \leq b_{i_s} \leq b_{i_{\max}}, b_{j_{\min}} \leq b_{j_s} \leq b_{j_{\max}} \quad (3.31)$$

$$\min \sum_{i=1}^M b_{i_s} \cdot c_i \cdot G_{i_s} + \sum_{j=M+1}^T b_{j_s} \cdot c_j \cdot G_{j_s} \quad (3.32)$$

subject to

$$\sum_{l=1}^n G_l = \sum_{l=1}^n D_l \quad (3.33)$$

$$G_{i_{\min}} \leq G_{i_s} \leq G_{i_{\max}}, G_{j_{\min}} \leq G_{j_s} \leq G_{j_{\max}} \quad (3.34)$$

$$\sum_{l=1}^n GSF_{k-l} \cdot (G_l - D_l) \leq \text{Limit}_k \quad (3.35)$$

for $k=1,2,\dots,m$ and all s .

where b_{j_s} is the unknown bidding strategic coefficient variable of wind GENCO j in scenario s (it equals to 1 for non-strategic price takers), G_{j_s} is the scheduled generation of conventional GENCO i or wind GENCO j in scenario s (MWh).

The control variables are b_{i_s} , b_{j_s} , G_{i_s} and G_{j_s} . If it is a conventional GENCO, the upper level objective function is (3.29), while if it is a wind GENCO, the upper level objective function should be replaced as (3.30a) and (3.30b) instead. Again, equation (3.31) is to set a limitation with the b_{i_s} and b_{j_s} selections to avoid the bidder to have infinite market power in theory. In the lower level optimization, LMP calculation still follows (3.8) and the expected payoff function for conventional GENCO i and wind

GENCO j follows (3.26) and (3.27) respectively.

Therefore, its final profit expectation of wind GENCO j for all wind generation output scenarios is considered as

a) $G_j > G_{j-s}$

$$profit_j = E[profit_{j-s}] = \sum_s P_s \cdot \left[\begin{array}{l} LMP_{j-s} \cdot G_{j-s} - c_j \cdot G_{j-s} \\ + LMP_{j-s} (G_{j-s} - G_j) \end{array} \right] \quad (3.36a)$$

b) $G_j < G_{j-s}$

$$profit_j = E[profit_{j-s}] = \sum_s P_s \cdot \left[LMP_{j-s} \cdot G_{j-s} - c_j \cdot G_{j-s} \right] \quad (3.36b)$$

It should be clarified that in this chapter, we consider short-term inelastic load demand, so we only minimize generation cost. Also, the model is a complete information model, which means everyone knows each other's bidding strategy.

3.3 Monte Carlo Simulation and Genetic Algorithm

3.3.1 Monte Carlo Simulation

Since wind generation is supposed to follow some statistic distributions in this chapter, it is natural to employ MC methods to describe and integrate it into this bidding problem [6, 27].

The MCS, applicable to both scheme I and II, is implemented as follows:

- 1) Suppose wind GENCOs output follows normal distribution, and their mean value and variance could be already known beforehand. Thus, their probability density functions (PDFs) can be derived as well. Use them as the inputs in this MCS.
- 2) Take s repeated random samplings for each wind GENCO j 's PDF to obtain

G_{j_s} and P_s for each MC sampled scenario s .

- 3) For each scenario s , perform a deterministic optimization based on GA and then LP to calculate all bidding strategies, all GENCO dispatches, all LMPs, and the profits for all GENCOs (conventional and wind).
- 4) Aggregate the results to get all GENCOs' profit expectation.

The number of random samplings s could be determined as follows: The MCS can stop based on whether a pre-defined convergence threshold ε_M has been reached or not. This stopping criterion is shown mathematically as follows [64-66]:

$$\frac{\sigma[E(X)]}{E(X)} = \frac{\sigma(X)}{\sqrt{s} \cdot E(X)} \leq \varepsilon_M \quad (3.37)$$

where X is the random variable representing the wind generation profit in this chapter, s is the MC sampling scenarios of the wind power generation, $E(X)$ is the mean value of X , and $\sigma(X)$ is the standard deviation of X .

Equation (3.37) shows that if ε_M is small, then s is large. This means that more computational power and time are needed to maintain an acceptable accuracy. Otherwise, if ε_M is large, then s is less, it means computational power and time are unnecessary and perhaps wasted for an unnecessary high level of accuracy. In practice, a delicate design of the convergence threshold ε_M needs to consider some compromise between accuracy and computing speed.

It is not necessary to know an exact s because a large enough s can also be accepted in reality. Therefore, there is another way to get the rough estimation of s . First, set an initial guess of s_0 , for example 1000. Then a MCS trial can be processed. With the

statistical results $\sigma(X)$ and $E(X)$ obtained from these 1000 samples, if (3.37) holds for the pre-defined threshold ε_M , then stop and return with all results. Otherwise, an update s value can be calculated based on the estimation of $\sigma(X)$ and $E(X)$ to meet (3.37). Thus, we can perform additional $s-s_0$ random MC draws. With the new results, (3.37) can be re-evaluated. This process is repeated till (3.37) holds with the least required s .

3.3.2 Genetic Algorithm

Essentially, this proposed optimization problem is to find the global Nash Equilibrium to each bidder. The formation of the proposed solution is a bi-level optimization, which is depicted in Figure 3.1. There are various approaches to solve this non-linear, non-convex, bi-level optimization. Here the GA is used in this chapter. Note that the term “biological generation,” instead of the commonly used term “generation” in the GA algorithm discussion, is used to avoid possible confusion with the electrical generation.

GA is based on the Darwinian principle of natural selection. Initially, a population of data structures is randomly chosen. Candidate solutions, encoded in a binary string of 0s and 1s, are used to model the optimization problem with a fitness function. Then during each biological generation of the evolutionary process, crossovers and mutations are applied to the data of the binary string such that a new, evolved population is created for the next generations towards a better solution. Further, the new population is then used in the next iteration of the algorithm to explore different areas of the solution space that the parent generations did not. Also, the less fitness ones of the existing populations will be replaced [7, 27]. Generally, the algorithm terminates when either a maximum number of generations is reached, or a satisfactory fitness level has been reached for the

population. If the algorithm is terminated due to a maximum number of generations, a satisfactory solution may or may not have been reached.

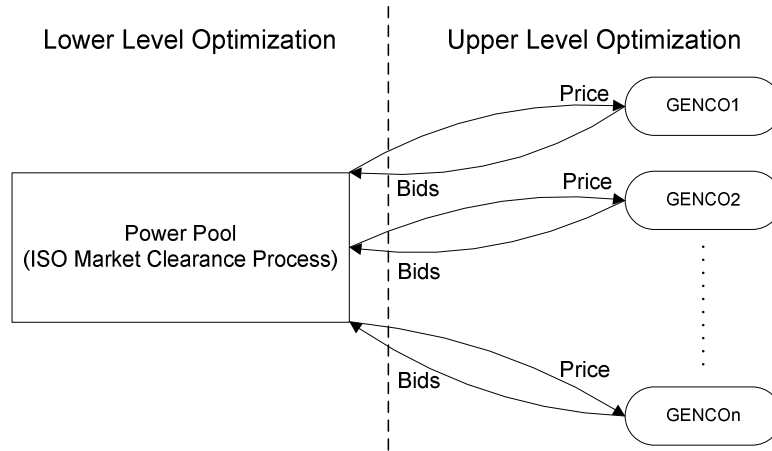


Figure 3.1 Framework of the proposed bi-level GA optimization process

For each scenario s , the simulation process is described for wind GENCO bidding strategy Schemes I & II, respectively.

a. For Wind GENCO Scheme I:

1) System initialization:

- Input all relevant data and initialization.
- Initialize all $b_{i,s}$ for all conventional GENCOs.
- Randomly initialize a population for each $b_{i,s}$.
- Set $i=1$ and the biological generation counter to zero.

2) Suppose bidding strategies of opponents' generator are fixed. Update conventional GENCO i 's bidding strategies until no unit will change its bidding strategy, while the current biological generation number is less than the maximum generation number.

- Solve LP of the ISO's dispatch model to obtain LMP and the dispatched generation output.
 - Calculate the fitness function for each member of the biological generation.
 - Select parents, crossover the selected to create new offspring and mutate these new offspring.
 - Increase the biological generation counter and go to the beginning of step 2).
 - If the current generation number is more than the maximum generation number, go to step 3).
- 3) $i=i+1$ and repeat 2) to find each conventional GENCO's optimal bidding strategies in response to the opponents' bidding strategies.
- 4) Go to 2) and repeat the procedure until no generator would change its bidding strategy, i.e., no one can gain more by unilaterally changing its bidding strategy.

b. For Wind GENCO Scheme II:

1) System initialization:

- Input all relevant data and initialization.
- Initialize all b_{i_s} for all conventional GENCOs and all b_{j_s} for all wind GENCOs.
- Randomly initialize a population for each b_{i_s} and b_{j_s} .
- Set $i=1$ and $j=M+1$ and the biological generation counter to zero.

2) Suppose bidding strategies of opponents' generator are fixed. Update conventional GENCO i 's bidding strategies until no unit will change its bidding strategy, while the current biological generation number is less than the maximum

biological generation number.

- Solve LP of the ISO's dispatch model to obtain LMP and the dispatched generation output.
 - Calculate the fitness function for each member of the generation.
 - Select parents, crossover the selected to create new offspring and mutate these new offspring.
 - Increase the biological generation counter and go to the beginning of step 2).
 - If the current biological generation number is more than the maximum generation number, go to step 3).
- 3) $i=i+1$ and repeat 2) to find each conventional GENCO's optimal bidding strategies in response to the opponents' bidding strategies.
- 4) Suppose bidding strategies of opponents' generator are fixed. Update wind GENCO j 's bidding strategies until no unit will change its bidding strategy, while the current biological generation number is less than the maximum generation number.
- Solve LP of the ISO's dispatch model to obtain LMP and the dispatched generation output.
 - Calculate the fitness function for each member of the biological generation.
 - Select parents, crossover the selected to create new offspring and mutate these new offspring.
 - Increase the biological generation counter and go to the beginning of step 4).
 - If the current biological generation number is more than the maximum

generation number, go to step 5).

5) $j=j+1$ and repeat 4) to find each wind GENCO's optimal bidding strategies in response to the opponents' bidding strategies.

6) Go to 2) and repeat the procedure until no generator would change its bidding strategy, i.e., no one can gain more by unilaterally changing its bidding strategy.

By combining all scenarios' results based on MCS and GA, the expected results can be derived. The whole computation process is wrapped up and the flow chart is shown in Figures 3.2 and 3.3 for Schemes I and II, respectively.

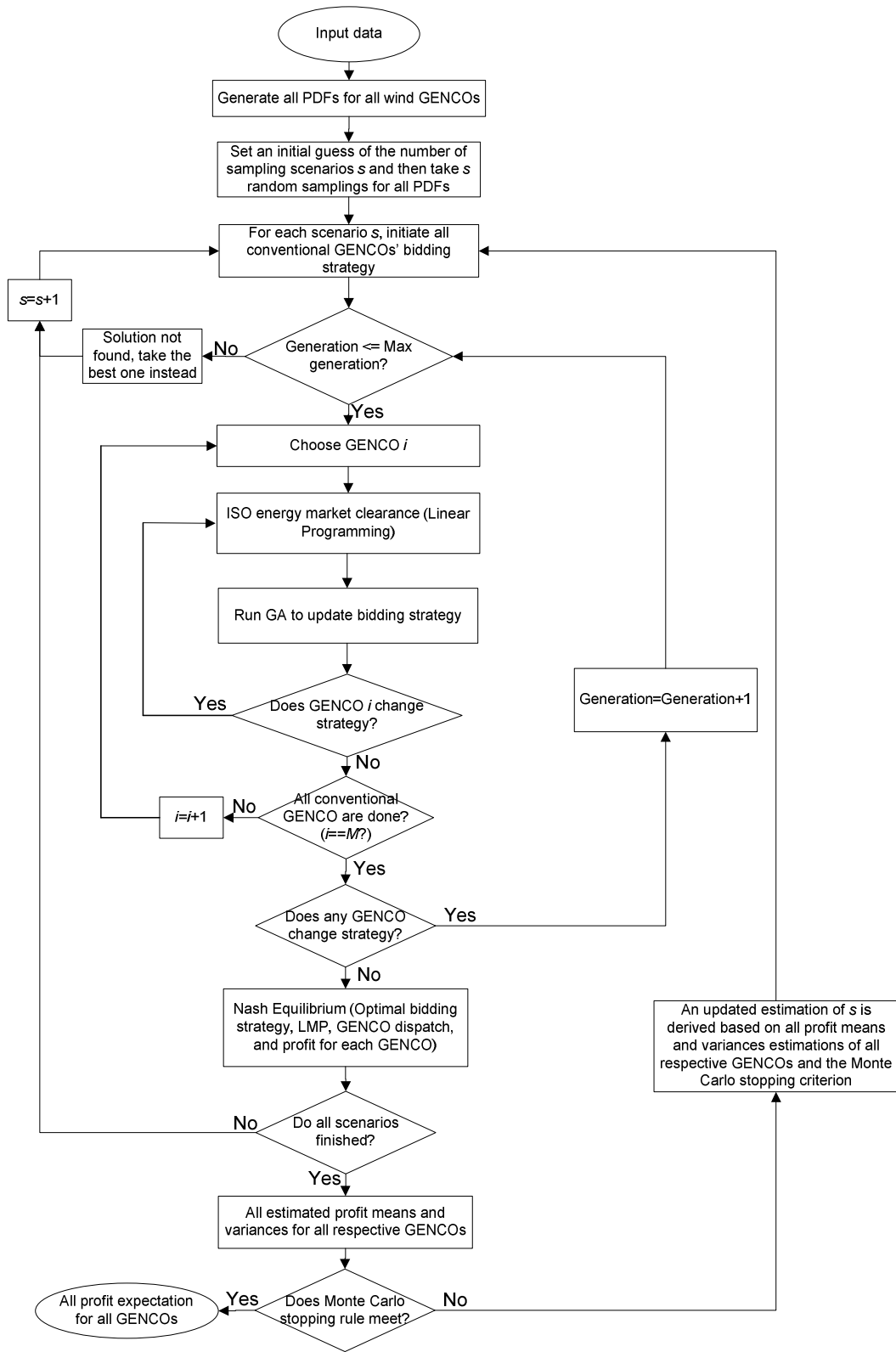


Figure 3.2 Flowchart of the proposed GA and MCS for wind generation bidding scheme I

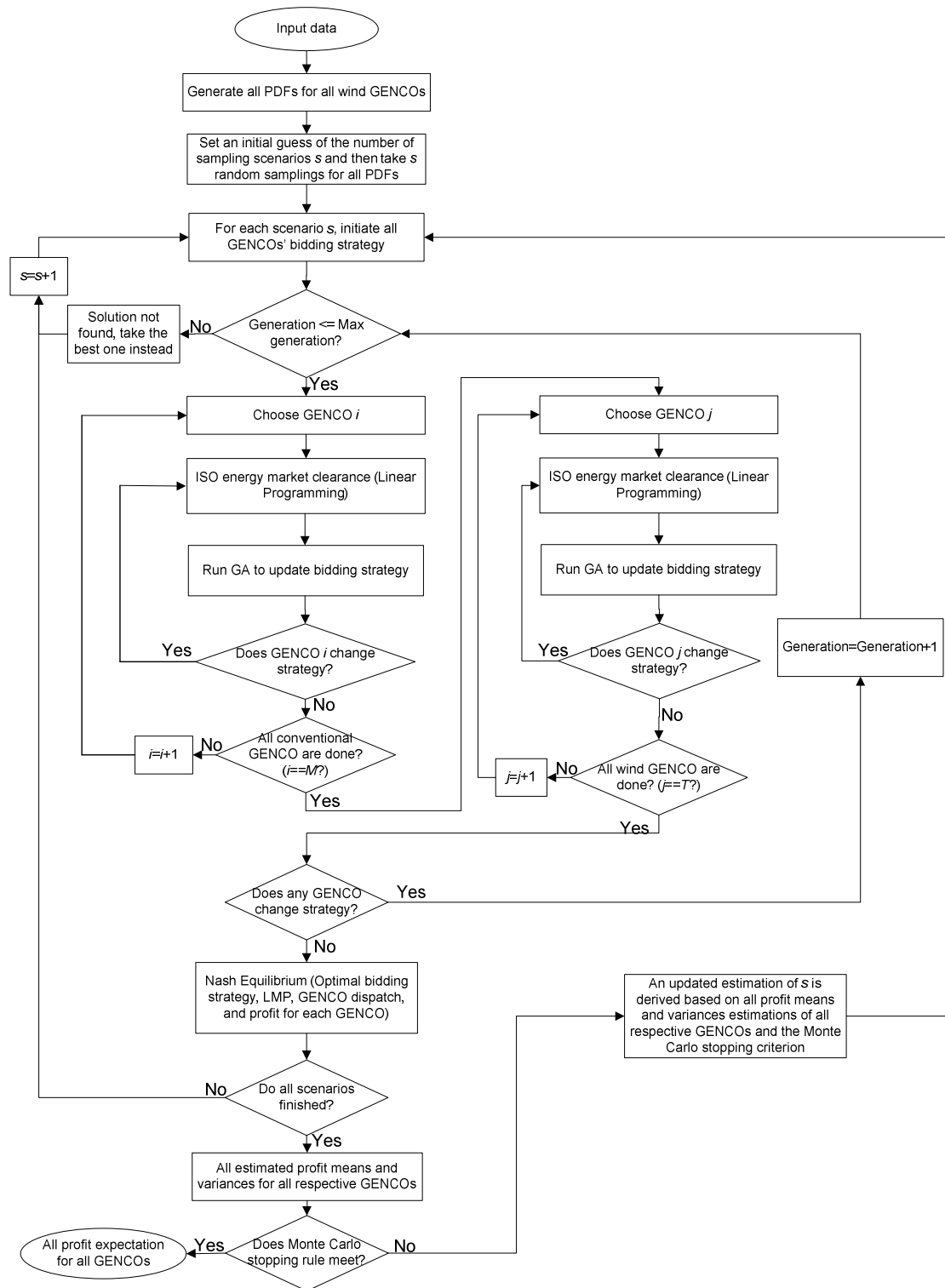


Figure 3.3 Flowchart of the proposed GA and MCS for wind generation bidding scheme II

3.4 Numerical Examples

The stopping criterion ε_M of MCS is set to 0.01 for all cases below [65]. In addition, for the parameters associated with GA applied to the cases below, we set the total biological generation to 100, population size to 50, crossover rate to 0.5, mutation rate to 0.01, and eight bits for bidding strategy coefficients (b_i and b_j). Also, the GA stopping criterion is that the difference between the previous profit and the current profit of each GENCO is less than 1% of the current profit for all scenarios in each case.

3.4.1 PJM Five-Bus System

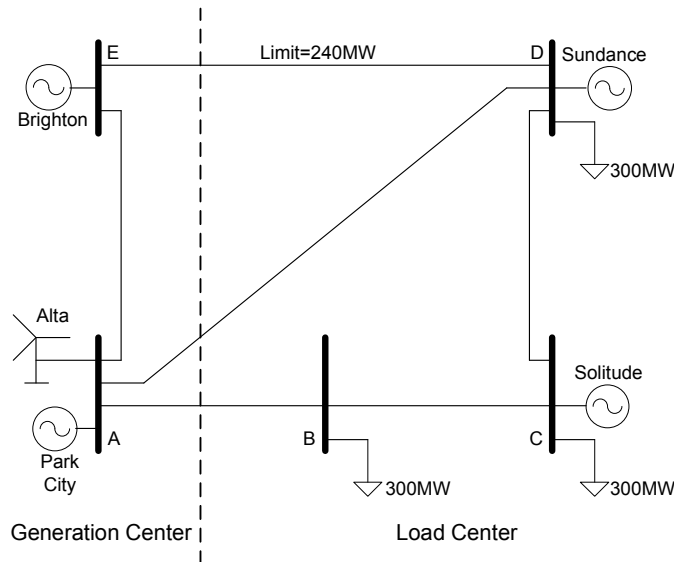


Figure 3.4 Modified PJM five-bus Example

This modified PJM five-bus system is shown in Figure 3.4 [14]. The transmission line profiles are shown in Table 3.1. On the left hand side of this system is the generation center, while the load center is on the right hand side. In this base case, its total load level is 900MW. In this modified test system, Alta is a wind generator which observes normal

distribution with a mean output 100 MW and standard variance 16.67 MW. Considering three times of standard variance is the practical limit of wind output, the wind power output will be within the interval [50MW, 150MW] with 99.7% confidence based on normal distribution. All other generators are conventional units, with unit min and max generation and cost listed in Table 3.2 according to each unit's type.

Table 3.1 Line Impedance and Flow Limit

| Line | AB | AD | AE | BC | CD | DE |
|-----------|------|------|------|------|------|------|
| X(%) | 2.81 | 3.04 | 0.64 | 1.08 | 2.97 | 2.97 |
| Limit(MW) | 999 | 999 | 999 | 999 | 999 | 240 |

Table 3.2 Generator Data

| Generator | Type | P_{\min} (MW) | P_{\max} (MW) | Marginal Cost(\$/MWh) |
|-----------|-------|-----------------|-----------------|-----------------------|
| Alta | Wind | 50 | 150 | 7 |
| Park City | Hydro | 0 | 100 | 15 |
| Solitude | Gas | 0 | 520 | 30 |
| Sundance | Gas | 0 | 300 | 35 |
| Brighton | Steam | 10 | 600 | 10 |

1) Scheme I - Wind Generation as a Constraint

Let Park City and Sundance be the two bidders involved within this case. The two bidding strategy coefficients for Park City and Sundance are constrained to be in [1, 3] and [1, 1.5], respectively, such that they may bid up to \$45/MWh and \$52.5MWh, respectively, in order to have a wider range to set the price.

Wind generation is considered to be a negative load in this scheme. Then 1000 sampling scenarios are taken in this case. The profit, generation and price expectation for

each generator are shown in Table 3.3.

Table 3.3 Profit Expectation for Each Generator in PJM Five-Bus System Scheme I

| Generator | Alta | Park City | Solitude | Sundance | Brighton |
|-----------------------|-------|-----------|----------|----------|----------|
| Expected profit(\$) | 1129 | 0 | 0 | 0 | 1664 |
| Expected Output(MW) | 100 | 0 | 212.82 | 0 | 587.19 |
| Expected Price(\$/MW) | 18.78 | 18.78 | 30 | 38.56 | 12.77 |

The running time for this case is 108 seconds under Intel Core i5-2520M CPU 2.5GHz, 4GB RAM and Windows-7 64 bit operation system environment. The GA convergence rate (i.e., ratio between number of scenarios converged to a Nash Equilibrium and total scenarios) is 1. It means that the probability of reaching a Nash Equilibrium solution under current system conditions is 100%. The average total generation cost of this scheme is \$12,959.

2) Scheme II - Wind Generation as a Bidder

All the assumptions and parameters are the same as in the previous case. The only difference is that Alta is also a price bidder of the whole bidding process at this time with bidding strategic coefficient constrained in [1, 5] such that the wind unit's bid can be up to \$35/MWh, which is in a comparable range of the other strategic units' bids. Thus, there are three bidders in this case. Also, 1000 sampling scenarios are taken in this case. The profit expectation is shown in Table 3.4.

Table 3.4 Profit Expectation for Each Generator in PJM Five-Bus System Scheme II

| Generator | Alta | Park City | Solitude | Sundance | Brighton |
|-----------------------|---------|-----------|----------|----------|----------|
| Expected profit(\$) | 1893.80 | 0 | 0 | 0 | 9593.3 |
| Expected Output(MW) | 69.84 | 0 | 238.38 | 0 | 591.77 |
| Expected Price(\$/MW) | 27.39 | 27.39 | 30 | 31.99 | 25.99 |

The running time for this case is 798 second under Intel Core i5-2520M CPU 2.5GHz, 4GB RAM and Windows-7 64 bit operation system environment. The GA convergence rate in this case is 0.99, i.e. the probability of reaching a Nash Equilibrium solution under the current system conditions is 99%. The average total generation cost of this system is \$13,773, which is about 6.3% higher than the previous case.

3) Analysis of Results with Sensitivity Study

If we compare the results of the above two cases in Tables 3.3 and 3.4, it shows that the profit of wind generator Alta in the Scheme II is more than in the Scheme I case even with less expected generation because the profit gains weight much more than the possible losses when under-production occurs. This implies that allowing wind unit to bid may financially help them cover their own uncertainty and reliability issues. The profit of Generator Solitude is 0, which means the LMP on this bus is always the same as its marginal cost in both cases, while generator Park City and Sundance also earn no profit due to zero production.

However, the unit Brighton is the biggest winner in Scheme II, because the LMP at its bus doubles and its expected output stays the same. Also, the total generation cost goes up by 6.3% which is also significant. Thus, there are pros and cons for allowing wind unit to participate in bidding. This implies the need of an update in the power market architecture and structure for adapting high penetration of wind power.

Further, sensitivity study based on different total system load levels is performed. The comparison graphs of wind unit Alta's profit and the total system cost are shown in the following figures.

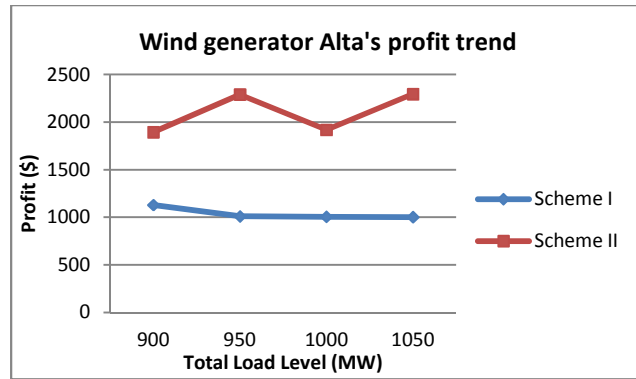


Figure 3.5 Comparison of Wind Generator Alta's Profit

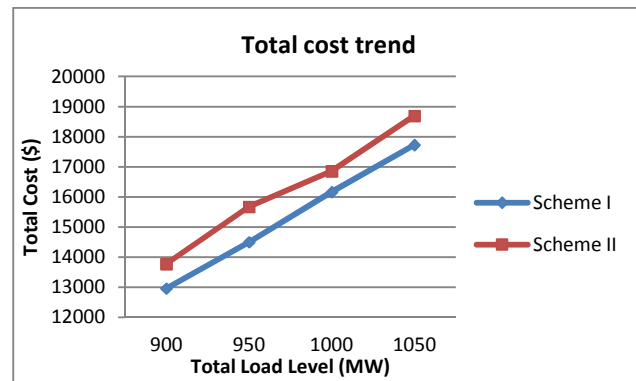


Figure 3.6 Comparison of System Total Cost

As seen in Figures 3.5 and 3.6, the load level increases in a 50MW step. At different load levels, Scheme II will lead the wind bidder to consistently earn more than in Scheme I, while the total system cost is higher than in Scheme I as well. At the studied four load levels, the GA always has a high convergence rate more than 99.5%, which guarantees the validity of the results.

Note, as the total system load level goes beyond 1100MW or even more, the convergence rate of GA is very low, i.e. lower than 50%. This means the total generation capacity is not sufficient. Thus, the sensitivity analysis is stopped at 1050MW load level, otherwise the result is not credible.

3.4.2 IEEE 118-Bus System

There are 186 branches, 91 loads, and 54 generators in the IEEE 118-bus test system. All the detailed information can be found in [67]. The original IEEE 118-bus system data does not contain the information of generator marginal costs and branch thermal limits. Therefore, generator marginal costs are constructed in this chapter as follows: two wind generators with marginal cost \$8, twenty cheap generators with marginal cost from \$10 to \$19.5 with \$0.5 increment; eighteen expensive generators with marginal cost from \$20 to \$23 and \$26 to \$39 with \$1 increment; and fourteen extremely expensive generators with marginal cost from \$40 to \$53 with \$1 increment. In addition, five thermal limits are introduced into the transmission system: 345MW for Line 69-77, 630MW for Line 68-81, 106MW for Line 83-85 and 94-100, 230MW for Line 80-98 [12]. Also, the maximum total generation is more than twice of the total load. In order to show the wind generation effect, each load is scaled up at 1.8 times of its original value in the whole system.

Suppose two wind GENCOs are located at Buses 59 and 61, respectively. Their generation output mean values are 155MW and 160MW, respectively. Also, they have the same standard variance at 33.33MW to make possible wind power output locate in the interval [55MW, 255MW] and [60MW, 260MW], respectively, with 99.7% confidence based on the normal distribution property. In addition, the two wind generations are independent random variables with each other. All other generators are conventional units.

1) Scheme I - Wind Generation as a Constraint

Let generators at Buses 65, 66 and 69 be the strategic players involved in this case. The three bidding strategy coefficients are constrained to be in [1, 2] such that the involved units may bid up to \$56/MWh which gives a sufficiently wide range for simulation test.

Wind generation is considered to be a negative load in this scheme with 1000 sampling scenarios. The profit expectation is shown in Table 3.5. (Here only the results of the strategic bidders and wind owners are listed).

Table 3.5 Profit Expectation for Each Generator in IEEE 118 Bus System Scheme I

| Generator at Bus | 59 | 61 | 65 | 66 | 69 |
|-----------------------|--------|--------|--------|--------|--------|
| Expected Profit(\$) | 4577.4 | 4727.9 | 5354.8 | 4839.9 | 6981.7 |
| Expected Output(MW) | 153.74 | 158.66 | 490.9 | 491 | 794.75 |
| Expected Price(\$/MW) | 37.85 | 37.87 | 37.90 | 37.86 | 37.84 |

The running time for this case is 596 seconds under Intel Core i5-2520M CPU 2.5GHz, 4GB RAM and Windows-7 64 bit operation system environment. The GA convergence rate (i.e., ratio between the number of scenarios converged to a Nash Equilibrium and the total number of scenarios) is 1, which means that the probability of having a Nash Equilibrium solution is 100% under the current system conditions. The average generation cost is \$176,430.

2) Scheme II - Wind Generation as a Bidder

All the assumptions and parameters are the same as in the previous case. The only difference is that the two wind units at Buses 59 and 61 are market players in the entire bidding process with bidding factor in the range of [1, 6]. Thus, we will have five bidders

in this case. Similar to the previous case, 1000 sampling scenarios are taken in this case. The profit expectations of five strategic bidders are shown in Table 3.6.

Table 3.6 Profit Expectation for Each Generator in IEEE 118 Bus System Scheme II

| Generator at Bus | 59 | 61 | 65 | 66 | 69 |
|-----------------------|--------|--------|--------|--------|--------|
| Expected profit(\$) | 4838.5 | 4952.5 | 5826.4 | 5328.9 | 7876.7 |
| Expected Output(MW) | 108.04 | 115.36 | 491 | 491.51 | 801.91 |
| Expected Price(\$/MW) | 38.84 | 38.85 | 38.87 | 38.84 | 38.83 |

The running time for this case is 1850 seconds under Intel Core i5-2520M CPU 2.5GHz, 4GB RAM and Windows-7 64 bit operation system environment. The GA convergence rate is 0.995, which means the probability of having a Nash Equilibrium solution is 99.5%. The average total generation cost is \$178,080, which is about 1% increase from Scheme I. Since the five strategic bidders represent a small portion of the total units, this 1% increase is considerable.

3) Analysis of Results

If we compare the results of these two cases in Tables 3.5 and 3.6, the observation shall be very similar to the one from the previous PJM five-bus system study. Both wind generation bidders may have tremendous profit uplift as a marginal unit even the probabilistic uncertainty is considered, because the gains from wind strategic bidding outweigh the cost of purchasing power due to insufficient wind production. From this perspective, this should encourage the renewable generation to aggressively play in the power market to gain more profits.

However, also similar to the PJM five-bus case study, the above benefit is at the cost of increased total production cost and more profit of other conventional generation

bidders. Thus, consumers will pay more.

Therefore, this implies the need of an update in the power market architecture and structure to better accommodate high penetration of wind power. Also, the high GA convergence rate guarantees the validity of the results.

3.5 Conclusions

The contribution of this chapter can be summarized as follows:

- Two bidding strategy schemes are modeled in this chapter to consider wind GENCOs, conventional GENCOs, and transmission constraints, while few literatures have studied the impact of wind GENCOs to bidding strategy. The first scheme considers wind power as negative loads, which is aligned with the ongoing practice that wind power must be dispatched with higher priority. The second scheme considers wind GENCOs as possible strategic bidders, which is aligned with the common expectation that wind power owners may participate in market competition in the future.
- In each scheme, a comprehensive bidding strategy model is proposed in a probabilistic approach using MCS. In each MC sample, a bi-level optimization model is employed with different objective functions for wind GENCOs. The Genetic Algorithm is employed as the solution method.
- Simulation results show that, when wind GENCOs act as strategic bidders to set the price, they can make significant profits as opposed to playing as a price taker. Note this result considers the probabilistic variability of wind output. However, this is at the expense of an increased production cost and other units'

profit, which means consumers will pay more. Thus, we can draw an important conclusion that when there is a high-penetration of wind power, likely an update of the existing market architecture and structure is necessary in terms of having a competitive electricity market under high-penetration renewables.

The future work may include the bidding strategy model with ancillary service models, detailed penalty model and effect of GENCO's collusion and coalition in the power market.

CHAPTER IV

SENSITIVITY ANALYSIS OF LOAD-DAMPING CHARACTERISTIC

4.1 Background of Different Load Categories

In power systems, the load may be mainly classified as in two categories: the frequency-sensitive load such as induction motors and the pure constant PQ load such as the heaters. They have different frequency response behaviors under various frequency conditions. The constant PQ load has constant load under any system frequency status, while the frequency sensitive load could have different load value as system frequency changes. Since different system has different frequency-load sensitivity due to the different ratio between the constant PQ load elements and the frequency sensitive load components, it is always desirable to have a mathematical description to quantify its effect for better system frequency analysis. In this chapter, a frequency sensitivity function of load-damping coefficient is calculated for system frequency stability use. And it indicates a new system frequency stability border considering the effect of this frequency sensitivity function.

4.2 Sensitivity Function Derivation

4.2.1 Single Machine (SISO) System

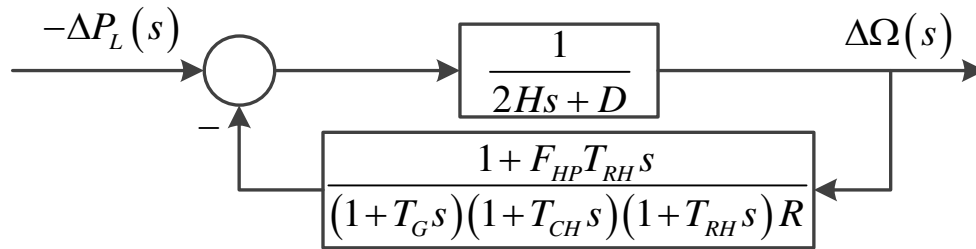


Figure 4.1 Load frequency control diagram with input $\Delta P_L(s)$ and output $\Delta\Omega(s)$

Here we consider a complete block diagram of the load-frequency control (LFC) for a simple single machine system, or single input-single output (SISO) system, in Figure 4.1 [20]. Where T_G is the governor time constant, T_{CH} is the steam chest time constant, T_{RH} is the reheat turbine time constant, F_{HP} is the high pressure power fraction of reheat turbine, H is the generator inertia constant, D is the load-damping coefficient, R is the governor speed regulation, $\Delta\Omega(s)$ is the Laplace transformation of the angular frequency deviation $\Delta\omega(t)$, $\Delta P_L(s)$ is the Laplace transformation of the load change perturbation (usually considered as a step function).

Here the machine model considers a reheat turbine, which is typical for frequency control, for illustrative purpose. Similar analysis and conclusions can be extended to other turbines like hydraulic ones. With commonly adopted hypothetic assumptions, this is the most simplified model. If a system is a multi-machine and multi-load system, it can be converted to an approximate SISO system using generation and load aggregation [36, 68-69]. The closed-loop transfer function relating the fixed load step change, $\Delta P_L(s)$, which is commonly assumed for LFC, to the angular frequency deviation from nominal reference frequency 60 Hz, $\Delta\Omega(s)$, is shown as follows:

$$\frac{\Delta\Omega(s)}{-\Delta P_L(s)} = \frac{1}{2Hs + D + \frac{1 + F_{HP}T_{RH}s}{(1 + T_Gs)(1 + T_{CH}s)(1 + T_{RH}s)}R} \quad (4.1)$$

By (4.1), the stability of this frequency-regulation system can be tested by Routh-Hurwitz array or root locus. And the output of angular frequency deviation can be obtained as:

$$\Delta\Omega(s) = \frac{-\Delta P_L(s)}{2Hs + D + \frac{1 + F_{HP}T_{RH}s}{(1+T_Gs)(1+T_{CH}s)(1+T_{RH}s)}R} \quad (4.2)$$

The proposed sensitivity analysis of the load-damping coefficient D , is to calculate $\frac{\partial\Delta\Omega(s)}{\partial D}$. As previously stated, this shows the potential frequency variation when the actual D value differs from the estimated value, or D is assumed to change continuously in a time period due to load control programs. This is important since the D value is usually obtained empirically. Thus, the growing penetration of demand response draws the research interest on the impact of the D value.

Taking partial derivative of D in (4.2), we can obtain the sensitivity of the frequency deviation, $\Delta\Omega$, w.r.t. the load-damping coefficient D , as follows:

$$\begin{aligned} \frac{\partial\Delta\Omega(s)}{\partial D} &= \frac{\Delta P_L(s)}{\left[2Hs + D + \frac{1 + F_{HP}T_{RH}s}{(1+T_Gs)(1+T_{CH}s)(1+T_{RH}s)}R\right]^2} \\ &= \left[\frac{\Delta\Omega(s)}{\Delta P_L(s)}\right]^2 \Delta P_L(s) \end{aligned} \quad (4.3)$$

Then S_D , the unit-less frequency sensitivity function of D , is derived by its definition as follows:

$$S_D = \frac{d\Delta\Omega(s)/\Delta\Omega(s)}{dD/D} = \frac{\partial\Delta\Omega(s)}{\partial D} \cdot \frac{D}{\Delta\Omega(s)} = \frac{\Delta\Omega(s)}{\Delta P_L(s)} \cdot D \quad (4.4)$$

4.2.2 Multi-Machines System

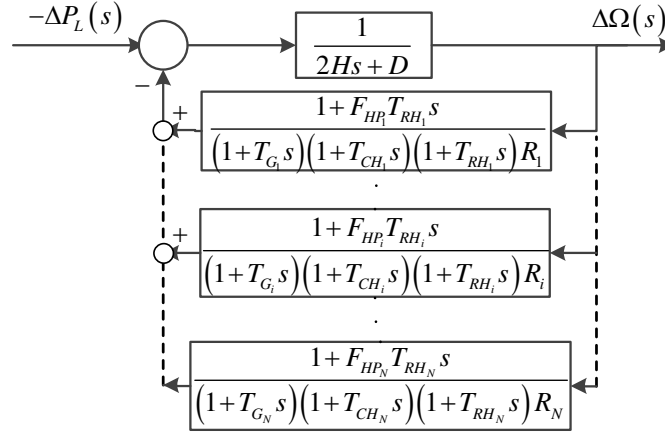


Figure 4.2 LFC block diagram of multiple generation machines case with input $\Delta P_L(s)$ and output $\Delta\Omega(s)$

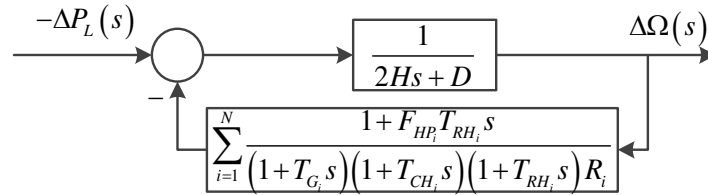


Figure 4.3 LFC equivalent block diagram of multiple generation machines case

For the case of multiple generation machines as shown in Figures 4.2 and 4.3, the transfer function is given by:

$$\begin{aligned} \frac{\Delta\Omega(s)}{-\Delta P_L(s)} &= \frac{\frac{1}{2Hs + D}}{1 + \frac{1}{2Hs + D} \left[\sum_{i=1}^N \frac{1 + F_{HP_i} T_{RH_i} s}{(1 + T_{G_i} s)(1 + T_{CH_i} s)(1 + T_{RH_i} s) R_i} \right]} \quad (4.5) \\ &= \frac{1}{(2Hs + D) + \sum_{i=1}^N \frac{1 + F_{HP_i} T_{RH_i} s}{(1 + T_{G_i} s)(1 + T_{CH_i} s)(1 + T_{RH_i} s) R_i}} \end{aligned}$$

where N is the number of generators.

The output of angular frequency deviation could be obtained as

$$\Delta\Omega(s) = \frac{-\Delta P_L(s)}{(2Hs + D) + \sum_{i=1}^N \frac{1 + F_{HP_i} T_{RH_i} s}{(1 + T_{G_i} s)(1 + T_{CH_i} s)(1 + T_{RH_i} s) R_i}} \quad (4.6)$$

Thus, the sensitivity of $\Delta\Omega$ w.r.t. D is given by:

$$\begin{aligned} \frac{\partial\Delta\Omega(s)}{\partial D} &= \frac{\Delta P_L(s)}{\left[(2Hs + D) + \sum_{i=1}^N \frac{1 + F_{HP_i} T_{RH_i} s}{(1 + T_{G_i} s)(1 + T_{CH_i} s)(1 + T_{RH_i} s) R_i} \right]^2} \\ &= \left[\frac{\Delta\Omega(s)}{\Delta P_L(s)} \right]^2 \Delta P_L(s) \end{aligned} \quad (4.7)$$

Then S_D , the unit-less multi-machines sensitivity function of D can be written as:

$$S_D = \frac{d\Delta\Omega(s)/\Delta\Omega(s)}{dD/D} = \frac{\partial\Delta\Omega(s)}{\partial D} \cdot \frac{D}{\Delta\Omega(s)} = \frac{\Delta\Omega(s)}{\Delta P_L(s)} \cdot D \quad (4.8)$$

Note that (4.3), and (4.7) have the same formulation of the sensitivity function.

Similarly, (4.4), and (4.8) show the same formulation of the unit-less sensitivity function.

4.3 Stability Analysis using Total Differential Equation

4.3.1 Total Differential Equation for Frequency Deviation

The angular frequency deviation $\Delta\Omega(s)$ is only considered to be related with external disturbance $\Delta P_L(s)$ for simplicity in early researches [8, 19-20, 36]. And its differential equation is as follows:

$$d\Delta\Omega(s) = \frac{\partial\Delta\Omega(s)}{\partial\Delta P_L(s)} d\Delta P_L(s) \quad (4.9)$$

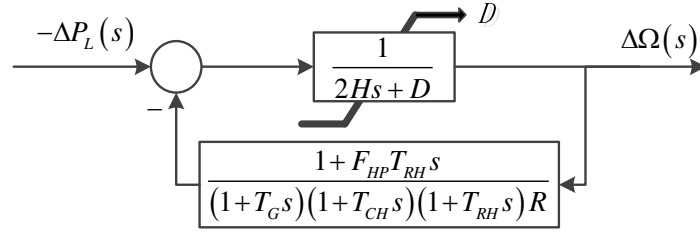


Figure 4.4 SISO LFC block diagram with input $\Delta P_L(s)$ and output $\Delta\Omega(s)$ and varied load-damping coefficient D

However, in (4.9), the effect of the load-damping coefficient D in this SFR model is ignored. This may not give complete information because the interrupted load may have a different load-damping coefficient than the rest of the loads. This is highly possible because many times interrupted or shed loads are induction motor loads which have a D value different from other types of loads. Also, D may be evaluated based on an out-of-date profile of load characteristic. In other words, the frequency variation $\Delta\Omega$ should be a function of ΔP_L and D rather than ΔP_L only as shown in Figure 4.4. Thus, it is interesting to investigate the impact of the load-damping coefficient.

With the assumption that $\Delta P_L(s)$ and D are mutually independent, (4.9) should be modified to include D as follows:

$$d\Delta\Omega(s) = \frac{\partial\Delta\Omega(s)}{\partial\Delta P_L(s)} d\Delta P_L(s) + \frac{\partial\Delta\Omega(s)}{\partial D} dD \quad (4.10)$$

Combining either (4.3), and (4.7) with (4.10), we have:

$$d\Delta\Omega(s) = \frac{\partial\Delta\Omega(s)}{\partial\Delta P_L(s)} d\Delta P_L(s) + \left[\frac{\Delta\Omega(s)}{\Delta P_L(s)} \right]^2 \Delta P_L(s) dD \quad (4.11)$$

Furthermore, taking partial derivative for $\Delta P_L(s)$ of equation either (4.2), or (4.6),

we have

$$\frac{\partial \Delta \Omega(s)}{\partial \Delta P_L(s)} = \frac{\Delta \Omega(s)}{\Delta P_L(s)} \quad (4.12)$$

Combining (4.12) with (4.11), we have

$$d\Delta \Omega(s) = \frac{\Delta \Omega(s)}{\Delta P_L(s)} d\Delta P_L(s) + \left[\frac{\Delta \Omega(s)}{\Delta P_L(s)} \right]^2 \Delta P_L(s) dD \quad (4.13)$$

In order to have its time domain description, Laplace inverse transformation is applied to (4.13). Thus, we have:

$$\begin{aligned} d\Delta \omega(t) &= L^{-1} [d\Delta \Omega(s)] \\ &= L^{-1} \left[\frac{\Delta \Omega(s)}{\Delta P_L(s)} d\Delta P_L(s) \right] + L^{-1} \left\{ \left[\frac{\Delta \Omega(s)}{\Delta P_L(s)} \right]^2 \Delta P_L(s) dD \right\} \end{aligned} \quad (4.14)$$

Integration of (4.14) gives:

$$\begin{aligned} \Delta \omega(t) &= \int L^{-1} [d\Delta \Omega(s)] \\ &= \int L^{-1} \left[\frac{\Delta \Omega(s)}{\Delta P_L(s)} d\Delta P_L(s) \right] + \int L^{-1} \left\{ \left[\frac{\Delta \Omega(s)}{\Delta P_L(s)} \right]^2 \Delta P_L(s) dD \right\} \end{aligned} \quad (4.15)$$

Another interesting point should be mentioned from (4.15) is about the effect of the load-damping coefficient D on the stability analysis in this SFR model in the next subsection.

4.3.2 Stability Analysis

a. When the Power System is Essentially Stable

If a power system is stable after disturbance, then its Laplace characteristic function's poles are all located on the left half plane in s -domain. That means the finite time-domain input $\Delta P_L(t)$ would not produce infinite time-domain output $\Delta \omega(t)$. It

suffices to say that the norm of the transfer function is bounded, i.e. $\left\| \frac{\Delta\Omega(s)}{\Delta P_L(s)} \right\| < \infty$ for $\forall t \in (0, \infty)$, from the perspective of control theory. Furthermore, from the perspective of power system design, $\Delta\omega(t)$ should be in a small finite range since the system is essentially stable. The bound of the frequency deviation is analyzed next.

From (4.15), if we consider ΔP_L a step function, by triangle inequality we have:

$$\begin{aligned}
\|\Delta\omega(t)\| &\leq \left\| \int L^{-1} \left[\frac{\Delta\Omega(s)}{\Delta P_L(s)} d\Delta P_L(s) \right] \right\| + \left\| \int L^{-1} \left\{ \left[\frac{\Delta\Omega(s)}{\Delta P_L(s)} \right]^2 \Delta P_L(s) dD \right\} \right\| \\
&\leq \left\| \int L^{-1} \left[\left\| \frac{\Delta\Omega(s)}{\Delta P_L(s)} \right\| d\Delta P_L(s) \right] \right\| + \left\| \int L^{-1} \left\{ \left\| \frac{\Delta\Omega(s)}{\Delta P_L(s)} \right\|^2 \Delta P_L(s) dD \right\} \right\| \\
&= \left\| \int L^{-1} [\varepsilon d\Delta P_L(s)] \right\| + \left\| \int L^{-1} \{ \varepsilon^2 \Delta P_L(s) dD \} \right\| \\
&= \left\| \int \varepsilon L^{-1} \left[\frac{d\Delta P_L}{s} \right] \right\| + \left\| \int \varepsilon^2 dD L^{-1} \left\{ \frac{\Delta P_L}{s} \right\} \right\| \\
&= \left\| \int \varepsilon \cdot 1(t-t_0) d\Delta P_L \right\| + \left\| \int \varepsilon^2 \cdot 1(t-t_0) \Delta P_L dD \right\| \\
&\leq \varepsilon \|\Delta P_L\| + \varepsilon^2 \|\Delta P_L\| \|D\|
\end{aligned} \tag{4.16}$$

where $\varepsilon = \left\| \frac{\Delta\Omega(s)}{\Delta P_L(s)} \right\|$ is a small value less than 1. Note that $1(t-t_0)$ is the unit step function,

t_0 is the start point of disturbance and it equals to 1 when t is t_0 .

Apparently, the bound of $\Delta\omega(t)$ from the traditional model ignoring the impact of D is given by:

$$\|\Delta\omega(t)\| \leq \varepsilon \|\Delta P_L\| \tag{4.17}$$

The difference between the new model and the conventional model is $\varepsilon^2 \|\Delta P_L\| \|D\|$

. This means the frequency deviation under both models are bounded, though by different boundaries.

b. When the Power System is Essentially Unstable

If the power system is unstable, then some of its Laplace characteristic function's poles are located on the right half plane in the s -domain. That means the finite time domain input $\Delta P_L(t)$ produces infinite time domain output $\Delta\omega(t)$. It suffices to the norm

$$\left\| \frac{\Delta\Omega(s)}{\Delta P_L(s)} \right\| \text{ which is larger than a very large value } M, \text{ i.e. } \left\| \frac{\Delta\Omega(s)}{\Delta P_L(s)} \right\| \geq M \text{ for } \forall t \in (0, \infty).$$

Then, a new relationship can be derived as follows:

$$\begin{aligned} \|\Delta\omega(t)\| &= \left\| \int L^{-1} \left[\frac{\Delta\Omega(s)}{\Delta P_L(s)} d\Delta P_L(s) \right] + \int L^{-1} \left\{ \left[\frac{\Delta\Omega(s)}{\Delta P_L(s)} \right]^2 \Delta P_L(s) dD \right\} \right\| \\ &= \left\| \int L^{-1} \left[\left\| \frac{\Delta\Omega(s)}{\Delta P_L(s)} \right\| \angle\theta \cdot d\Delta P_L(s) \right] + \int L^{-1} \left\{ \left\| \frac{\Delta\Omega(s)}{\Delta P_L(s)} \right\|^2 \angle 2\theta \cdot \Delta P_L(s) dD \right\} \right\| \\ &\geq \left\| \int L^{-1} \left[M e^{j\theta} d\Delta P_L(s) \right] + \int L^{-1} \left\{ M^2 e^{j2\theta} \Delta P_L(s) dD \right\} \right\| \\ &= \left\| \int M e^{j\theta} L^{-1} \left[\frac{d\Delta P_L}{s} \right] + \int M^2 e^{j2\theta} dD L^{-1} \left\{ \frac{\Delta P_L}{s} \right\} \right\| \tag{4.18} \\ &= \left\| \int M e^{j\theta} \cdot 1(t-t_0) d\Delta P_L + \int M^2 e^{j2\theta} \cdot 1(t-t_0) \Delta P_L dD \right\| \\ &= \left\| M e^{j\theta} \cdot 1(t-t_0) \Delta P_L + M^2 e^{j2\theta} \cdot 1(t-t_0) \Delta P_L D \right\| \\ &= \left\| M e^{j\theta} (1 + M D e^{j\theta}) \Delta P_L \right\| \end{aligned}$$

where θ is the phase angle of $\frac{\Delta\Omega(s)}{\Delta P_L(s)}$.

Equation (4.18) indicates that even if ΔP_L and D are very small values (much less than 1) in per unit, $\left\| M^2 e^{j2\theta} \cdot 1(t-t_0) \Delta P_L D \right\| = \left\| M^2 \Delta P_L D \right\|$ may still be a very large number compared with $\left\| M e^{j\theta} \cdot 1(t-t_0) \Delta P_L \right\| = \left\| M \Delta P_L \right\|$, which is the lower bound based on the conventional model. Therefore, the effect of dD to $d\Delta\omega(t)$ cannot be neglected in this

case. This means it can accelerate the system frequency deviation and make instability situation worse than using the conventional equation (4.9).

4.4 Largest Dip of Frequency Change $\Delta f_{\max}(t)$

As shown in the previous analysis in Section 4.3, the frequency deviation in a stable case is bounded with the upper bound given by equation (4.16). Therefore, it is interesting to solve the largest angular frequency dip $\Delta\omega_{\max}(t)$ [i.e., $\Delta f_{\max}(t)$] or its Laplace transform $\Delta\Omega(s)$ [70]. This is because the largest frequency dip is one of the key specifications that power system operators want to know and compare against power systems stability criterion. It can be obtained by Laplace inverse transformation next.

At the largest angular frequency dip $\Delta\omega_{\max}(t)$, the partial derivative of $\Delta\omega(t)$ must be zero, i.e.,

$$\frac{\partial\Delta\omega(t)}{\partial t} = L^{-1}(s\Delta\Omega(s) - \Delta\omega(0)) = 0 \quad (4.19)$$

Here, $\Delta\omega(0)=0$ because at the very beginning there is no angular frequency deviation.

$$\text{Thus, } \frac{\partial\Delta\omega(t)}{\partial t} = L^{-1}(s\Delta\Omega(s)) = 0 \quad (4.20)$$

Hence, we have equations for the following two cases:

For SISO system case:

$$\begin{aligned} \frac{\partial\Delta\omega(t)}{\partial t} &= L^{-1}(s\Delta\Omega(s)) \\ &= L^{-1} \left[\frac{-s\Delta P_L(s)}{2Hs + D + \frac{1 + F_{HP}T_{RH}s}{(1 + T_Gs)(1 + T_{CH}s)(1 + T_{RH}s)R}} \right] = 0 \end{aligned} \quad (4.21)$$

For multi-machines system case:

$$\begin{aligned} \frac{\partial \Delta \omega(t)}{\partial t} &= L^{-1}(s \Delta \Omega(s)) \\ &= L^{-1} \left[\frac{-s \Delta P_L(s)}{(2Hs + D) + \sum_{i=1}^N \frac{1 + F_{HP_i} T_{RH_i} s}{(1 + T_{G_i} s)(1 + T_{CH_i} s)(1 + T_{RH_i} s) R_i}} \right] = 0 \end{aligned} \quad (4.22)$$

Solving (4.21)-(4.22) can give the time t in both cases, when $\frac{\partial \Delta \omega(t)}{\partial t} = 0$. If $\Delta \omega(t)$

is an oscillation response, i.e. there are several points such that $\frac{\partial \Delta \omega(t)}{\partial t} = 0$, then choose

the smallest t as t_{\max} since the first swing in a stable case gives the largest frequency dip.

Thus, the critical time t_{\max} and corresponding largest dip $\Delta \omega_{\max}(t)$ can be derived

respectively. Then, multiplication of $\Delta \omega(t)$, $\Delta \omega_{\max}(t)$ and $\frac{\partial \Delta \omega(t)}{\partial t}$ with $\frac{60}{2\pi}$ can derive

the largest dip of frequency change $\Delta f(t)$, $\Delta f_{\max}(t)$ and $\frac{\partial \Delta f(t)}{\partial t}$ in Hertz, respectively.

4.5 Proof of the Alignment of the Maximum Sensitivity and the Largest Frequency Dip

In a stable case, when $\frac{\partial \Delta \omega(t)}{\partial D}$ or $\frac{\partial \Delta f(t)}{\partial D}$ reaches its maximum, the necessary

condition is that its derivative with time t should be equal to zero, i.e. $\partial \left(\frac{\partial \Delta \omega(t)}{\partial D} \right) / \partial t = 0$.

Then, applying Laplace transformation to $\partial \left(\frac{\partial \Delta \omega(t)}{\partial D} \right) / \partial t$ with zero initial condition, i.e.

$\frac{\partial \omega(0)}{\partial D} = 0$ and considering equation (4.3), or (4.7) which has the same formulation, we

have:

$$s \frac{\partial \Delta \Omega(s)}{\partial D} - \frac{\partial \omega(0)}{\partial D} = s \frac{[\Delta \Omega(s)]^2}{\Delta P_L(s)} = s \frac{[\Delta \Omega(s)]^2}{\frac{\Delta P_L}{s}} = \frac{[s \Delta \Omega(s)]^2}{\Delta P_L} = 0 \quad (4.23)$$

For a general time t function $g(t)$, its Laplace transform is given by:

$$L \left[\frac{d^2 g(t)}{dt^2} \right] = s^2 G(s) - s g(0) - g'(0). \text{ Thus, we have}$$

$$s^2 G(s) = L \left[\frac{d^2 g(t)}{dt^2} \right] + s g(0) + g'(0) \quad (4.24)$$

where $G(s)$ and $g(t)$ are defined as $G(s) = [\Delta \Omega(s)]^2$ and $g(t) = L^{-1} [(\Delta \Omega(s))^2] =$

$\int_0^t \Delta \omega(t-\tau) \Delta \omega(\tau) d\tau$ in this chapter. In addition, we have $g(0)=0$ and $g'(0)=[\Delta \omega(0)]^2$,

which can be derived by the definition of $g(t)$.

Therefore, taking inverse Laplace transform on both sides of (4.24), we have:

$$L^{-1} [s^2 G(s)] = \frac{d^2 g(t)}{dt^2} + L^{-1} [s g(0)] + L^{-1} [g'(0)] \quad (4.25)$$

To solve (4.23) to obtain the critical time t_{max} , the inverse Laplace transformation is applied to (4.23). Also, (4.25) is used as well. Here we consider the general initial condition $\Delta \omega(0)=0$, which means no frequency deviation initially. Thus, we have

$$\begin{aligned}
\frac{\partial \left(\frac{\partial \Delta \omega(t)}{\partial D} \right)}{\partial t} &= \frac{L^{-1} [s \Delta \Omega(s)]^2}{\Delta P_L} = \frac{L^{-1} [s^2 (\Delta \Omega(s))^2]}{\Delta P_L} \\
&= \frac{\frac{d^2}{dt^2} \left(L^{-1} [\Delta \Omega(s)]^2 \right) + L^{-1} [s g(0)] + L^{-1} [g'(0)]}{\Delta P_L} \quad (4.26) \\
&= \frac{\frac{d^2}{dt^2} \int_0^t \Delta \omega(t-\tau) \Delta \omega(\tau) d\tau}{\Delta P_L} + \frac{g(0) L^{-1} [s]}{\Delta P_L} + \frac{L^{-1} [g'(0)]}{\Delta P_L} \\
&= \frac{\Delta \omega(0)}{\Delta P_L} \cdot \frac{d \Delta \omega(t)}{dt} + \frac{[\Delta \omega(0)]^2}{\Delta P_L} \cdot \uparrow(t) = 0
\end{aligned}$$

where $\uparrow(t)$ is the impulse function with magnitude of 1. Thus, from (4.26) we have

$$\frac{\partial \Delta \omega(t)}{\partial t} = -\Delta \omega(0) \cdot \uparrow(t) . \text{ Since } \Delta \omega(0)=0 \text{ (i.e., no frequency deviation initially),}$$

therefore equation (4.26) indicates that solving $\partial \left(\frac{\partial \Delta \omega(t)}{\partial D} \right) / \partial t = 0$ is equivalent to

$$\text{solving } \frac{\partial \Delta \omega(t)}{\partial t} = 0 .$$

An alternative proof is given in Appendix A.

Hence, we can conclude that the maximum of $\frac{\partial \Delta \omega(t)}{\partial D}$ is aligned with the maximum of $\Delta \omega(t)$ (i.e., the largest frequency dip). Therefore, the error of evaluating D gives the largest impact on frequency deviation right at the time when the largest frequency deviation occurs. This further shows the importance of obtaining accurate the load-damping coefficient, D . This important feature can be easily observed in the simulation results.

4.6 Numerical Simulations

As listed below, four case studies have been performed.

- Single machine system – Stable & Unstable Cases
- Multi-machines system – Stable & Unstable Cases

4.6.1 Single Machine (SISO) System

In this case the simulation time period is 20 seconds. Consider a typical aggregated power system containing a load and a single generator with a reheat turbine. Assume the system parameters are $T_{RH}=7$ sec, $T_G=0.2$ sec, $T_{CH}=0.3$ sec, $F_{HP}=0.3$, $H=5$ sec, $D=1$, $R=0.05$. Here a load increase is considered as the external disturbance. Consider a step load change, $\Delta P_L=0.1$ p.u. [20], which can be attributed to a demand response signal. In addition, let the ΔD be a set of values with 20% increments: 20%, 40%, 60%, 80% and 100%. The scenario of 100% increase of D can be roughly viewed as the extreme case that all loads are actually frequency sensitive while it is thought only half of the loads are sensitive. From all the given parameters, it can be calculated that this power system is stable. The Simulink diagram of a single machine case study is illustrated in Figure 4.5.

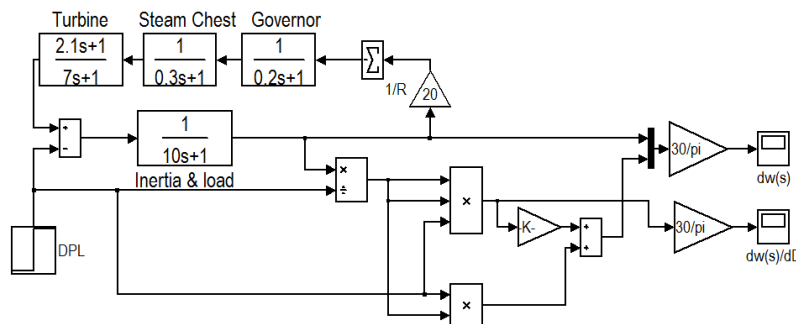


Figure 4.5 Simulink diagram of a SISO system

A1: Single Machine System – Stable Case

Figure 4.6 shows the six curves: the “external disturbance” curve is obtained using (4.9) by ignoring the impact of dD , while the five “total disturbance” curves are obtained with (4.10) and (4.3) to address the impact from various dD values. If the six curves in Figure 4.6 are compared, they are very similar and close.

Figure 4.6 is derived from (4.21). The textboxes in Figures 4.6 and 4.7 show the critical time $t_{\max}=2.25 \text{ sec}$ at the largest frequency dip, when $\Delta f_{\max}(t)=0.112\text{Hz}$ as shown in Figure 4.6 or when $\partial\Delta f(t)/\partial t=0$ as shown in Figure 4.7.

The sensitivity curve of frequency deviation, Δf , w.r.t. load-damping coefficient, D , is shown in Figure 4.8. As shown in the figure, the sensitivity function curve is relatively small, as opposed to the case in unstable case shown later in this chapter.

An important observation in Figure 4.8 is that $\partial\Delta f(t)/\partial D$ reaches its maximum also at the critical time $t_{\max}=2.25 \text{ sec}$ when the maximum frequency dip occurs. This verifies the conclusion in the last paragraph in Section 4.5 that the error of D gives the largest impact on frequency deviation right at the time when the largest frequency deviation occurs. This further demonstrates the importance of obtaining the accurate D value.

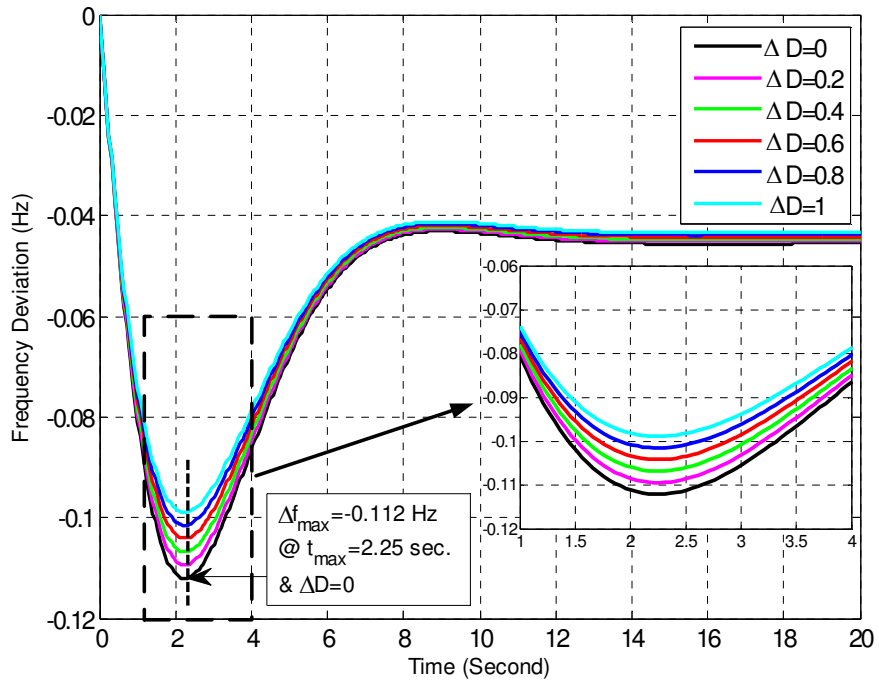


Figure 4.6 $\Delta f(t)$ curves of a SISO system

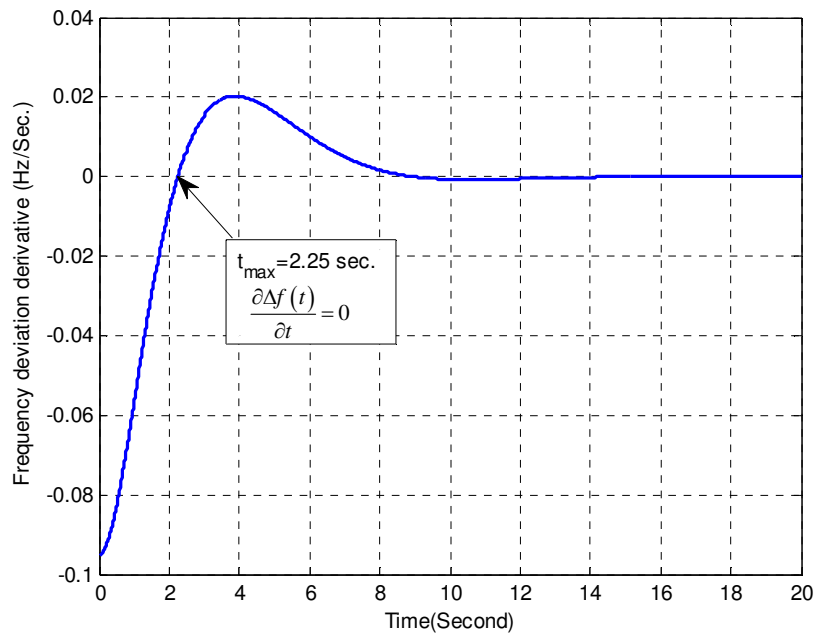


Figure 4.7 $\frac{\partial \Delta f(t)}{\partial t}$ curve with critical time of a SISO system

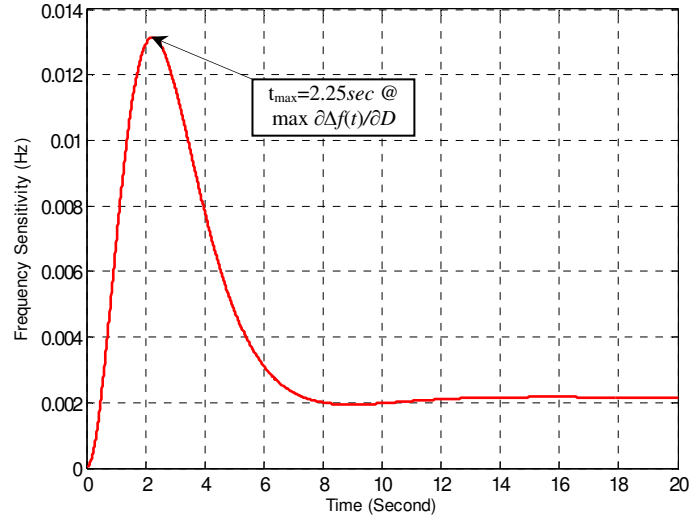


Figure 4.8 $\partial\Delta f(t)/\partial D$ curve of a SISO system indicating that the max $\partial\Delta f(t)/\partial D$ occurs when the largest $\Delta f(t)$ occurs

A2: Single Machine System – Unstable Case

In this case, we assume some disturbance happens to make the generation governor unstable at the time $t=0$ second. In this simulation, the parameter in the governor control in Figure 4.5 is changed from $0.2s+1$ to $-0.2s+1$, for demonstration purpose, to produce a pole in the right half of the s plane as in Figure 4.9. Here the simulation time period is 1.4 sec, because the system frequency is already close to the instability threshold (57Hz, [19-20]) at 1.4 sec. After that, the system frequency will sharply deviate from 60 Hz.

The comparison result is shown in Figure 4.10 with different dD values. The sensitivity of the frequency deviation Δf to the load-damping coefficient D is shown in Figure 4.11. These two figures indicate that the power system is unstable and has a trend to be even worse than anticipated using the conventional model in (4.9), and the load-damping coefficient D can exert larger effect on SFR. So, it may accelerate the system

frequency collapse in this case. Therefore, the effect of load-damping coefficient D can be significant.

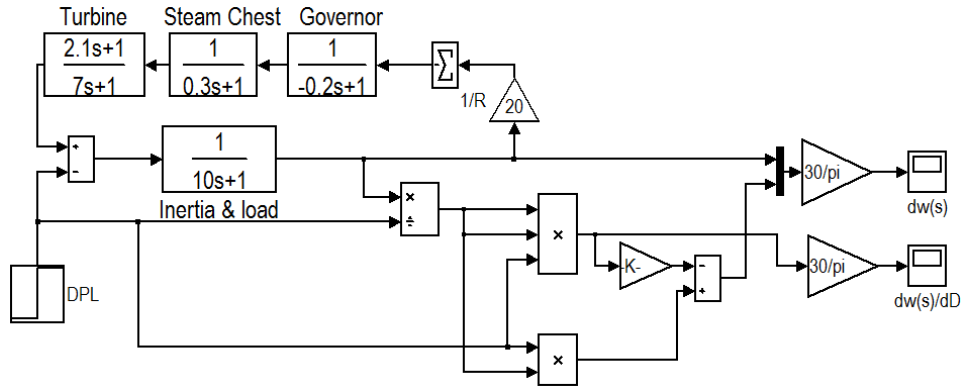


Figure 4.9 Simulink diagram with a right half s -plane pole of a SISO system

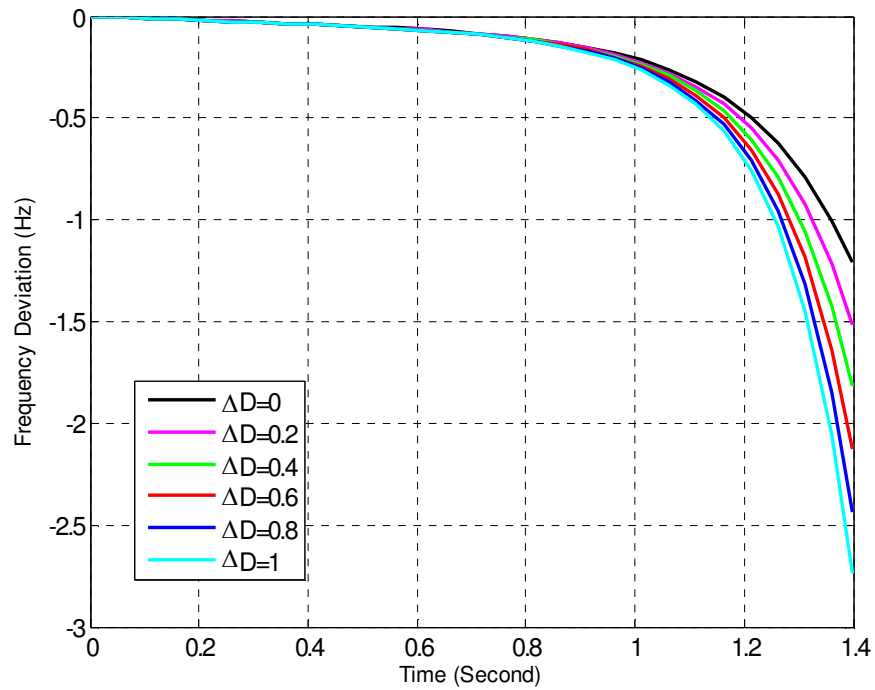


Figure 4.10 $\Delta f(t)$ curves of a SISO system in Case A2

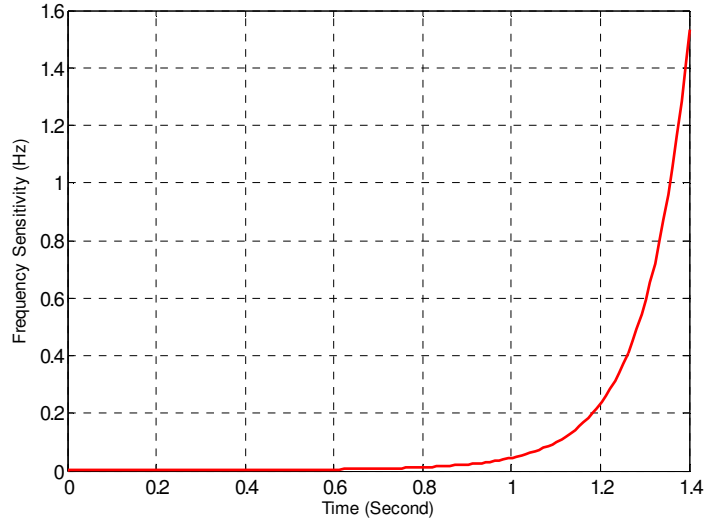


Figure 4.11 $\partial\Delta f(t)/\partial D$ curve of a SISO system in Case A2

4.6.2 Multi-machines System

In this and the next subsections, a two-machine system is considered. Let $T_{RH1}=7$ sec, $T_{G1}=0.2$ sec, $T_{CH1}=0.3$ sec, $F_{HP1}=0.3$, $R_1=0.1$, $T_{RH2}=11$ sec, $T_{G2}=0.35$ sec, $T_{CH2}=0.25$ sec, $F_{HP2}=0.2$, $R_2=0.1$, $H=5$ sec, and $D=1$. Further, consider a 10% load increase on the first system input, i.e., $\Delta P_{L1}=0.1$ p.u. [20]. Also consider the actual D is 20%, 40%, 60%, 80%, and 100%, respectively, higher than the expected value. The Simulink diagram is shown in Figure 4.12.

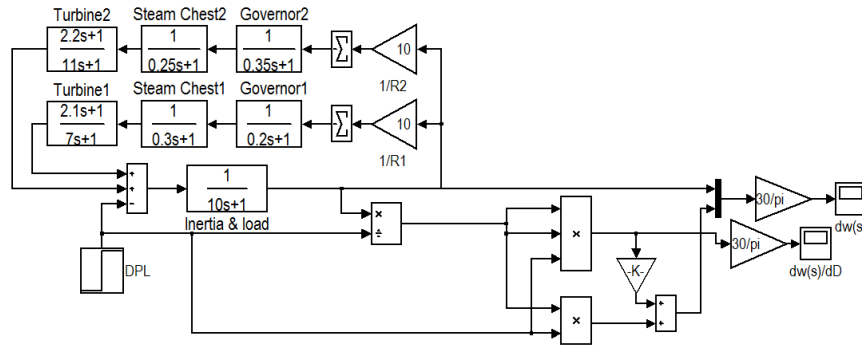


Figure 4.12 Simulink diagram of multi-machines system

B1: Multi-machines System – Stable Case

In this case the simulation time period is 20 sec. The six curves obtained from (4.9) and (4.10) based on various dD values are shown in Figure 4.13. The results of $\partial\Delta f(t)/\partial t$ and $\partial\Delta f(t)/\partial D$ are shown in Figures 4.14 and 4.15, respectively. The critical time, $t_{\max}=2.53$ sec, and the largest frequency dip, $\Delta\omega_{\max}(t)=0.1258$ Hz, are given in the textboxes of Figures 4.13 and 4.14. Observations and conclusion are very similar to the ones in Case A1. For example, the impact of the load-damping coefficient on SFR is relatively small and bounded if compared with unstable cases; $\partial\Delta f(t)/\partial D$ reaches its maximum right at the critical time $t_{\max}=2.53$ sec; and the error of D gives the largest impact on frequency deviation right at the time when the largest frequency deviation occurs.

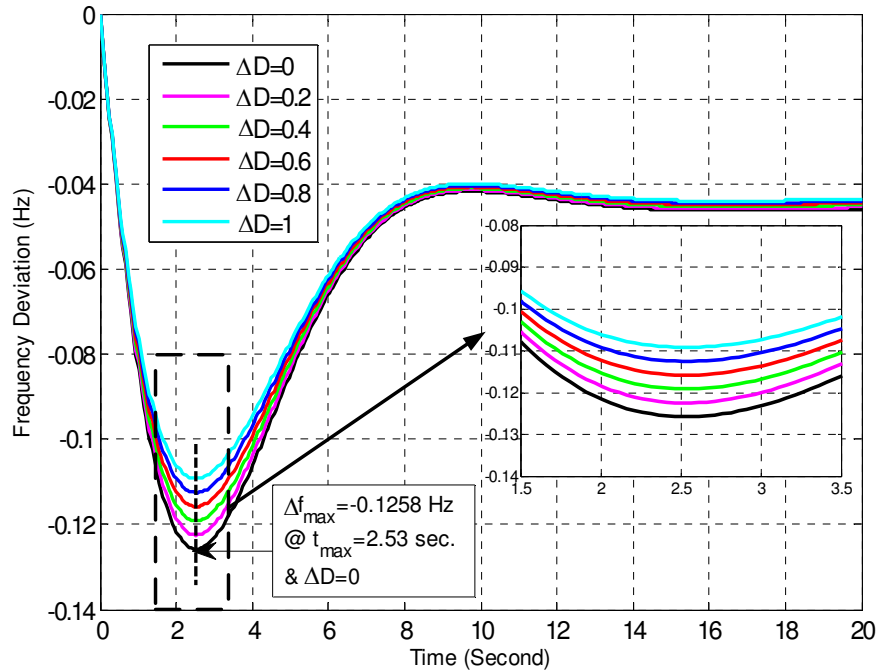


Figure 4.13 $\Delta f(t)$ curves of multi-machines system

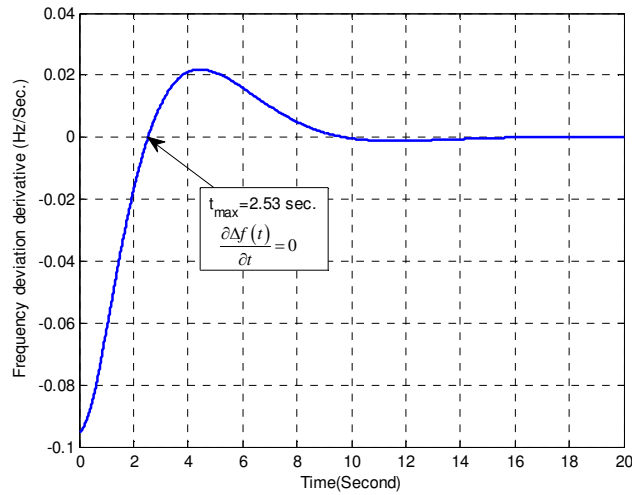


Figure 4.14 $\frac{\partial \Delta f(t)}{\partial t}$ curve with critical time of multi-machines system

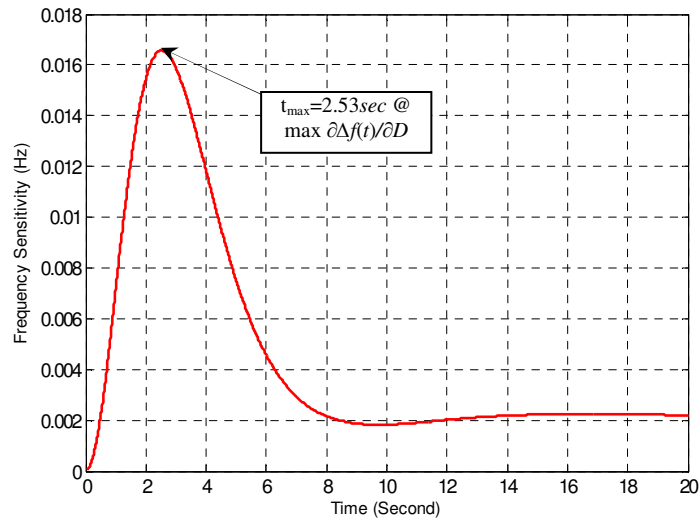


Figure 4.15 $\frac{\partial \Delta f(t)}{\partial D}$ curve of multi-machines system indicating the max $\frac{\partial \Delta f(t)}{\partial D}$ occurs when the largest $\Delta f(t)$ occurs

B2: Multi-machines System – Unstable Case

Similar to Case A2, here we assume a fault on Governor 2 at $t=0$ causes the parameter to change from $0.35s+1$ to $-0.35s+1$ as in Figure 4.12 for demonstration purpose. This leads to a pole in the right half of the s plane as in Figure 4.16. The

simulation results are shown up to 2.4 *sec*. After that, the system frequency will sharply deviate from 60 Hz. The comparison result is shown in Figure 4.17. The sensitivity $\partial\Delta f(t)/\partial D$ curve is shown in Figure 4.18.

Similar to Case A2, Figure 4.17 shows that the frequency response using (4.10) is worse than the conventional model using (4.9). Thus, the consideration of D may lead to acceleration of frequency instability and less response time for corrective actions.

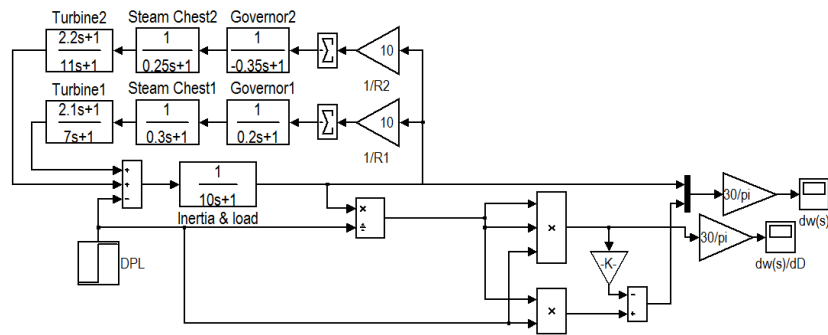


Figure 4.16 Simulink diagram with a right half s -plane pole of multi-machines system

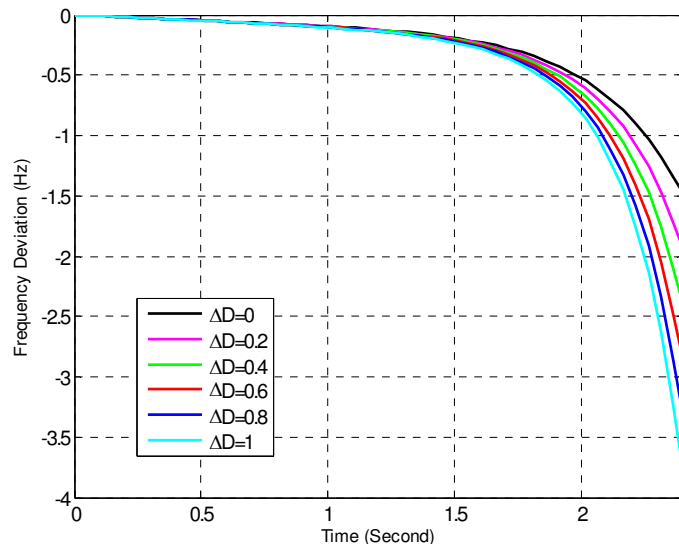


Figure 4.17 $\Delta f(t)$ curves of multi-machines system in Case B2

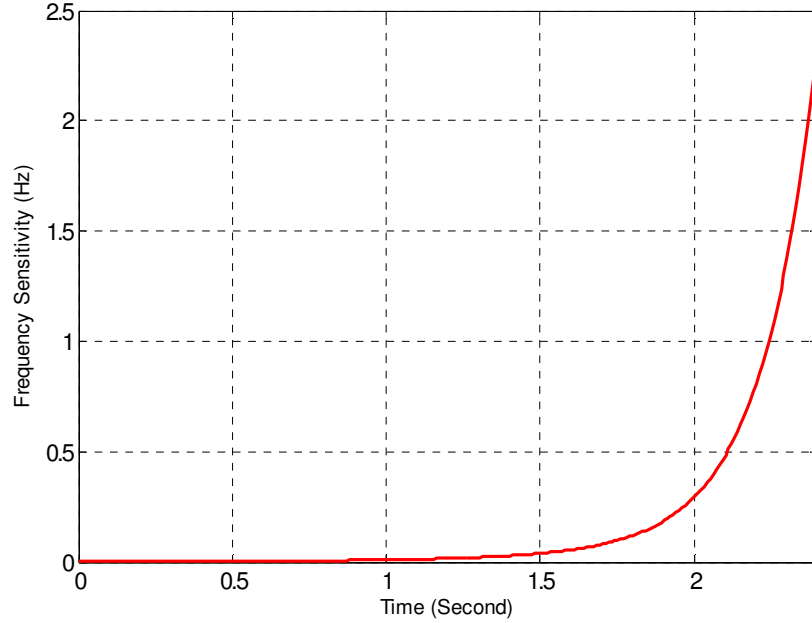


Figure 4.18 $\partial\Delta f(t)/\partial D$ curve of multi-machines system in Case B2

4.7 Conclusions

The increasing penetration of controllable load calls the interests to re-examine the load-frequency response. This chapter investigates the impact of the load-damping coefficient, because many load control programs target frequency-sensitive motor loads which may have a significantly different load-damping coefficient D , from the rest of the loads.

This chapter investigates the effect of frequency-sensitive load on the power system frequency regulation based on the typical SFR model. Theoretic analysis as well as simulation studies show that the impact of an inaccurate load-damping coefficient is relatively small and bounded when the power system is essentially stable; while the system frequency deviation may be accelerated when the power system is indeed unstable after disturbance.

This chapter also derives analytical calculation of the largest frequency deviation and the corresponding critical time by inverse Laplace transformation. This can be a useful indicator for power system operators for decision-making of load control or interruption.

Further, this chapter proves that the error of D gives the largest impact on frequency deviation right at the time when the largest frequency deviation occurs. Simulation studies verify this conclusion, which also demonstrates the importance of obtaining the accurate D value.

The future research work may be about a strategic design of a robust load shedding scheme considering the variation of the load-damping coefficient. Also, sensitivity study of other parameters and other generator models such as hydraulic turbines, perhaps in a large-scale system, can be investigated.

CHAPTER V

MODELING DYNAMIC DEMAND RESPONSE USING MONTE CARLO SIMULATION AND INTERVAL MATHEMATICS FOR BOUNDARY ESTIMATION

5.1 Background of Flat Load Level

For personnel in the system planning and operation departments in a power utility company, a flat load profile is always their desire because flat load curve could be easily dispatched and less reserve is needed to balance the possible gaps between generation and load. Besides, during the peak hours, if the peak load could be reduced to a lower flat level, then it could not only avoid the price spikes but also reduce power losses. This is because fewer loads means less power flow across transmission lines, thus results in lower temperature of lines and corresponding lower line resistance which could further decrease power losses on lines. Besides, flat load level, also meaning its derivative LMP invariant in system, could suppress price volatility in power market as well if the whole system topology is unchanged. To realize flat load level, there are two approaches in practice: DLC and demand response. The former one is under ISO or utility companies' regulation, while the latter one is based on control of load itself. In this chapter, a closed loop feedback control of demand response scheme is proposed and modeled. Based on this adjustment process, it could shave the peak load to a desirable load level in finite steps, therefore it could be adopted for both online or offline application.

5.2 LSE's Load Response Formulation

For better description, some assumptions are made and are listed as follows:

- Each generation company (GENCO) has only one generator candidate unit and

bids a constant price for a single block for simplicity, while in practice a monotonically increasing multi-block bid model is commonly used. Each load service entity (LSE) has only one load candidate unit and its bids could be adjusted in real time.

- Power losses on transmission lines are neglected with a linearized DC power flow model.
- Unit commitment is already settled down and is fixed since this chapter deals with intra-hour dispatches. For instance, this chapter considers 12 trading periods of 5-minute real time market within an hour. Unit commitment within an hour usually does not change.
- Demand response is considered at bus level rather than feeder level. That is to say, the main focus is on the aggregated response of multiple end-users at the LSE level to study their behavior in the system dispatch model.

5.2.1 Conventional Economic Dispatch

Suppose we have a lossless DC-based linear programming model. In general, the core of a well-known economic dispatch problem is to solve a generation production cost optimization. If the power loss on transmission lines is omitted, then economic dispatch Scheme I could be written as follows:

$$\min \sum_{i=1}^N c_i \cdot G_i \quad (5.1)$$

$$s.t. \sum_{i=1}^N G_i = \sum_{i=1}^N D_i \quad (5.2)$$

$$G_i^{\min} \leq G_i \leq G_i^{\max} \quad (5.3)$$

for $i = 1, 2, \dots, N$

$$\sum_{i=1}^N GSF_{k-i} \cdot (G_i - D_i) \leq Limit_k \quad (5.4)$$

for $k = 1, 2, \dots, M$

where c_i is the marginal cost of generation at Bus i , G_i is the generation at Bus i , D_i is the demand at Bus i , G_i^{\min} is the minimum generation at Bus i , G_i^{\max} is the maximum generation at Bus i , GSF_{k-i} is the generation shift factor from Bus i to line k , $Limit_k$ is the thermal limit of transmission line k , N is the number of buses and M is the number of transmission lines.

For Scheme I, the generation production cost is minimized in (5.1). Constraint (5.2) ensures the balance of supply and demand. Constraint (5.3) represents the generation capacity limit. Constraint (5.4) represents the transmission line constraints.

If we consider responsive or elastic load into (5.1) of Scheme I, then the economic dispatch Scheme II is as follows:

$$\min \sum_{i=1}^N (c_i \cdot G_i - d_i \cdot D_i) \quad (5.5)$$

$$s.t. \quad \sum_{i=1}^N G_i = \sum_{i=1}^N D_i \quad (5.6)$$

$$G_i^{\min} \leq G_i \leq G_i^{\max} \quad (5.7)$$

for $i = 1, 2, \dots, N$

$$\sum_{i=1}^N GSF_{k-i} \cdot (G_i - D_i) \leq Limit_k \quad (5.8)$$

for $k = 1, 2, \dots, M$

$$D_i^{\min} \leq D_i \leq D_i^{\max} \quad (5.9)$$

for $i = 1, 2, \dots, N$

where d_i is the load cost at Bus i , D_i^{\min} is the minimum demand at Bus i , D_i^{\max} is the maximum demand at Bus i .

The difference between Schemes I and II is that the load items appear in the objective function (5.5), which means that the load variables could be adjusted in dispatch process. (5.6), (5.7) and (5.8) are the same as (5.2), (5.3) and (5.4) in Scheme I. In addition, the limitation of individual load amount is described in (5.9). If $d_i = -H$, here H is a very large positive number as penalty parameter. It is easy to see this scheme will exclude or avoid load shedding in dispatch process autonomously, then the Scheme II will degrade into Scheme I.

However, regardless of Scheme I or II, the c_i and d_i are fixed time-invariant constants. That means this dispatch is somewhat like “one time use” static dispatch.

5.2.2 Controllable Load Response Feedback Control Model

The elastic economic dispatch model in Scheme III considering flexible and adjustable load cost $d_i(t)$ is represented as follows:

$$\min \sum_{i=1}^N (c_i \cdot G_i(t) - d_i(t) \cdot D_i(t)) \quad (5.10)$$

$$s.t. \quad \sum_{i=1}^N G_i(t) = \sum_{i=1}^N D_i(t) \quad (5.11)$$

$$G_i^{\min} \leq G_i(t) \leq G_i^{\max} \quad (5.12)$$

$$D_i^{\min} \leq D_i(t) \leq D_i^{\max} \quad (5.13)$$

for $i = 1, 2, \dots, N$ and arbitrary t

$$\sum_{i=1}^N GSF_{k-i} \cdot (G_i(t) - D_i(t)) \leq Limit_k \quad (5.14)$$

for $k = 1, 2, \dots, M$ and arbitrary t

where t is the discrete time domain step, $G_i(t)$ is the generation at Bus i at time t , $D_i(t)$ is the demand at Bus i at time t , $d_i(t)$ is the load cost at Bus i at time t . The demand response is treated as negative generation and the production cost objective function is minimized in (5.10). Constraint (5.11) ensures the balance of supply and demand. Constraint (5.12) and (5.13) represent the generation limits and load capacity limits, respectively. Constraint (5.14) represents the transmission line capacity limits.

In the above model, $d_i(t)$ is an instantaneous, flexible, and adjustable parameter which may change at step t in discrete time domain. Note that $d_i(t)$ could be a positive or negative bid signal of LSE if the LSE would like to respond ISO's directions to curtail potential peak load times or encourage consumption in valley hours. However, since the peak reduction is more concerned in real practices due to security consideration, the discussion in this chapter is based on the load reduction case. In (5.10)-(5.14), all variables except c_i are in terms of the discrete step t . The process is time variant and thus dynamic. c_i is the generation marginal cost and considered fixed in this chapter such that we can focus on the demand response study.

Again, the goal of this work is to provide a mathematical model which can describes the dynamic process that an ISO reduces the total load of LSEs to a certain lower level. The reduction of load to a certain level is aligned with the goal of reducing the transmission congestions, LMP spikes, and transmission line power loss,

simultaneously [62].

To construct a feedback of load dispatch, it is natural to utilize the gap between the existing and desired load level. This gap, $GAP(t)$, is a reference signal given by:

$$GAP(t) = \sum_i^N D_i(t) - D_{ST} \quad (5.15)$$

Here, $\sum_i^N D_i(t)$ represents the total load under the LSE while D_{ST} is the target load level of this LSE. For each economic dispatch round, the ISO sends out the economic incentive and load gap signals to LSEs, which adjust their load cost $d_i(t)$ based on this load gap signal and their end-users' condition and return the updated bids to the ISO again. The process continues back and forth until the load gap falls in an acceptable threshold.

In this model, the key is to build a way to make $d_i(t)$ change appropriately such that it can guide the present load level reach the desired level D_{ST} . Here, we propose a possible $d_i(t)$ construction pattern in a 2nd-order polynomial formulation as follows:

$$d_i(t) = \alpha_i \frac{(GAP(t-1))^2}{L^2} + \beta_i \frac{(GAP(t-1))}{L} + d_i(t-1) \quad (5.16)$$

where α_i and β_i are designed positive coefficients. Eq. (5.16) indicates that the present $d_i(t)$ could be adjusted in real-time based on the previous time step information such as $d_i(t-1)$ and $GAP(t-1)$. Also in (5.16), L is used to distribute $d_i(t)$ across the entire system load rather than focusing on just some parts of the system. It should be mentioned that the order of polynomial function of $d_i(t)$ may be higher but more complicated. The 2nd-order polynomial is chosen to make it aligned with the common generation cost model.

The derivative of $d_i(t)$ versus $GAP(t-1)$ in (5.16) is given as follows:

$$\frac{\partial d_i(t)}{\partial (GAP(t-1))} = \frac{2\alpha_i}{L^2}(GAP(t-1)) + \frac{\beta_i}{L} \quad (5.17)$$

It is easy to find that the derivative of $d_i(t)$ in (5.17) is determined by the sign of $GAP(t-1) = \sum_i^N D_i(t-1) - D_{ST}$ since α_i , β_i and L are positive parameters. If $GAP(t-1)$ is positive, then the derivative is also positive, and vice versa. However, if it is the 1st-order linear function relation between $d_i(t)$ and $GAP(t-1)$, then (5.17) is modified as in (5.18).

$$\frac{\partial d_i(t)}{\partial (GAP(t-1))} = \frac{\beta_i}{L} \quad (5.18)$$

If β_i and L are fixed, then this derivative value is fixed. $d_i(t)$ could either increase or decrease in one direction. Sometimes, this may lead to diverging results due to unidirectional movement. This also shows why it is not appropriate to apply a linear model in (5.16).

The whole process is summarized as follows: At the beginning, the mismatch error (i.e., $\sum_i^N D_i(t) - D_0$) may be large and $d_i(t)$ changes greatly. That can make $D_i(t)$ change by a large size at early steps. Each time $d_i(t)$ will be adjusted by the previous step result. Then, based on (5.16), the change in $d_i(t)$ will decrease until convergence is finally attained. If the process converges, $GAP(t) = \sum_i^N D_i(t) - D_{ST}$ will be equal to zero and the number of steps can be determined. It is a typical feedback control and behavior learning process. The flow chart corresponding to this controllable demand response process is illustrated in Figure 5.1. Note that if the algorithm is terminated due to a maximum number of time steps, a satisfactory load level solution may not have been reached.

The process can also be described graphically as in Figure 5.2. The black curve is the demand curve, while the blue one is the supply curve. If the original supply-demand equilibrium point is B_1 with an associated load D_1 then the equilibrium point could be moved to B_2 with corresponding load D_2 on the red demand response curve based on interactions among ISO, LSEs, and end-users. This process is also simultaneously concerned with load cost adjustment. It is worth mentioning that if all conditions are ideal, then this movement could be achieved in just one step. However, in reality, because each individual end-user may respond differently to incentives with uncertain behaviors, this process may need several steps of adjustment, even with oscillation of load change over a short period. The proposed Monte Carlo simulation model and interval mathematic model are two approaches to identify the possibility that the demand response may not reach its target load level.

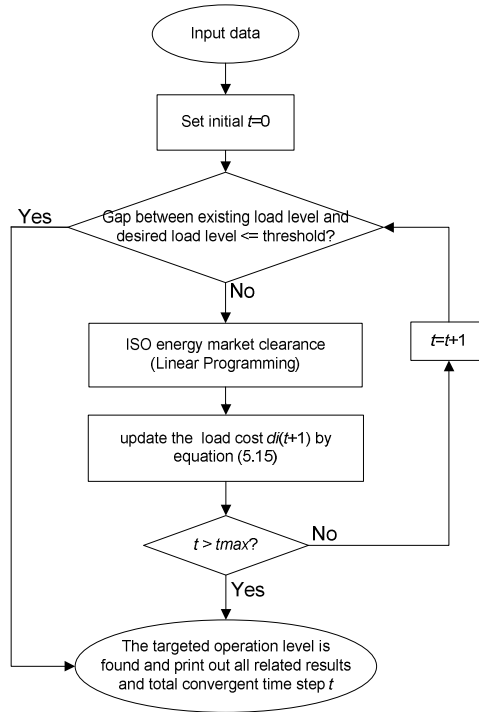


Figure 5.1 Flow chart of controllable demand response process

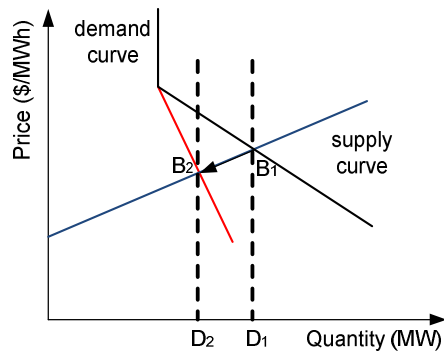


Figure 5.2 Demand elasticity change to adjust load level

5.2.3 Monte Carlo Simulation of LSEs' Response Uncertainty

Though an ISO could rely on the demand response process of Section 5.2.2 to obtain the expected load dispatch in a limited number of steps, LSEs may not be able to respond to the expected level exactly because of various factors such as the uncertainty

regarding individual end-user, unknown weather conditions, and some operation limits. Thus, it is appropriate to consider the LSEs' response variation into this problem. Another question to address is how to model the impact of the demand response uncertainty on the entire system. Assume a stochastic uncertainty of individual load demand response to an ISO's expected dispatch corresponds to a normal distribution in a pre-estimate interval which deviates from the ISO's expected dispatch μ by some percentage. To estimate the boundaries of a power system's key indices due to the load response uncertainty, it is straightforward to employ MC methods in order to describe and calculate this controllable demand response problem [6, 27].

The MCS is implemented as follows:

- 1) Take s scenarios for MCS and set the initial scenario index $S=1$.
- 2) At start time $t=0$, with all initial values, perform elastic economic dispatch based on Equations (5.10)-(5.14) to derive the ISO's expected dispatch level. Record all related data.
- 3) Suppose actual load response of each LSE i to an ISO's expected dispatch level follows a normal distribution, and the uncertainty interval is known beforehand. Randomly pick one value from this interval as $D_i(t)$, the actual response of load i for next step.
- 4) Update the load cost $d_i(t+1)$ based on (5.16).
- 5) $t=t+1$ and go back to 2) until $GAP(t)$ is less than a preset convergence threshold ε or maximum time step t reached.
- 6) $S=S+1$ and return to 2) until stop iteration $S=s$ is met.
- 7) Compare and sort the recorded data to find the minimum and maximum value

of the indices outputs for boundaries determination.

The whole process is shown in Figure 5.3.

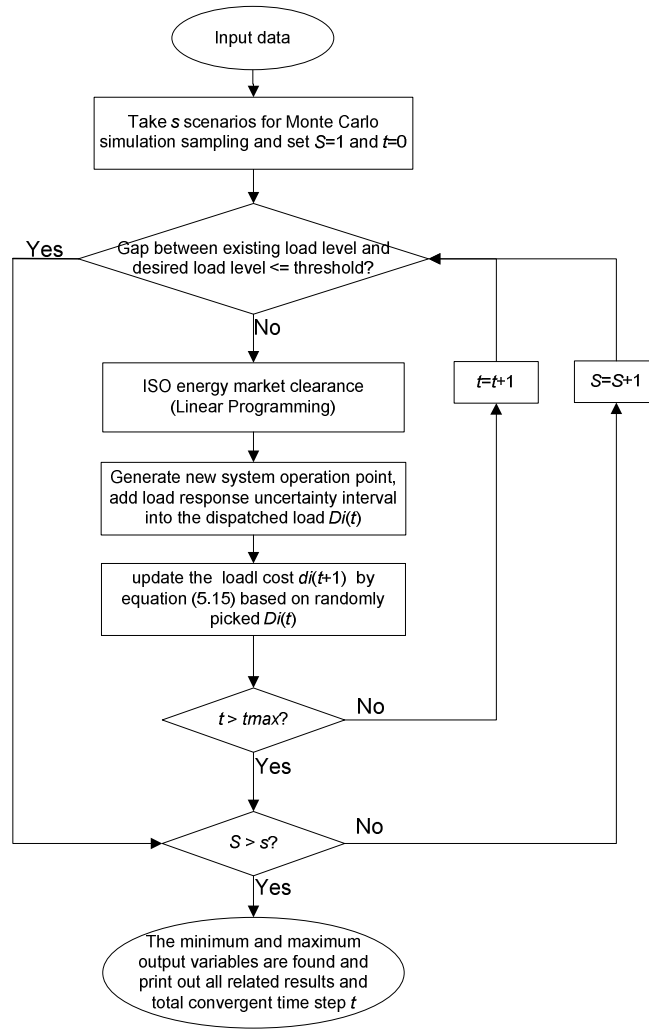


Figure 5.3 Flow chart of output boundary calculation by Monte Carlo simulation

The number of random samplings s could be determined as follows: The MCS can stop based on whether a pre-defined convergence threshold ε_M has been reached or not. This stopping criterion is shown mathematically as follows [64-66]:

$$\frac{\sigma[E(Z)]}{E(Z)} = \frac{\sigma(Z)}{\sqrt{s} \cdot E(Z)} \leq \varepsilon_M \quad (5.19)$$

where Z is the random variable representing the load cost, s is the MC sampling scenarios of the controllable load response, $E(Z)$ is the mean value of Z , and $\sigma(Z)$ is the standard deviation of Z .

Certainly, if a large amount of s is taken, it can meet a small threshold ε_M . However, this may not be efficient. To achieve good results without an unnecessary large amount of s samples, the following strategy can be used. First, we can start with an initial small value of s . Then, we can compute $E(Z)$ and $\sigma(Z)$ after s samples are finished. Using the computed $E(Z)$ and $\sigma(Z)$, we can update the s value with (5.19). Thus, it is not necessary to start with a large amount of s value, while still achieving satisfactory results.

5.2.4 Boundary Calculation with LSEs' Response Uncertainty

In Section 5.2.3, the Monte Carlo simulation is easy to implement, but may suffer from a long consumption time and extensive use of computational sources. To overcome these drawbacks, various technologies were proposed [71-75]. Naturally, interval mathematics is a good alternative for determining the output boundary of given input intervals, because it can obtain reasonable results with a relatively acceptable computational time. It has already been successfully applied in the boundary estimation of various indices in power flow calculation with parameter uncertainty. It is based on directly and explicitly derived Jacobian matrices [71-75], although very few examples are used in the area of optimal power flow for assessment of uncertainty impacts. In this

chapter, the boundary approach of interval mathematics, based on fundamental linear relation shown as follows [71], is employed.

For a general nonlinear vector function description $Y=F(X)$, consider its first order linear approximation at the initial point (X_0, Y_0) : $Y=Y_0+K(X-X_0)$, then for the i th element of output Y , Y_i , it is given by:

$$Y_i = Y_{0i} + \sum_{j=1}^m K_{ij} \times (X_j - X_{0j}) \quad (5.20)$$

where Y_{0i} and X_{0j} are initial estimated values of Y_i and X_j , m is the number of input element X_j , K is the Jacobian sensitivity coefficient matrix evaluated based on initial point (X_0, Y_0) , and K_{ij} represent the (i, j) element of K .

Suppose the range of X_j is represented in $[X_j^{\min}, X_j^{\max}]$ as defined, i.e. $X_j \in [X_j^{\min}, X_j^{\max}]$, then the range of Y_i could be determined briefly by iterative calculation as follows:

At each iteration, solve the minimum value Y_j^{\min}

- 1) If the sign of K_{ij} is positive, then $X_j = X_j^{\min}$
- 2) If the sign of K_{ij} is negative, then $X_j = X_j^{\max}$

Else, solve the maximum value Y_j^{\max}

- 1) If the sign of K_{ij} is positive, then $X_j = X_j^{\max}$
- 2) If the sign of K_{ij} is negative, then $X_j = X_j^{\min}$

When Y_j^{\min} and Y_j^{\max} derived, then the boundary of output Y_j is solved. Continue with this iteration process until ΔY is less than a predefined convergent threshold.

The Jacobian matrix can be used to determine search direction and update the minimum or maximum output value for each iteration. In addition, if the signs of the elements in the Jacobian matrix change, then $X_j = (X_j^{\min} + X_j^{\max})/2$ to overcome an unstable oscillation of the solution.

In this chapter, X represents $D_i(t)$, and Y represents the $d_i(t)$. Thus, $GAP(t)$ is an intermediate variable connecting $d_i(t)$ and $D_i(t)$. In other words, once we have $D_i(t)$, we can obtain $GAP(t)$ based on Equation (5.15). Then, we can obtain $d_i(t)$ since it is modeled using Equation (5.16). Therefore, with a combination of (5.15) and (5.17), the Jacobian matrix of the sensitivity between $d_i(t)$ and $D_i(t)$ is given by:

$$\begin{aligned} \frac{\partial d_i(t)}{\partial D_i(t-1)} &= \frac{\partial d_i(t)}{\partial(GAP(t-1))} \cdot \frac{\partial(GAP(t-1))}{\partial D_i(t-1)} \\ &= \frac{\partial d_i(t)}{\partial(GAP(t-1))} \cdot 1 = \frac{2\alpha_i}{L^2}(GAP(t-1)) + \frac{\beta_i}{L} \end{aligned} \quad (5.21)$$

Based on the Jacobian matrix between $\mathbf{d}(t)$ and the bus load $\mathbf{D}(t-1)$, we have

$$\begin{bmatrix} d_1(t) \\ \vdots \\ d_i(t) \\ \vdots \\ d_j(t) \\ \vdots \\ d_N(t) \end{bmatrix} = \begin{bmatrix} \frac{\partial d_1(t)}{\partial D_1(t-1)} & \cdots & \frac{\partial d_1(t)}{\partial D_i(t-1)} & \cdots & \frac{\partial d_1(t)}{\partial D_j(t-1)} & \cdots & \frac{\partial d_1(t)}{\partial D_N(t-1)} \\ \vdots & \ddots & \vdots & \ddots & \vdots & \ddots & \vdots \\ \frac{\partial d_i(t)}{\partial D_1(t-1)} & \cdots & \frac{\partial d_i(t)}{\partial D_i(t-1)} & \cdots & \frac{\partial d_i(t)}{\partial D_j(t-1)} & \cdots & \frac{\partial d_i(t)}{\partial D_N(t-1)} \\ \vdots & \ddots & \vdots & \ddots & \vdots & \ddots & \vdots \\ \frac{\partial d_j(t)}{\partial D_1(t-1)} & \cdots & \frac{\partial d_j(t)}{\partial D_i(t-1)} & \cdots & \frac{\partial d_j(t)}{\partial D_j(t-1)} & \cdots & \frac{\partial d_j(t)}{\partial D_N(t-1)} \\ \vdots & \ddots & \vdots & \ddots & \vdots & \ddots & \vdots \\ \frac{\partial d_N(t)}{\partial D_1(t-1)} & \cdots & \frac{\partial d_N(t)}{\partial D_i(t-1)} & \cdots & \frac{\partial d_N(t)}{\partial D_j(t-1)} & \cdots & \frac{\partial d_N(t)}{\partial D_N(t-1)} \end{bmatrix} \begin{bmatrix} \Delta D_1(t-1) \\ \vdots \\ \Delta D_i(t-1) \\ \vdots \\ \Delta D_j(t-1) \\ \vdots \\ \Delta D_N(t-1) \end{bmatrix} + \begin{bmatrix} d_1(t-1) \\ \vdots \\ d_i(t-1) \\ \vdots \\ d_j(t-1) \\ \vdots \\ d_N(t-1) \end{bmatrix} \quad (5.22)$$

where

$$K = \begin{bmatrix} \frac{\partial d_1(t)}{\partial D_1(t-1)} & \dots & \frac{\partial d_1(t)}{\partial D_i(t-1)} & \dots & \frac{\partial d_1(t)}{\partial D_j(t-1)} & \dots & \frac{\partial d_1(t)}{\partial D_N(t-1)} \\ \vdots & \ddots & \vdots & \ddots & \vdots & \ddots & \vdots \\ \frac{\partial d_i(t)}{\partial D_1(t-1)} & \dots & \frac{\partial d_i(t)}{\partial D_i(t-1)} & \dots & \frac{\partial d_i(t)}{\partial D_j(t-1)} & \dots & \frac{\partial d_i(t)}{\partial D_N(t-1)} \\ \vdots & \ddots & \vdots & \ddots & \vdots & \ddots & \vdots \\ \frac{\partial d_j(t)}{\partial D_1(t-1)} & \dots & \frac{\partial d_j(t)}{\partial D_i(t-1)} & \dots & \frac{\partial d_j(t)}{\partial D_j(t-1)} & \dots & \frac{\partial d_j(t)}{\partial D_N(t-1)} \\ \vdots & \ddots & \vdots & \ddots & \vdots & \ddots & \vdots \\ \frac{\partial d_N(t)}{\partial D_1(t-1)} & \dots & \frac{\partial d_N(t)}{\partial D_i(t-1)} & \dots & \frac{\partial d_N(t)}{\partial D_j(t-1)} & \dots & \frac{\partial d_N(t)}{\partial D_N(t-1)} \end{bmatrix}$$

is the N by N dimension

Jacobian matrix for the vectors $\partial d(t)$ versus $\partial D(t-1)$.

Other important variables such as LMP can be obtained using similar approaches.

The flowchart of this problem, considering the controllable demand response with boundary calculation process, is described as follows in Figure 5.4.

The maximum output calculation process is very similar to the minimum one.

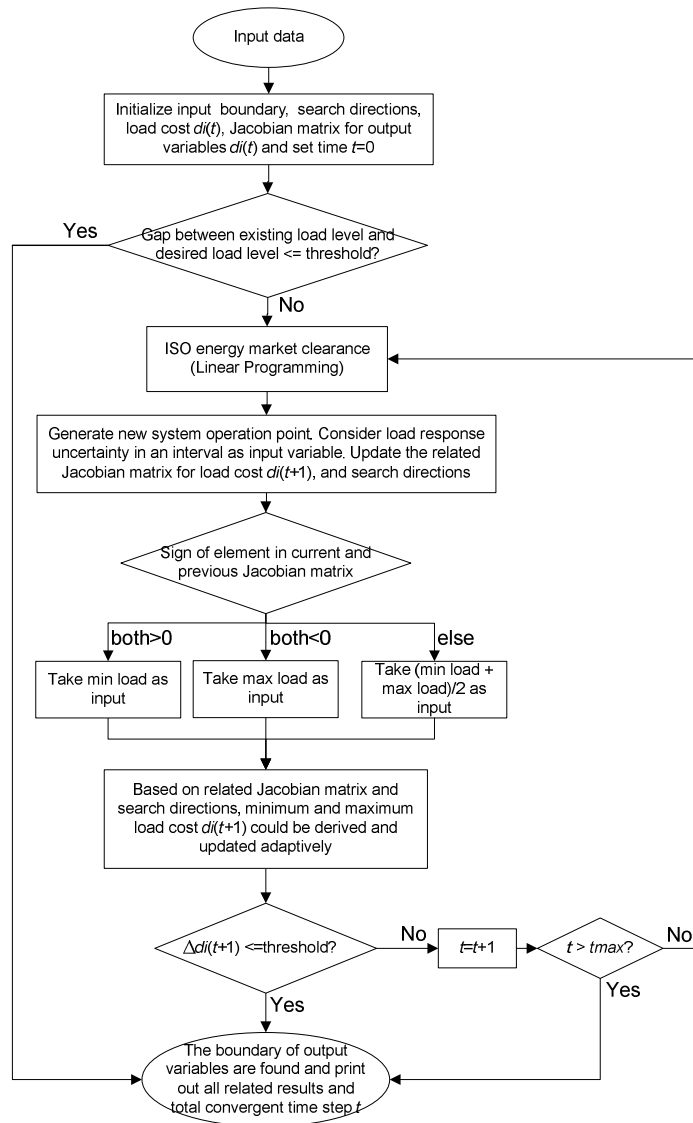


Figure 5.4 Flow chart of output boundary calculation by interval mathematics

5.3 Simulation Results

A modified PJM five-bus system, shown in Figure 5.5 [27], is used in this simulation study. On the left side of this system is the generation center, while the load center is located on the right side. The system has five GENCOs and three LSEs. The

generation, load, and line data are given in Tables 5.1-5.3. The controllable load response model without uncertainty is simulated to verify the proposed approach. Then, Monte Carlo simulation and interval mathematics for boundary estimation are applied to obtain the min and max boundaries of various quantities.

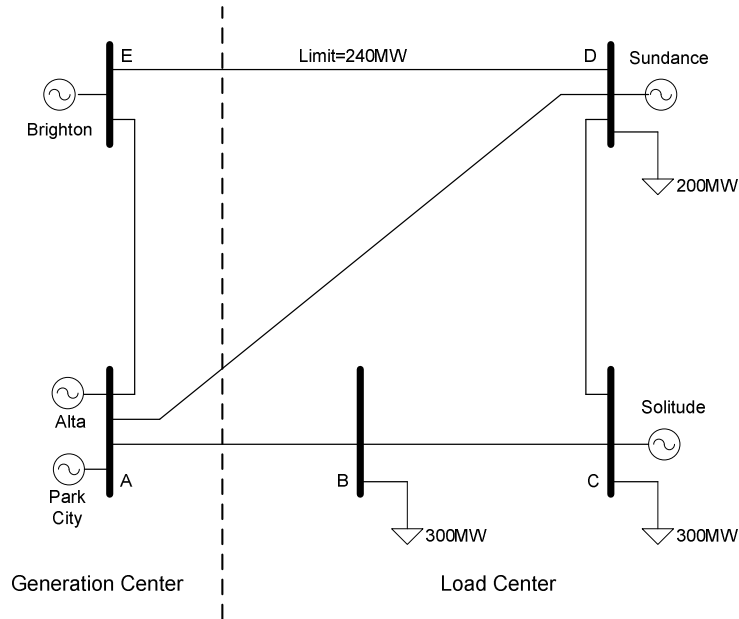


Figure 5.5 Modified PJM Five-Bus System

Table 5.1 Line Impedance and Flow Limit Data

| Line | AB | AD | AE | BC | CD | DE |
|-----------|------|------|------|------|------|------|
| X(%) | 2.81 | 3.04 | 0.64 | 1.08 | 2.97 | 2.97 |
| Limit(MW) | 999 | 999 | 999 | 999 | 999 | 240 |

Table 5.2 Load Data

| Load Location | P_{\min} (MW) | P_{\max} (MW) | Initial Load Cost(\$/MWh) |
|---------------|-----------------|-----------------|---------------------------|
| Bus B | 200 | 300 | 30 |
| Bus C | 200 | 300 | 30 |
| Bus D | 200 | 300 | 40 |

Table 5.3 Generation Data

| Generator | P_{\min} (MW) | P_{\max} (MW) | Marginal Cost(\$/MWh) |
|-----------|-----------------|-----------------|-----------------------|
| Alta | 10 | 110 | 5 |
| Park City | 10 | 100 | 15 |
| Solitude | 10 | 520 | 30 |
| Sundance | 10 | 300 | 35 |
| Brighton | 10 | 600 | 10 |

5.3.1 Controllable Load Response Result

In this deterministic case, no uncertainty is considered. The α_i values are 0.001, 0.002, and 0.003 for Buses B, C and D, respectively; while the β_i values are 0.3, 0.2, and 0.1 for Buses B, C and D, respectively. The total load level of the entire system is 800 MW, including 600 MW base load and 200 MW available demand response capacity. The initial load cost is \$30/MWh at Bus B, \$30/MWh at Bus C, and \$30/MWh at Bus D. The desired reference total load level is 740 MW. Each step is a 5-minute trading cycle which is aligned with some ISO’s actual real-time energy market time interval. The results are shown in Figs. 5.6 to 5.9 below.

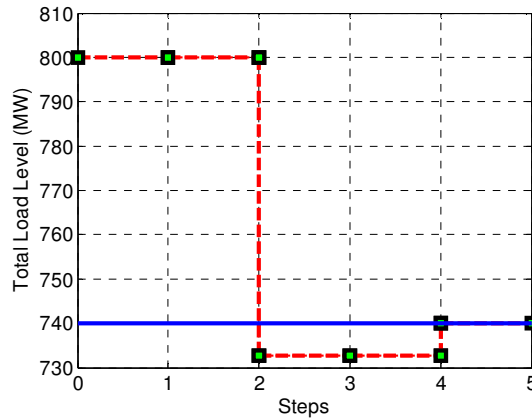


Figure 5.6 Total load level adjustment of the modified PJM Five-Bus system

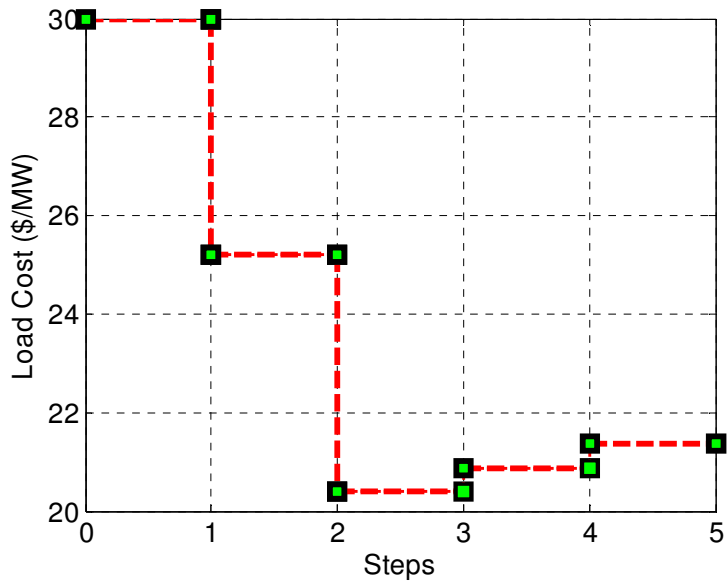


Figure. 5.7 Load cost adjustment at Bus B

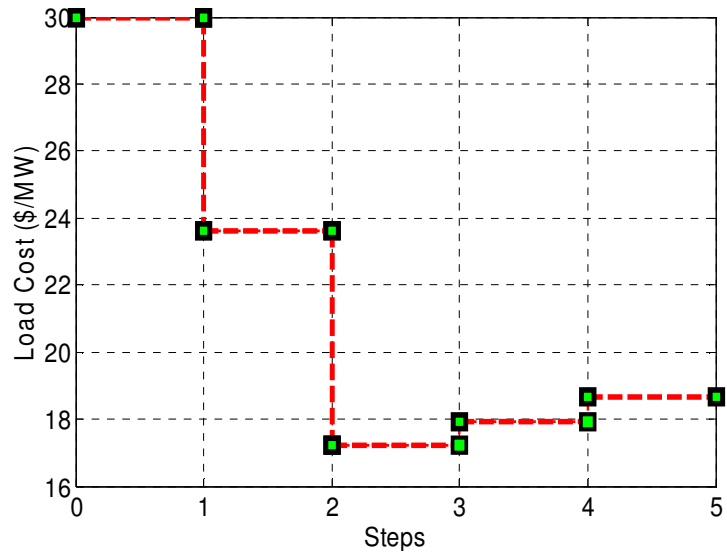


Figure 5.8 Load cost adjustment at Bus C

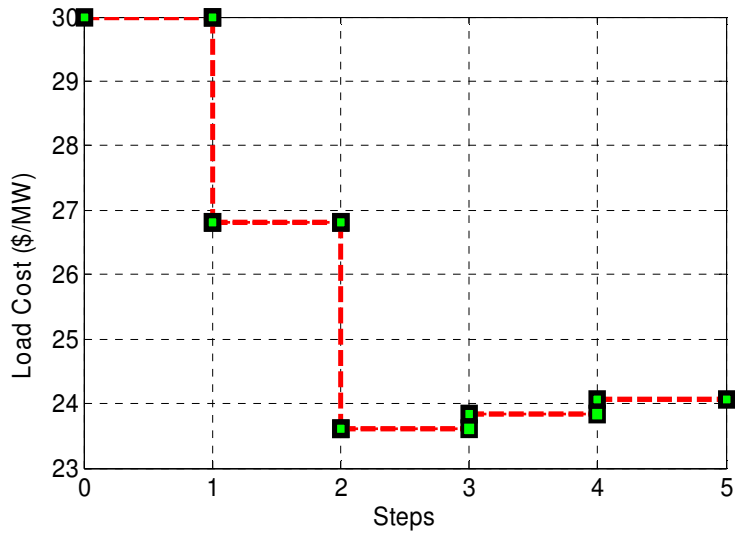


Figure 5.9 Load cost adjustment at Bus D

Figure 5.6 shows the initial load level 800MW could decrease to the desired load level in only five steps (i.e., five trading periods of 5 minutes each) based on the controllable demand response model. Figures 5.7-5.9 show the load shedding cost adjustment process of Bus B, C and D corresponding to the load change in Figure 5.6. In Figs. 9-11, the load shedding costs of Bus B, C, and D decrease to 18.66\$/MW, 21.36\$/MW, and 24.05\$/MW at step 5 compared to the initial load cost. It indicates that the end-users of LSEs would be more likely to reduce their load. All figures indicate that the process converges after five steps. Note that the number of steps also depends on the initial start point. If different initial load cost values are chosen, the number of steps may vary, but it still converges in finite steps based on Equation (5.16). In addition, it could be applied offline for estimation purpose of the day-ahead market or hour-ahead market simulation. Moreover, it should be mentioned that this model can be applied flexibly for increasing load to a high targeted level if ISO wants more load connected in the system to

balance unexpected extra generation at some off-peak hours. In such cases, the coefficients in the model may need to be changed accordingly.

5.3.2 Output Variable Boundary Determination

In this case, 10000 scenarios are taken for MCS sampling. Assume that the uncertainty stems only from the end-users' behavior. A normal distribution is applied to describe end-users' uncertainty in this MCS. The uncertainty of load response is 5% deviation of μ , i.e. the load response is in the interval $[0.95\mu, 1.05\mu]$ after the first dispatch, where μ is the ISO dispatched responsive load, and the standard variance σ is 0.0167μ to ensure 99.7% confidence in the interval $[0.95\mu, 1.05\mu]$ based on normal distribution. The whole process is based on Section 5.2.3. In addition, the interval mathematics based on Section 5.2.4 is also applied in this case and is compared with the result of MCS. All results are listed in the following tables.

Table 5.4 Load Cost Boundary by Monte Carlo Simulation

| Boundary approach of Monte Carlo simulation | | | | |
|---|------------------------|------------------------|------------------------------------|------------------------------------|
| load # | max load cost (\$/MWh) | min load cost (\$/MWh) | $\mu+3\sigma$ lower bound (\$/MWh) | $\mu-3\sigma$ upper bound (\$/MWh) |
| load at Bus B | 18.9623 | 17.1945 | 19.3012 | 17.3377 |
| load at Bus C | 21.8187 | 19.2723 | 22.4315 | 19.7283 |
| load at Bus D | 24.6751 | 21.3500 | 25.6469 | 22.0338 |

Table 5.5 Load Cost Boundary by Interval Mathematics

| Boundary approach of interval mathematics | | |
|---|------------------------|------------------------|
| load # | max load cost (\$/MWh) | min load cost (\$/MWh) |
| load at Bus B | 19.4222 | 17.9903 |
| load at Bus C | 22.1778 | 20.7251 |
| load at Bus D | 24.9333 | 23.4599 |

From Tables 5.4 and 5.5, the boundary data is shown and is listed for comparison. Here, the boundary analysis results are based on the final, converged step. From Figures 5.9-5.11 in Section 5.3.1, it is obvious that the final load costs at step five are contained in the intervals calculated in Tables 5.4 and 5.5. All boundaries calculated from interval mathematics are close to the counterparts calculated from the MCS. Hence, the validity of interval mathematics can be verified by the MCS. This interval mathematics can bring confidence to ISO for the worst case estimation when the uncertainty of controllable load response is considered.

Note, since MCS takes 10000 samples while the interval mathematics only considers two scenarios (min and max boundaries), the interval mathematics approach takes less than 1% of the MCS computing time. The interval mathematics gives higher computational efficiency compared to MCS. However, interval mathematics approach provides min and max boundaries, but not the statistical measures like μ and σ which can be obtained from MCS. Therefore, market participants may take different tools, either MCS or interval mathematics, to analysis the potential risks depending on their own needs.

5.4 Conclusions

Electricity is typically difficult to store, and supply must be balanced with demand at all times to maintain system reliability and stability. Power system load demand is always fluctuating continuously. If the production cost of peak units is much higher than regular and normal base units, then the market price is high during peak hours. Therefore, there is an increasing need to promote the demand response programs including at the end-users side such that LSEs may reduce load and avoid price spikes

during peak hours.

This chapter presents a new controllable demand response model. It is a dynamic load adjustment feedback process rather than a conventional static “one time use” open-loop process. Moreover, this model also clearly describes the interactions among all participants in a power market. The load cost is adjusted based on the difference between the present and targeted load levels in this model. Within a finite time period, this model can lower the total load level to a desired level in order to meet the reliability needs of ISOs during peak hours. In addition, the uncertainty of the demand response behavior of individual end-users is estimated by Monte Carlo simulation and interval mathematics for boundary analysis. Finally, this model can help shave load during peak hours as an effective tool for system operators in applying load adjustment.

Future work may include the study of the sizing and the siting of demand response programs and the integration of renewable energy resources.

CHAPTER VI CONCLUSIONS AND RECOMMENDATIONS

6.1. Summary of Contributions

In Chapter III, wind power integration into the power grid is discussed with economic efficiency considered. The wind generation access into power market bidding process is conducted into two bidding schemes and compared: the wind generation as negative loads; and wind generation as one of game players in power market.

In the first scheme, wind generation is taken as zero generation cost in the system and will always be the first to get dispatched regardless of its intermittency and uncertainty. Although it can guarantee the wind generation penetration quantity in the whole system, the profit of the wind generation may not be satisfied enough to encourage wind farm owners to produce more clean energy due to its lower price. While in the second scheme, wind generation could exert its market power to earn a higher price position. Base on wind intermittency or uncertainty, a market rule is made as: if the wind generation could not meet its need of required generation quantity position, it suffers from profit forfeit for purchasing the gap amount of electricity from the spot market of ISO as a penalty; but if the wind generation could produce more, it can earn more from expectation as an extra bonus. The result shows that even the wind generation may be subject to some losses due to the probability distribution of wind generation, the entire revenue or profit is much more than the first scheme. Therefore, wind generation should participate in bidding process of power market from generation side rather than from the load side for load balance use to earn more profit, but this new bidding framework as the

second scheme should require a restructured market framework to fit for promotion of wind generation.

In Chapter IV, the system frequency security analysis is carried out from the load side instead of from the generation side. In this regard, the sensitivity functions about the effect of varying load-damping characteristic D on frequency response change are rigorously derived based on the SFR models at first. Thus, an exact mathematical description rather than repetitive simulation with discrete load-damping characteristic D increment based on experience could be obtained for the purpose of quantifying frequency excursion away from the 60Hz frequency balance point.

In addition, these sensitivity functions could be used for system frequency stability analysis such as helping determine the system frequency stability status and margin when it is deviated far away from the normal steady operation point under large external disturbances for system operators. It reminds the operators not to forget to consider the frequency sensitive load effect on system stability assessment and analysis as well as estimating effect of external interruptions.

Besides, the largest frequency dip of a stable power system is also solved mathematically. The alignment of occurring time of the largest frequency dip and the max load-damping characteristic sensitivity function moment is observed and rigorously proven. This is also verified in simulation studies. This phenomenon can be valuable to provide an alternative way to derive the critical time when the largest frequency dip occurs due to an external perturbation. It is also useful to estimate the largest frequency drop for system security consideration if the equation of derivative of frequency response function with time t equals to zero is not easy to solve directly.

In Chapter V, a new dynamic load response model is proposed. It can be used for reducing peak hours load and transmission congestion. It can help realize a flatter load profile as well.

First, this load response process is built as a closed loop feedback control model, which uses flexible load cost to direct load dispatch change to the desired load level. In this model, the actual load level is the feedback signal and also the system output. The error between actual load level and the desired load level is the input of the controller. And the load cost is the output of the controller. The relation between the input and output of the controller is based on a second order polynomial function description. If the existing load level is higher than the desired load level, then the load cost is growing up to reduce actual load in dispatch; otherwise, it is decreasing to increase actual load in the next step. The whole process goes on until the error between the ideal load level and the actual load level is less than a preset threshold value.

Further, the load response scheme in this work also respects the loads' willingness to accept and respond with incentive signals. Since the willingness to respond or even adjust towards ideal load level under the directions from ISO is different for each load, it is also of benefit to consider the stochastic uncertainty from each individual end load user's response in this work to avoid possible DLC implementation in practice due to its economical inefficiency. MCS and interval mathematics are employed for the load response boundary estimation of output variables.

The whole process could be realized autonomously in finite steps even with the uncertainty consideration from each individual end load user's responses. All these

properties make this controllable load response model fit for many applications such as long-term or short-term planning and online operation.

6.2. Future Works

The following items may be considered in future works for this dissertation.

- **On Bidding Strategy for Wind Generation Considering Conventional Generation and Transmission Constraints**
 - Bidding strategy model with incomplete information
 - Considering stochastic uncertainty effects among each player in the power market
- **On Sensitivity Analysis of Load-Damping Characteristic in Power System Frequency Regulation**
 - A strategic design of a robust load shedding scheme considering the variation of the load-damping coefficient
 - Sensitivity study of other parameters and other generator models such as hydraulic turbines, perhaps in a large-scale system, can be investigated.
- **On Controllable Demand Response Modeling**
 - Large scale system demand response application considering size and site of load and load priority
 - Other control approaches on demand response with various energy market uncertainties

LIST OF REFERENCES

- [1] D. Kirschen and G. Strbac, *Fundamentals of Power System Economics*, John Wiley & Sons, 2005.
- [2] D. Zhang, Y. Wang, and P. B. Luh, "Optimization Based Bidding Strategies in the Deregulated Market," *IEEE Trans. on Power Syst.*, vol. 15, no. 3, pp. 981-986, Aug. 2000.
- [3] T. Li and M. Shahidehpour, "Strategic Bidding of Transmission-Constrained GENCOs with Incomplete Information," *IEEE Trans. on Power Syst.*, vol. 20, no. 1, pp. 437-447, Feb. 2005.
- [4] T. Li and M. Shahidehpour, "Risk-Constrained FTR Bidding Strategy in Transmission Markets," *IEEE Trans. on Power Syst.*, vol. 20, no. 2, pp. 1014-1021, May 2005.
- [5] J. Wang, M. Shahidehpour, Z. Li and A. Botterud, "Strategic Generation Capacity Expansion Planning With Incomplete Information," *IEEE Trans. on Power Syst.*, vol. 24, no. 2, pp. 1002-1010, May 2009.
- [6] F. S. Wen and A. K. David, "Optimal Bidding Strategies and Modeling of Imperfect Information among Competitive Generators," *IEEE Trans. on Power Syst.*, vol. 16, no. 1, pp. 15-21, Feb. 2001.
- [7] C. W. Richter, Jr. and G. B. Sheble, "A Profit-Based Unit Commitment GA for the Competitive Environment," *IEEE Trans. on Power Syst.*, vol. 15, no. 2, pp. 715-721, May 2000.
- [8] P. M. Anderson and M. Mirheydar, "An Adaptive Method for Setting Underfrequency Load Shedding Relays," *IEEE Trans. on Power Syst.*, vol. 7, no. 2, pp. 647-655, May 1992.

- [9] U.S. Department of Energy, “Benefits of Demand Response in Electricity Markets and Recommendations for Achieving Them: A Report to the United States Congress Pursuant to Section 1252 of the Energy Policy Act of 2005,” Feb. 2006.
- [10] F. Li and R. Bo, “Congestion and Price Prediction Under Load Variation,” *IEEE Trans. on Power Syst.*, vol. 24, no. 2, pp. 911-922, May 2009.
- [11] R. Bo and F. Li, “Efficient Estimation of Critical Load Levels Using Variable Substitution Method,” *IEEE Trans. on Power Syst.*, vol. 26, no. 4, pp. 2472-2482, Oct. 2011.
- [12] R. Bo and F. Li, “Probabilistic LMP Forecasting Considering Load Uncertainty,” *IEEE Trans. on Power Syst.*, vol. 24, no. 3, pp. 1279-1289, Aug. 2009.
- [13] F. Li, “Continuous Locational Marginal Pricing (CLMP),” *IEEE Trans. on Power Syst.*, vol. 22, no. 4, pp. 1638-1646, Nov. 2007.
- [14] F. Li and R. Bo, “DCOPF-Based LMP simulation: Algorithm, Comparison with ACOPF, and sensitivity,” *IEEE Trans. on Power Syst.*, vol. 22, no. 4, pp. 1475-1485, Nov. 2007.
- [15] A. Faruqui, S. Sergici, and J. Palmer, “The Impact of Dynamic Pricing on Low Income Customers,” Institute for Electric Efficiency White Paper, Washington, D.C., Sep. 2010.
- [16] A. Faruqui, S. Sergici, and L. Wood, “Moving Toward Utility-Scale Deployment of Dynamic Pricing in Mass Markets,” Institute for Electric Efficiency, Jun. 2009.
- [17] A. Faruqui and L. Wood, “Quantifying the Benefits of Dynamic Pricing in the Mass Market,” The Edison Electric Institute, Jan. 2008.

- [18] K. Herter, S. Wayland, and J. Rasin, "Small Business Demand Response with Communicating Thermostats: SMUD's Summer Solutions Research Pilot," LBNL-2742E, Sep. 2009.
- [19] H. Saadat, *Power System Analysis*, 2nd Edition, McGraw Hill, 2002.
- [20] P. Kundur, *Power System Stability and Control*, Electric Power Research Institute, 1994.
- [21] A. K. David and F. S. Wen, "Market Power in Electricity Supply," *IEEE Trans. on Ener. Conv.*, vol.16, no. 4, pp. 352-360, Dec. 2001.
- [22] H. Yamin, S. Al-Agtash, and M. Shahidehpour, "Security-Constrained Optimal Generation Scheduling for GENCOs," *IEEE Trans. on Power Syst.*, vol. 19, no. 3, pp. 1365-1372, Aug. 2004.
- [23] T. Peng and K. Tomsovic, "Congestion Influence on Bidding Strategies in an Electricity Market," *IEEE Trans. on Power Syst.*, vol. 18, no. 3, pp.1054-1061, Aug. 2003.
- [24] E. Bompard, Y. C. Ma, R. Napoli, G. Gross, and T. Guler, "Comparative Analysis of Game Theory Models for Assessing the Performances of Network Constrained Electricity Markets," *IET Gener. Transm. Distrib.*, vol. 4, no. 3, pp. 386-399, Mar. 2010.
- [25] Y. He and Y. H. Song, "The Study of the Impacts of Potential Coalitions on Bidding Strategies of GENCOs," *IEEE Trans. on Power Syst.*, vol. 18, no. 3, pp. 1086-1093, Aug. 2003.

- [26] Y. He, Y. H. Song, and X. F. Wang, "Bidding Strategies Based on Bid Sensitivities in Generation Auction Markets," *IEE Proc.-Gener. Transm. Distrib.*, vol. 149, no.1, pp. 21-26, Jan. 2002.
- [27] V. P. Gountis and A. G. Bakirtzis, "Bidding Strategies for Electricity Producers in a Competitive Electricity Marketplace," *IEEE Trans. on Power Syst.*, vol. 19, no. 1, pp.356-365, Feb. 2004.
- [28] Y. Yang, Y. Zhang, F. Li, and H. Cheng, "Computing All Nash Equilibria of Multiplayer Games in Electricity Markets by Solving Polynomial Equations," *IEEE Trans. on Power Syst.*, vol. 27, no.1, pp. 81-91, Feb. 2012.
- [29] L. Xu and R. Baldick, "Transmission-Constrained Residual Demand Derivative in Electricity Markets," *IEEE Trans. on Power Syst.*, vol. 22, no. 4, pp. 1563-1573, Nov. 2007.
- [30] L. Xu, R. Baldick, and Y. Sutjandra, "Transmission-Constrained Inverse Residual Demand Jacobian Matrix in Electricity Markets," *IEEE Trans. on Power Syst.*, vol. 26, no. 4, pp. 2311-2318, Nov. 2011.
- [31] L. Xu, R. Baldick, and Y. Sutjandra, "Bidding Into Electricity Markets: A Transmission-Constrained Residual Demand Derivative Approach," *IEEE Trans. on Power Syst.*, vol. 26, no. 3, pp. 1380-1388, Aug. 2011.
- [32] S. N. Singh and I. Erlich, "Strategies for Wind Power Trading in Competitive Electricity Markets," *IEEE Trans. on Ener. Conv.*, vol. 23, no. 1, pp. 249-256, Mar. 2008.

- [33] J. Matevosyan and L. Soder, "Minimization of Imbalance Cost Trading Wind Power on the Short-Term Power Market," *IEEE Trans. on Power Syst.*, vol. 21, no. 3, pp. 1396-1404, Aug. 2006.
- [34] J. M. Morales, A. J. Conejo, and J. Perez-Ruiz, "Short-Term Trading for a Wind Power Producer," *IEEE Trans. on Power Syst.*, vol. 25, no. 1, pp. 554-564, Feb. 2010.
- [35] X. Liu and W. Xu, "Economic Load Dispatch Constrained by Wind Power Availability: A Here-and-Now Approach," *IEEE Trans. on Sust. Ener.*, vol.1, no. 1, pp.2-9, Apr. 2010.
- [36] P. M. Anderson and M. Mirheydar, "A Low-Order System Frequency Response Model," *IEEE Trans. on Power Syst.*, vol. 5, no. 3, pp. 720-729, Aug. 1990.
- [37] S. Mukherjee, S. Teleke, and V. Bandaru, "Frequency Response and Dynamic Power Balancing in Wind and Solar Generation," *IEEE PES General Meeting*, Jul. 2011.
- [38] L. Yao and H. Lu, "A Two-Way Direct Control of Central Air-Conditioning Load Via the Internet," *IEEE Trans. on Power Deli.*, vol. 24, no. 1, pp. 240-248, Jan. 2009.
- [39] L. Yao, W. Chang, and R. Yen, "An Iterative Deepening Genetic Algorithm for Scheduling of Direct Load Control," *IEEE Trans. on Power Syst.*, vol. 20, no. 3, pp. 1414-1421, Aug. 2005.
- [40] N. Ruiz, I. Cobelo, and J. Oyarzabal, "A Direct Load Control Model for Virtual Power Plant Management," *IEEE Trans. on Power Syst.*, vol. 24, no. 2, pp.959-966, May 2009.

- [41] V. V. Terzija, "Adaptive Underfrequency Load Shedding Based on the Magnitude of the Disturbance Estimation," *IEEE Trans. on Power Syst.*, vol. 21, no. 3, pp. 1260-1266, Aug. 2006.
- [42] Y. Halevi and D. Kottick, "Optimization of Load Shedding System," *IEEE Trans. on Power Syst.*, vol. 8, no. 2, pp. 207-213, Jun. 1993.
- [43] X. Lin, H. Weng, Q. Zou and P. Liu, "The Frequency Closed-Loop Control Strategy of Islanded Power Systems," *IEEE Trans. on Power Syst.*, vol. 23, no. 2, pp. 796-803, May 2008.
- [44] D. L. H. Aik, "A General-Order System Frequency Response Model Incorporating Load Shedding: Analytic Modeling and Applications," *IEEE Trans. on Power Syst.*, vol. 21, no. 2, pp. 709-717, May 2006.
- [45] N. Amjady and F. Fallahi, "Determination of Frequency Stability Border of Power System to Set the Thresholds of Under Frequency Load Shedding Relays," *Energy Conv. and Mgmt.*, vol. 51, no. 10, pp. 1864-1872, Oct. 2010.
- [46] H. Bevrani, G. Ledwich, Z. Dong, and J. J. Ford, "Regional Frequency Response Analysis under Normal and Emergency Conditions," *Electric Power Systems Research*, vol. 79, no. 5, pp. 837-845, May 2009.
- [47] H. Omara and F. Bouffard, "A Methodology to Study the Impact of an Increasingly Nonconventional Load Mix on Primary Frequency Control," *IEEE PES General Meeting*, Jul. 2009.
- [48] N. Lu, D. P. Chassin, and S.E. Widergren, "Modeling Uncertainties in Aggregated Thermostatically Controlled Loads Using a State Queueing Model," *IEEE Trans. on Power Syst.*, vol. 20, no. 2, pp. 725-733, May 2005.

- [49] Y. Liu and F. F. Wu, "Generator Bidding in Oligopolistic Electricity Markets Using Optimal Control: Fundamentals and Application," *IEEE Trans. on Power Syst.*, vol. 21, no.3, pp. 1050-1061, Aug. 2006.
- [50] Y. Liu and F. F. Wu, "Prisoner Dilemma: Generator Strategic Bidding in Electricity Markets," *IEEE Trans. on Auto. Cont.*, vol. 52, no. 6, pp. 1143-1149, Jun. 2007.
- [51] F. Alvarado, "The Stability of Power System Markets," *IEEE Trans. on Power Syst.*, vol. 14, no. 2, pp.505-511, May 1999.
- [52] A. R. Kian, J. J. B. Cruz, and R. J. Thomas, "Bidding Strategies in Oligopolistic Dynamic Electricity Double-Sided Auctions," *IEEE Trans. on Power Syst.*, vol. 20, no. 1, pp. 50-58, Feb. 2005.
- [53] J. Nutaro and V. Protopopescu, "The Impact of Market Clearing Time and Price Signal Delay on the Stability of Electric Power Markets," *IEEE Trans. on Power Syst.*, vol. 24, no. 3, pp. 1337-1345, Aug. 2009.
- [54] M. D. Ilic, L. Xie, and J.-Y. Joo, "Efficient Coordination of Wind Power and Price-Responsive Demand-Part I: Theoretical Foundations," *IEEE Trans. on Power Syst.*, vol. 26, no. 4, pp. 1875-1884, Nov. 2011.
- [55] M. D. Ilic, L. Xie, and J.-Y. Joo, "Efficient Coordination of Wind Power and Price-Responsive Demand-Part II: Case Studies," *IEEE Trans. on Power Syst.*, vol. 26, no. 4, pp. 1885-1893, Nov. 2011.
- [56] U.S. Department of Energy, "Benefits of Demand Response in Electricity Markets and Recommendations for Achieving Them: A Report to the United

- States Congress Pursuant to Section 1252 of the Energy Policy Act of 2005,” Feb. 2006.
- [57] California Energy Commission, “Proposed Load Management Standards,” Draft Committee Report, CEC-400-2008-027-CTD, Nov. 2008.
- [58] K. Herter, P. McAuliffe, and A. Rosenfeld, “An Exploratory Analysis of California Residential Customer Response to Critical Peak Pricing of Electricity,” *Energy*, vol. 32, no. 1, pp. 25-34, Jan. 2007.
- [59] K. Herter and S. Wayland, “Residential Response to Critical Peak Pricing of Electricity: California Evidence,” *Energy*, vol. 35, no. 4, pp. 1561-1567, Apr. 2010.
- [60] K. Herter, “Residential Implementation of Critical-Peak Pricing of Electricity,” *Energy Policy*, vol. 35, no. 4, pp. 2121-2130, Apr. 2007.
- [61] A. Stothert and I. MacLeod, “Competitive Bidding as a Control Problem,” *IEEE Trans. on Power Syst.*, vol. 15, no. 1, pp. 88-94, Feb. 2000.
- [62] A. Nourai, V. I. Kogan, and C. M. Schafer, “Load Leveling Reduces T&D Line Losses,” *IEEE Trans. on Power Syst.*, vol. 23, no. 4, pp. 2168-2173, Oct. 2008.
- [63] A. J. Wood and B. F. Wollenberg, *Power Generation, Operation, and Control*, John Wiley & Sons, 1996.
- [64] R. Billinton and G. Bai, “Generating Capacity Adequacy Associated With Wind Energy,” *IEEE Trans. on Ener. Conv.*, vol. 19, no. 3, pp. 641-646, Sep. 2004.
- [65] R. Billinton, H. Chen, and R. Ghajar, “A Sequential Simulation Technique for Adequacy Evaluation of Generating Systems Including Wind Energy,” *IEEE Trans. on Ener. Conv.*, vol. 11, no. 4, pp. 728-734, Dec. 1996.

- [66] R. Billinton and L. Gan, "Monte Carlo Simulation Model for Multiarea Generation System Reliability Studies," *IEE Proceedings-C*, vol. 140, no. 6, pp. 532-538, Nov. 1993.
- [67] Univ. Washington, Power System Test Case Archive. [Online]. Available: <http://www.ee.washington.edu/research/pstca/>.
- [68] A. Karakas, F. Li, and S. Adhikari, "Aggregation of Multiple Induction Motors using MATLAB-based Software Package," *IEEE PES Power System Conf. and Expo. (PSCE) 2009*, Seattle, WA, Mar. 15-18, 2009.
- [69] F. Nozari, M.D. Kankam, and W.W. Price, "Aggregation of Induction Motors for Transient Stability Load Modeling," *IEEE Trans. on Power Syst.*, vol. 2, no. 4, pp. 1096-1103, Nov. 1987.
- [70] I. Egado, F. Fernandez-Bernal, P. Centeno, and L. Rouco, "Maximum Frequency Deviation Calculation in Small Isolated Power Systems," *IEEE Trans. Power Syst.*, vol. 24, no. 4, pp. 1731-1738, Nov. 2009.
- [71] A. Dimitrovski and K. Tomsovic, "Boundary Load Flow Solutions," *IEEE Trans. on Power Syst.*, vol. 19, no. 1, pp. 348-355, Feb. 2004.
- [72] Z. Wang and F. L. Alvarado, "Interval Arithmetic in Power Flow Analysis," *IEEE Trans. on Power Syst.*, vol. 7, no.3, pp. 1341-1349, Aug. 1992.
- [73] A. Vaccaro, C. A. Canizares, and K. Bhattacharya, "A Range Arithmetic-Based Optimization Model for Power Flow Analysis Under Interval Uncertainty," *IEEE Trans. on Power Syst.*, vol. 28, no. 2, pp. 1179-1186, May 2013.

- [74] A. Vaccaro and D. Villacci, "Radial Power Flow Tolerance Analysis by Interval Constraint Propagation," *IEEE Trans. on Power Syst.*, vol. 24, no. 1, pp. 28-39, Feb. 2009.
- [75] A. Vaccaro, C. A. Canizares, and D. Villacci, "An Affine Arithmetic-Based Methodology for Reliable Power Flow Analysis in the Presence of Data Uncertainty," *IEEE Trans. on Power Syst.*, vol. 25, no. 2, pp. 624-632, May 2010.

APPENDICES

APPENDIX A

A.1 Alternative Proof of the Alignment of the Maximum Sensitivity and the Largest Frequency Dip

In a stable case, when $\frac{\partial \Delta \omega(t)}{\partial D}$ or $\frac{\partial \Delta f(t)}{\partial D}$ reaches its maximum, the necessary condition is that its derivative with time t should be equal to zero, i.e. $\partial \left(\frac{\partial \Delta \omega(t)}{\partial D} \right) / \partial t = 0$.

. When the largest frequency dip $\Delta \omega(t)$ occurs, its derivative with time t should also be equal to zero, i.e. $\frac{\partial \Delta \omega(t)}{\partial t} = 0$. If the maximum sensitivity and the largest frequency dip are aligned, then it means that solving $\partial \left(\frac{\partial \Delta \omega(t)}{\partial D} \right) / \partial t = 0$ is equivalent to solving $\frac{\partial \Delta \omega(t)}{\partial t} = 0$. That is to say, from $\frac{\partial \Delta \omega(t)}{\partial t} = 0$, it could deduce $\partial \left(\frac{\partial \Delta \omega(t)}{\partial D} \right) / \partial t = 0$ and from $\partial \left(\frac{\partial \Delta \omega(t)}{\partial D} \right) / \partial t = 0$, $\frac{\partial \Delta \omega(t)}{\partial t} = 0$ could be derived as well. Here we consider the general initial condition $\Delta \omega(0)=0$, which means no frequency deviation initially.

i. Proof of $\frac{\partial \Delta \omega(t)}{\partial t} = 0 \Rightarrow \partial \left(\frac{\partial \Delta \omega(t)}{\partial D} \right) / \partial t = 0$

Base on multi-variables calculus theory, rewritten $\partial \left(\frac{\partial \Delta \omega(t)}{\partial D} \right) / \partial t = 0$ as

$$\partial \left(\frac{\partial \Delta \omega(t)}{\partial D} \right) / \partial t = \frac{\partial^2 \Delta \omega(t)}{\partial D \partial t} = \partial \left(\frac{\partial \Delta \omega(t)}{\partial t} \right) / \partial D = 0 \quad (\text{A.1})$$

If $\frac{\partial \Delta \omega(t)}{\partial t} = 0$, then from (A.1), it is obvious that $\partial \left(\frac{\partial \Delta \omega(t)}{\partial D} \right) / \partial t =$

$$\partial \left(\frac{\partial \Delta \omega(t)}{\partial t} \right) / \partial D = 0.$$

ii. Proof of $\partial \left(\frac{\partial \Delta \omega(t)}{\partial D} \right) / \partial t = 0 \Rightarrow \frac{\partial \Delta \omega(t)}{\partial t} = 0$

If $\partial \left(\frac{\partial \Delta \omega(t)}{\partial D} \right) / \partial t = 0$, then by (3.33), it is equivalent as $\partial \left(\frac{\partial \Delta \omega(t)}{\partial t} \right) / \partial D = 0$.

Thus, the possible satisfied solution should be either $\frac{\partial \Delta \omega(t)}{\partial t}$ is some constant without D

or $\frac{\partial \Delta \omega(t)}{\partial t}$ is a general time t function which does not contain D in its mathematical

description. Since if it is as a time t function, $\frac{\partial \Delta \omega(t)}{\partial t}$ does contain D (because

$$\frac{\partial \Delta \omega(t)}{\partial t} = L^{-1}(s\Delta\Omega(s) - \omega(0)) = L^{-1}(s\Delta\Omega(s)) \text{ and } \Delta\Omega(s) \text{ contains } D \text{ in (4.2), (4.6),}$$

(4.10) and (4.14)), therefore, the possible solution is that $\frac{\partial \Delta \omega(t)}{\partial t}$ is some constant

without D . In addition, if $\frac{\partial \Delta \omega(t)}{\partial t} = C$ as a non-zero constant (either positive or negative),

then $\Delta\omega(t) = Ct$, which means the absolute frequency deviation will continue growing up.

However, as for a stable system assumption, this is impossible to occur. Therefore, the

only possible case is $\frac{\partial \Delta \omega(t)}{\partial t} = 0$ as a zero constant.

Therefore, combining **i** and **ii**, it indicates that $\partial\left(\frac{\partial\Delta\omega(t)}{\partial D}\right)/\partial t = 0 \Leftrightarrow$

$$\frac{\partial\Delta\omega(t)}{\partial t} = 0 .$$

Hence, we can conclude that the maximum of $\frac{\partial\Delta\omega(t)}{\partial D}$ is aligned with the maximum of $\Delta\omega(t)$ (i.e., the largest frequency dip). Therefore, the error of evaluating D gives the largest impact on frequency deviation right at the time when the largest frequency deviation occurs. This further shows the importance of obtaining accurate the load-damping coefficient, D . This important feature can be easily observed in the simulation results.

APPENDIX B

B.1 Sensitivity Analysis Extension to Generator Inertia Coefficient H and Governor Speed Coefficient R in Power System Analysis

In Chapter IV, it gives the sensitivity analysis to the load damping coefficient D and its application in system stability analysis. However, it is not the only parameter that could change during power system operation in a long time range. In fact, the sensitivity analysis could also be extended to other coefficients such as generator inertia coefficient H and governor speed coefficient R in a typical LFC system as the load damping coefficient D shown in Chapter IV. In this appendix, the sensitivity function of generator inertia coefficient H and governor speed coefficient R and their application in system frequency stability analysis are given. The analysis process is similar in Chapter IV. To be succinct, the system figures of SISO and multi-machines case and assumptions are omitted in this session. All the relevant system block diagrams could be referred in Chapter IV.

B.2 Sensitivity Function Derivation

B.2.1 Single Machine (SISO) System

The closed-loop transfer function relating the fixed load step change, $\Delta P_L(s)$, which is commonly assumed for LFC, to the angular frequency deviation from nominal reference frequency 60 Hz, $\Delta\Omega(s)$, is shown as follows:

$$\frac{\Delta\Omega(s)}{-\Delta P_L(s)} = \frac{1}{2Hs + D + \frac{1 + F_{HP}T_{RH}s}{(1 + T_Gs)(1 + T_{CH}s)(1 + T_{RH}s)R}} \quad (\text{B.1})$$

Let $G(s) = \frac{1 + F_{HP} T_{RH} s}{(1 + T_G s)(1 + T_{CH} s)(1 + T_{RH} s)}$, then (B.1) could be rewritten as a brief

$$\text{format } \frac{\Delta\Omega(s)}{-\Delta P_L(s)} = \frac{1}{2Hs + D + G(s)/R}.$$

By (B.1), the stability of this frequency-regulation system can be tested by Routh-Hurwitz array or root locus. And the output of angular frequency deviation can be obtained as:

$$\Delta\Omega(s) = \frac{-\Delta P_L(s)}{2Hs + D + G(s)/R} \quad (\text{B.2})$$

The proposed sensitivity analysis of the generator inertia coefficient H and the governor speed coefficient R is to calculate $\partial\Delta\Omega(s)/\partial H$ and $\partial\Delta\Omega(s)/\partial R$. As previously stated, this shows the potential frequency variation when the actual H and R value differs from the estimated value. This is important since the H and R value is usually obtained empirically. Thus, the growing penetration of intermittent renewable energy in power grid draws the research interest on the impact of the H and R value.

Taking partial derivative of H or R in (B.2), we can obtain the sensitivity of the frequency deviation, $\Delta\Omega$, w.r.t. the generator inertia coefficient, H , or the governor speed coefficient, R , as follows:

$$\frac{\partial\Delta\Omega(s)}{\partial H} = \frac{\Delta P_L(s) \cdot 2s}{[2Hs + D + G(s)/R]^2} = \left[\frac{\Delta\Omega(s)}{\Delta P_L(s)} \right]^2 \Delta P_L(s) \cdot 2s \quad (\text{B.3})$$

$$\frac{\partial\Delta\Omega(s)}{\partial R} = \frac{-\Delta P_L(s)}{\left[2Hs + D + \frac{G(s)}{R} \right]^2} \cdot \frac{G(s)}{R^2} = - \left[\frac{\Delta\Omega(s)}{\Delta P_L(s)} \right]^2 \frac{\Delta P_L(s) G(s)}{R^2} \quad (\text{B.4})$$

Then S_H or S_R , the unit-less sensitivity function of H or R , is derived by its definition as follows:

$$S_H = \frac{d\Delta\Omega(s)/\Delta\Omega(s)}{dH/H} = \frac{\partial\Delta\Omega(s)}{\partial H} \cdot \frac{H}{\Delta\Omega(s)} = \frac{\Delta\Omega(s)}{\Delta P_L(s)} \cdot 2Hs \quad (\text{B.5})$$

$$\begin{aligned} S_R &= \frac{d\Delta\Omega(s)/\Delta\Omega(s)}{dR/R} = \frac{\partial\Delta\Omega(s)}{\partial R} \cdot \frac{R}{\Delta\Omega(s)} \\ &= -\left[\frac{\Delta\Omega(s)}{\Delta P_L(s)}\right]^2 \frac{\Delta P_L(s)G(s)}{R^2} \cdot \frac{R}{\Delta\Omega(s)} = -\frac{\Delta\Omega(s)}{\Delta P_L(s)} \cdot \frac{G(s)}{R} \end{aligned} \quad (\text{B.6})$$

B.2.2 Multi-Machines System

For the case of multiple generation machines, the transfer function is given by:

$$\frac{\Delta\Omega(s)}{-\Delta P_L(s)} = \frac{1}{(2Hs + D) + \sum_{i=1}^N \frac{G_i(s)}{R_i}} \quad (\text{B.7})$$

The output of angular frequency deviation could be obtained as

$$\Delta\Omega(s) = \frac{-\Delta P_L(s)}{(2Hs + D) + \sum_{i=1}^N \frac{G_i(s)}{R_i}} \quad (\text{B.8})$$

Thus, the sensitivity of $\Delta\Omega$ w.r.t. H or R is given by:

$$\frac{\partial\Delta\Omega(s)}{\partial H} = \frac{\Delta P_L(s) \cdot 2s}{\left[(2Hs + D) + \sum_{i=1}^N \frac{G_i(s)}{R_i}\right]^2} = \left[\frac{\Delta\Omega(s)}{\Delta P_L(s)}\right]^2 \Delta P_L(s) \cdot 2s \quad (\text{B.9})$$

$$\frac{\partial\Delta\Omega(s)}{\partial R_i} = \frac{-\Delta P_L(s)}{\left[(2Hs + D) + \sum_{i=1}^N \frac{G_i(s)}{R_i}\right]^2} \cdot \frac{G_i(s)}{R_i^2} = -\left[\frac{\Delta\Omega(s)}{\Delta P_L(s)}\right]^2 \frac{\Delta P_L(s)G_i(s)}{R_i^2} \quad (\text{B.10})$$

Then S_H or S_{R_i} , the unit-less multi-machines sensitivity function of H or R_i can be

written as:

$$S_H = \frac{d\Delta\Omega(s) / \Delta\Omega(s)}{dH / H} = \frac{\partial\Delta\Omega(s)}{\partial H} \cdot \frac{H}{\Delta\Omega(s)} = \frac{\Delta\Omega(s)}{\Delta P_L(s)} \cdot 2Hs \quad (\text{B.11})$$

$$\begin{aligned} S_{R_i} &= \frac{d\Delta\Omega(s) / \Delta\Omega(s)}{dR_i / R_i} = \frac{\partial\Delta\Omega(s)}{\partial R_i} \cdot \frac{R_i}{\Delta\Omega(s)} \\ &= - \left[\frac{\Delta\Omega(s)}{\Delta P_L(s)} \right]^2 \frac{\Delta P_L(s) G_i(s)}{R_i^2} \cdot \frac{R_i}{\Delta\Omega(s)} = - \frac{\Delta\Omega(s)}{\Delta P_L(s)} \cdot \frac{G_i(s)}{R_i} \end{aligned} \quad (\text{B.12})$$

Note that (B.3), and (B.9); (B.4), and (B.10) have the same format of the sensitivity function. Similarly, (B.5), and (B.11); (B.6), and (B.12) show the same format of the unit-less sensitivity function.

B.3 Stability Analysis Using Total Differential Equation

B.3.1 Total Differential Equation for Frequency Deviation

The angular frequency deviation $\Delta\Omega(s)$ is only considered to be related with external disturbance $\Delta P_L(s)$ for simplicity in early researches. And its differential equation is as follows:

$$d\Delta\Omega(s) = \frac{\partial\Delta\Omega(s)}{\partial\Delta P_L(s)} d\Delta P_L(s) \quad (\text{B.13})$$

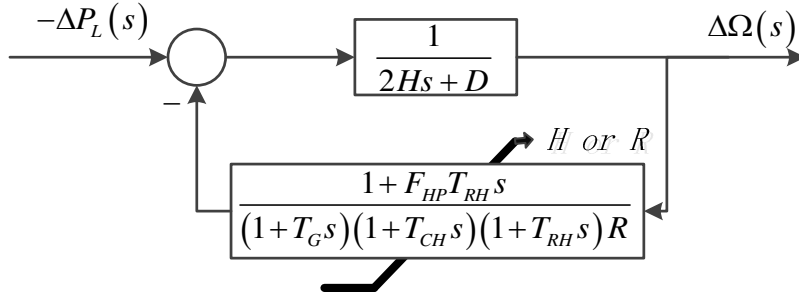


Figure B.1 SISO LFC block diagram with input $\Delta P_L(s)$ and output $\Delta\Omega(s)$ and varied generator inertia coefficient H or governor speed coefficient R

However, in (B.13), the effect of the generator inertia coefficient H and the governor speed coefficient R is ignored in this SFR model. This may not give complete information because the interrupted generator inertia or governor speed may have a different characteristic coefficient than the rest of the generator inertia or governor speed. This is highly possible because many times interrupted generation drop or intermittent renewable generation integration could result the initial generator inertia or governor speed change. Also, H or R may be evaluated based on an out-of-date profile of generation characteristic. In other words, the frequency variation $\Delta\Omega$ should be a function of ΔP_L and H or R rather than ΔP_L only as shown in Figure B.1. Thus, it is interesting to investigate the impact of the load-damping coefficient.

With the assumption that $\Delta P_L(s)$ and H or R are mutually independent, (B.13) should be modified to include H or R as follows:

$$d\Delta\Omega_H(s) = \frac{\partial\Delta\Omega(s)}{\partial\Delta P_L(s)} d\Delta P_L(s) + \frac{\partial\Delta\Omega(s)}{\partial H} dH \quad (\text{B.14})$$

$$\begin{aligned}
d\Delta\Omega_R(s) &= \frac{\partial\Delta\Omega(s)}{\partial\Delta P_L(s)}d\Delta P_L(s) + \frac{\partial\Delta\Omega(s)}{\partial R}dR \\
&= \frac{\partial\Delta\Omega(s)}{\partial\Delta P_L(s)}d\Delta P_L(s) + \sum_{i=1}^N \frac{\partial\Delta\Omega(s)}{\partial R_i}dR_i
\end{aligned} \tag{B.15}$$

Combining either (B.3) or (B.9) with (B.14) for dH , and either (B.4) or (B.10) with (B.15) for dR , we have:

$$d\Delta\Omega_H(s) = \frac{\partial\Delta\Omega(s)}{\partial\Delta P_L(s)}d\Delta P_L(s) + \left[\frac{\Delta\Omega(s)}{\Delta P_L(s)} \right]^2 \Delta P_L(s) \cdot 2sdH \tag{B.16}$$

$$\begin{aligned}
d\Delta\Omega_R(s) &= \frac{\partial\Delta\Omega(s)}{\partial\Delta P_L(s)}d\Delta P_L(s) - \left[\frac{\Delta\Omega(s)}{\Delta P_L(s)} \right]^2 \frac{\Delta P_L(s)G(s)}{R^2}dR \\
&= \frac{\partial\Delta\Omega(s)}{\partial\Delta P_L(s)}d\Delta P_L(s) - \sum_{i=1}^N \left[\frac{\Delta\Omega(s)}{\Delta P_L(s)} \right]^2 \frac{\Delta P_L(s)G_i(s)}{R_i^2}dR_i
\end{aligned} \tag{B.17}$$

Furthermore, taking partial derivative for $\Delta P_L(s)$ of equation either (B.2), or (B.8), we have

$$\frac{\partial\Delta\Omega(s)}{\partial\Delta P_L(s)} = \frac{\Delta\Omega(s)}{\Delta P_L(s)} \tag{B.18}$$

Combining (B.18) with (B.16) or (B.17), we have

$$d\Delta\Omega_H(s) = \frac{\Delta\Omega(s)}{\Delta P_L(s)}d\Delta P_L(s) + \left[\frac{\Delta\Omega(s)}{\Delta P_L(s)} \right]^2 \Delta P_L(s) \cdot 2sdH \tag{B.19}$$

$$\begin{aligned}
d\Delta\Omega_R(s) &= \frac{\Delta\Omega(s)}{\Delta P_L(s)}d\Delta P_L(s) - \left[\frac{\Delta\Omega(s)}{\Delta P_L(s)} \right]^2 \frac{\Delta P_L(s)G(s)}{R^2}dR \\
&= \frac{\Delta\Omega(s)}{\Delta P_L(s)}d\Delta P_L(s) - \sum_{i=1}^N \left[\frac{\Delta\Omega(s)}{\Delta P_L(s)} \right]^2 \frac{\Delta P_L(s)G_i(s)}{R_i^2}dR_i
\end{aligned} \tag{B.20}$$

In order to have its time domain description, Laplace inverse transformation is applied to (B.19) and (B.20). Thus, we have:

$$\begin{aligned}
d\Delta\omega_H(t) &= L^{-1} [d\Delta\Omega(s)] = L^{-1} \left[\frac{\Delta\Omega(s)}{\Delta P_L(s)} d\Delta P_L(s) \right] \\
&+ L^{-1} \left\{ \left[\frac{\Delta\Omega(s)}{\Delta P_L(s)} \right]^2 \Delta P_L(s) \cdot 2sdH \right\}
\end{aligned} \tag{B.21}$$

$$\begin{aligned}
d\Delta\omega_R(t) &= L^{-1} [d\Delta\Omega(s)] = L^{-1} \left[\frac{\Delta\Omega(s)}{\Delta P_L(s)} d\Delta P_L(s) \right] \\
&- L^{-1} \left\{ \left[\frac{\Delta\Omega(s)}{\Delta P_L(s)} \right]^2 \frac{\Delta P_L(s) G(s)}{R^2} dR \right\} = L^{-1} \left[\frac{\Delta\Omega(s)}{\Delta P_L(s)} d\Delta P_L(s) \right] \\
&- \sum_{i=1}^N L^{-1} \left\{ \left[\frac{\Delta\Omega(s)}{\Delta P_L(s)} \right]^2 \frac{\Delta P_L(s) G_i(s)}{R_i^2} dR_i \right\}
\end{aligned} \tag{B.22}$$

Integration of (B.21) and (B.22) gives:

$$\begin{aligned}
\Delta\omega_H(t) &= \int L^{-1} [d\Delta\Omega(s)] = \int L^{-1} \left[\frac{\Delta\Omega(s)}{\Delta P_L(s)} d\Delta P_L(s) \right] \\
&+ \int L^{-1} \left\{ \left[\frac{\Delta\Omega(s)}{\Delta P_L(s)} \right]^2 \Delta P_L(s) \cdot 2sdH \right\}
\end{aligned} \tag{B.23}$$

$$\begin{aligned}
\Delta\omega_R(t) &= \int L^{-1} [d\Delta\Omega(s)] = \int L^{-1} \left[\frac{\Delta\Omega(s)}{\Delta P_L(s)} d\Delta P_L(s) \right] \\
&- \int L^{-1} \left\{ \left[\frac{\Delta\Omega(s)}{\Delta P_L(s)} \right]^2 \frac{\Delta P_L(s) G(s)}{R^2} dR \right\} = \int L^{-1} \left[\frac{\Delta\Omega(s)}{\Delta P_L(s)} d\Delta P_L(s) \right] \\
&- \sum_{i=1}^N \int L^{-1} \left\{ \left[\frac{\Delta\Omega(s)}{\Delta P_L(s)} \right]^2 \frac{\Delta P_L(s) G_i(s)}{R_i^2} dR_i \right\}
\end{aligned} \tag{B.24}$$

Another interesting point should be mentioned from (B.23) and (B.24) is about the effect of the generator inertia coefficient H or speed governor coefficient R on the stability analysis in this SFR model in the next subsection.

B.3.2 Stability Analysis

a. When the Power System is Essentially Stable

If a power system is stable after disturbance, then its Laplace characteristic function's poles are all located on the left half plane in s -domain. That means the finite time-domain input $\Delta P_L(t)$ would not produce infinite time-domain output $\Delta\omega(t)$. It suffices to say that the norm of the transfer function is bounded, i.e. $\left\| \frac{\Delta\Omega(s)}{\Delta P_L(s)} \right\| < \infty$ for $\forall t \in (0, \infty)$, from the perspective of control theory. Furthermore, from the perspective of power system design, $\Delta\omega(t)$ should be in a small finite range since the system is essentially stable. The bound of the frequency deviation is analyzed next.

From (B.23) and (B.24), if we consider ΔP_L a step function, by triangle inequality we have both as follows:

$$\begin{aligned}
\|\Delta\omega_H(t)\| &\leq \left\| \int L^{-1} \left[\frac{\Delta\Omega(s)}{\Delta P_L(s)} d\Delta P_L(s) \right] \right\| + \left\| \int L^{-1} \left\{ \left[\frac{\Delta\Omega(s)}{\Delta P_L(s)} \right]^2 \Delta P_L(s) \cdot 2sdH \right\} \right\| \\
&\leq \left\| \int L^{-1} \left[\left\| \frac{\Delta\Omega(s)}{\Delta P_L(s)} \right\| d\Delta P_L(s) \right] \right\| + \left\| \int L^{-1} \left\{ \left\| \frac{\Delta\Omega(s)}{\Delta P_L(s)} \right\|^2 \Delta P_L(s) \cdot 2sdH \right\} \right\| \\
&= \left\| \int L^{-1} [\varepsilon d\Delta P_L(s)] \right\| + \left\| \int L^{-1} \{ \varepsilon^2 \Delta P_L(s) \cdot 2sdH \} \right\| \\
&= \left\| \int \varepsilon L^{-1} \left[\frac{d\Delta P_L}{s} \right] \right\| + \left\| \int \varepsilon^2 dH \cdot L^{-1} \{ \Delta P_L \} \right\| \tag{B.25} \\
&= \left\| \int \varepsilon \cdot 1(t-t_0) d\Delta P_L \right\| + \left\| \int \varepsilon^2 \cdot \uparrow(t-t_0) \Delta P_L dH \right\| \\
&\leq \varepsilon \|\Delta P_L\| + \varepsilon^2 \left\| \uparrow(t-t_0) \right\| \|\Delta P_L\| \|H\|
\end{aligned}$$

or

$$\begin{aligned}
\|\Delta\omega_R(t)\| &\leq \left\| \int L^{-1} \left[\frac{\Delta\Omega(s)}{\Delta P_L(s)} d\Delta P_L(s) \right] \right\| + \left\| \int L^{-1} \left\{ \left[\frac{\Delta\Omega(s)}{\Delta P_L(s)} \right]^2 \frac{\Delta P_L(s) G(s)}{R^2} dR \right\} \right\| \\
&\leq \left\| \int L^{-1} \left[\frac{\Delta\Omega(s)}{\Delta P_L(s)} d\Delta P_L(s) \right] \right\| + \sum_{i=1}^N \left\| \int L^{-1} \left\{ \left[\frac{\Delta\Omega(s)}{\Delta P_L(s)} \right]^2 \frac{\Delta P_L(s) G_i(s)}{R_i^2} dR_i \right\} \right\| \\
&\leq \left\| \int L^{-1} \left[\left\| \frac{\Delta\Omega(s)}{\Delta P_L(s)} \right\| d\Delta P_L(s) \right] \right\| + \sum_{i=1}^N \left\| \int L^{-1} \left\{ \left\| \frac{\Delta\Omega(s)}{\Delta P_L(s)} \right\|^2 \|G_i(s)\| \frac{\Delta P_L(s)}{R_i^2} dR_i \right\} \right\| \\
&= \left\| \int L^{-1} [\varepsilon d\Delta P_L(s)] \right\| + \sum_{i=1}^N \left\| \int L^{-1} \left\{ \varepsilon^2 \|G_i(s)\| \frac{\Delta P_L(s)}{R_i^2} dR_i \right\} \right\| \quad (\text{B.26}) \\
&= \left\| \int \varepsilon L^{-1} \left[\frac{d\Delta P_L}{s} \right] \right\| + \sum_{i=1}^N \left\| \int \varepsilon^2 \frac{dR_i}{R_i^2} \|G_i(s)\| \cdot L^{-1} \{ \Delta P_L(s) \} \right\| \\
&= \left\| \int \varepsilon \cdot 1(t-t_0) d\Delta P_L \right\| + \sum_{i=1}^N \left\| \int \varepsilon^2 \frac{dR_i}{R_i^2} \|G_i(s)\| \cdot 1(t-t_0) \Delta P_L \right\| \\
&\leq \varepsilon \|\Delta P_L\| + \sum_{i=1}^N \varepsilon^2 \|\Delta P_L\| \|G_i(s)\| / \|R_i\|
\end{aligned}$$

where $\varepsilon = \|\Delta\Omega(s)/\Delta P_L(s)\|$, and $\|G_i(s)\| = \frac{\|1 + F_{HP_i} T_{RH_i} s\|}{\|1 + T_{G_i} s\| \|1 + T_{CH_i} s\| \|1 + T_{RH_i} s\|}$ which is also

bounded.

Apparently, the bound of $\Delta\omega(t)$ from the traditional model ignoring the impact of H or R is given by:

$$\|\Delta\omega(t)\| \leq \varepsilon \|\Delta P_L\| \quad (\text{B.27})$$

The difference between the new model with H or R and the conventional model is $\varepsilon^2 \| \int (t-t_0) \| \Delta P_L \| \| H \|$ or $\varepsilon^2 \| \Delta P_L \| \| G(s) \| / \| R \|$ respectively. This means the frequency deviation under both models are bounded, though by different boundaries.

b. When the Power System is Essentially Unstable

If the power system is unstable, then some of its Laplace characteristic function's poles are located on the right half plane in the s -domain. That means the finite time domain input $\Delta P_L(t)$ produces infinite time domain output $\Delta\omega(t)$. It suffices to the norm $\|\Delta\Omega(s)/\Delta P_L(s)\|$ which is larger than a very large value M , i.e. $\|\Delta\Omega(s)/\Delta P_L(s)\| \geq M$ for $\forall t \in (0, \infty)$.

Then, a new relationship can be derived as follows:

$$\begin{aligned}
 \|\Delta\omega_H(t)\| &= \left\| \int L^{-1} \left[\frac{\Delta\Omega(s)}{\Delta P_L(s)} d\Delta P_L(s) \right] + \int L^{-1} \left\{ \left[\frac{\Delta\Omega(s)}{\Delta P_L(s)} \right]^2 \Delta P_L(s) \cdot 2sdH \right\} \right\| \\
 &= \left\| \int L^{-1} \left[\left\| \frac{\Delta\Omega(s)}{\Delta P_L(s)} \right\| \angle\theta \cdot d\Delta P_L(s) \right] + \int L^{-1} \left\{ \left\| \frac{\Delta\Omega(s)}{\Delta P_L(s)} \right\|^2 \angle 2\theta \cdot \Delta P_L(s) \cdot 2sdH \right\} \right\| \\
 &\geq \left\| \int L^{-1} \left[M e^{j\theta} d\Delta P_L(s) \right] + \int L^{-1} \left\{ M^2 e^{j2\theta} \Delta P_L(s) \cdot 2sdH \right\} \right\| \\
 &= \left\| \int M e^{j\theta} L^{-1} \left[\frac{d\Delta P_L}{s} \right] + \int M^2 e^{j2\theta} dHL^{-1} \{ \Delta P_L \} \right\| \\
 &= \left\| \int M e^{j\theta} \cdot 1(t-t_0) d\Delta P_L + \int M^2 e^{j2\theta} \cdot \uparrow(t-t_0) \Delta P_L dH \right\| \\
 &= \left\| M e^{j\theta} \cdot 1(t-t_0) \Delta P_L + M^2 e^{j2\theta} \cdot \uparrow(t-t_0) \Delta P_L H \right\|
 \end{aligned} \tag{B.28}$$

or

$$\begin{aligned}
\|\Delta\omega_R(t)\| &= \left\| \int L^{-1} \left[\frac{\Delta\Omega(s)}{\Delta P_L(s)} d\Delta P_L(s) \right] - \int L^{-1} \left\{ \left[\frac{\Delta\Omega(s)}{\Delta P_L(s)} \right]^2 \frac{\Delta P_L(s) G(s)}{R^2} dR \right\} \right\| \\
&= \left\| \int L^{-1} \left[\left\| \frac{\Delta\Omega(s)}{\Delta P_L(s)} \right\| \angle\theta \cdot d\Delta P_L(s) \right] - \int L^{-1} \left\{ \sum_{i=1}^N \left\| \frac{\Delta\Omega(s)}{\Delta P_L(s)} \right\|^2 \angle 2\theta \cdot \|G_i(s)\| \angle\beta_i \cdot \frac{\Delta P_L(s)}{R_i^2} dR_i \right\} \right\| \\
&= \left\| \int L^{-1} \left[\left\| \frac{\Delta\Omega(s)}{\Delta P_L(s)} \right\| \angle\theta \cdot d\Delta P_L(s) \right] - \sum_{i=1}^N \int L^{-1} \left\{ \left\| \frac{\Delta\Omega(s)}{\Delta P_L(s)} \right\|^2 \angle 2\theta \cdot \|G_i(s)\| \angle\beta_i \cdot \frac{\Delta P_L(s)}{R_i^2} dR_i \right\} \right\| \\
&\geq \left\| \int L^{-1} \left[M e^{j\theta} d\Delta P_L(s) \right] - \sum_{i=1}^N \int L^{-1} \left\{ M^2 \|G_i(s)\| e^{j2\theta} e^{j\beta_i} \frac{\Delta P_L(s)}{R_i^2} dR_i \right\} \right\| \\
&= \left\| \int M e^{j\theta} L^{-1} \left[\frac{d\Delta P_L}{s} \right] - \sum_{i=1}^N \int M^2 \|G_i(s)\| e^{j(2\theta+\beta_i)} \frac{dR_i}{R_i^2} L^{-1} \left\{ \frac{\Delta P_L}{s} \right\} \right\| \quad (\text{B.29}) \\
&= \left\| \int M e^{j\theta} \cdot 1(t-t_0) d\Delta P_L - \sum_{i=1}^N \int M^2 \|G_i(s)\| e^{j(2\theta+\beta_i)} \cdot 1(t-t_0) \Delta P_L \frac{dR_i}{R_i^2} \right\| \\
&= \left\| M e^{j\theta} \Delta P_L - \sum_{i=1}^N M^2 \|G_i(s)\| e^{j(2\theta+\beta_i)} \Delta P_L / R_i \right\|
\end{aligned}$$

where β_i is the phase angle of $G_i(s)$.

Equations (B.28) and (B.29) indicate that even if ΔP_L and H or R are very small values (much less than 1) in per unit, $\|M^2 e^{j2\theta} \uparrow (t-t_0) \Delta P_L H\| = \|M^2 \uparrow (t-t_0) \Delta P_L H\|$ and

$\left\| \sum_{i=1}^N M^2 \|G_i(s)\| e^{j(2\theta+\beta_i)} \cdot 1(t-t_0) \Delta P_L / R_i \right\| = \left\| \sum_{i=1}^N M^2 \|G_i(s)\| \Delta P_L / R_i \right\|$ may still be a very

large number compared with $\|M e^{j\theta} 1(t-t_0) \Delta P_L\| = \|M \Delta P_L\|$, which is the lower bound based on the conventional model. Therefore, the effect of dH or dR to $d\Delta\omega(t)$ cannot be neglected in this case. This means it can accelerate the system frequency deviation and make instability situation worse than using the conventional equation (B.13).

B.4 Numerical Simulation Results

As listed below, four case studies have been performed for sensitivity function effect of the generator inertia coefficient H and the governor speed coefficient R on power system frequency response respectively.

- Single machine system – Stable & Unstable Cases
- Multi-machines system – Stable & Unstable Cases

B.4.1 Single Machine (SISO) System

In this case the simulation time period is 20 seconds. Consider a typical aggregated power system containing a load and a single generator with a reheat turbine. Assume the system parameters are $T_{RH}=7$ sec, $T_G=0.2$ sec, $T_{CH}=0.3$ sec, $F_{HP}=0.3$, $H=5$ sec, $D=1$, $R=0.05$. Here a load increase is considered as the external disturbance. Consider a step load change, $\Delta P_L=0.1$ p.u. In addition, let the ΔH or ΔR be a set of values with 20% increments: 20%, 40%, 60%, 80% and 100%, respectively. From all the given parameters, it can be calculated that this power system is stable.

B.4.1.1 Single Machine System – Stable Case

Figures B.2 and B.3 show the six curves: the “external disturbance” curve is obtained using (B.13) by ignoring the impact of dH or dR , while the five “total disturbance” curves are obtained with (B.14) or (B.15) and (B.3) or (B.4) to address the impact from various dH or dR values. If the six curves in Figure B.2 are compared, they are close but not similar. In Figure B.3, the six curves are similar and bounded but not close. Note that the largest dips of the six curves in Figures B.2 and B.3 are not aligned at the same moment as in Chapter IV.

The sensitivity curve of frequency deviation, Δf , w.r.t. the generator inertia coefficient H , and the governor speed coefficient R is shown in Figures B.4 and B.5. As shown in the figures, the sensitivity function curve is relatively small, as opposed to the case in unstable case shown later in this chapter.

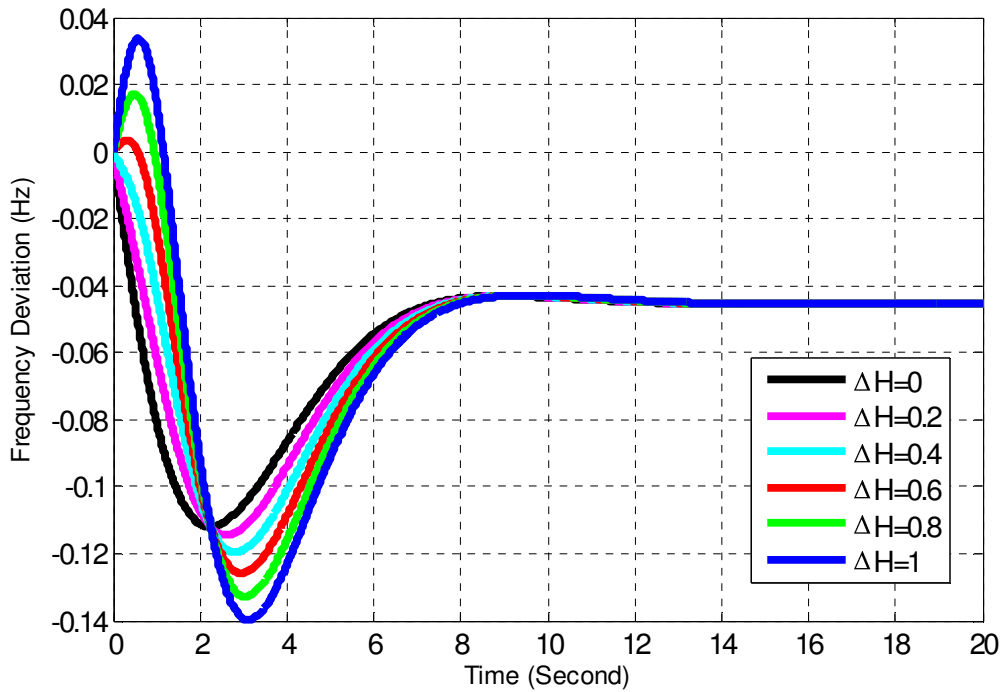


Figure B.2 $\Delta f(t)$ curves with H change of a SISO system

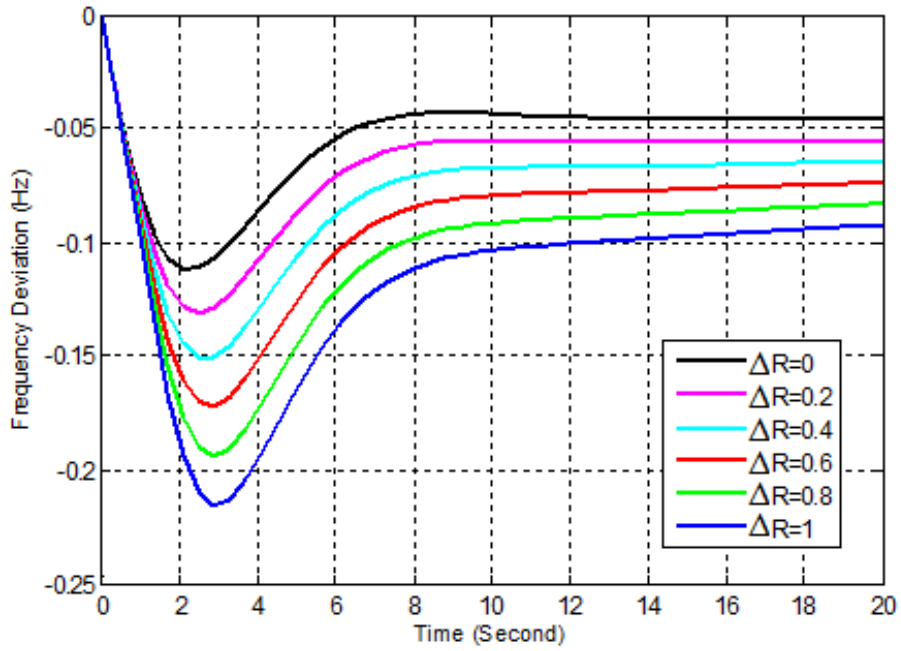


Figure B.3 $\Delta f(t)$ curves with R change of a SISO system

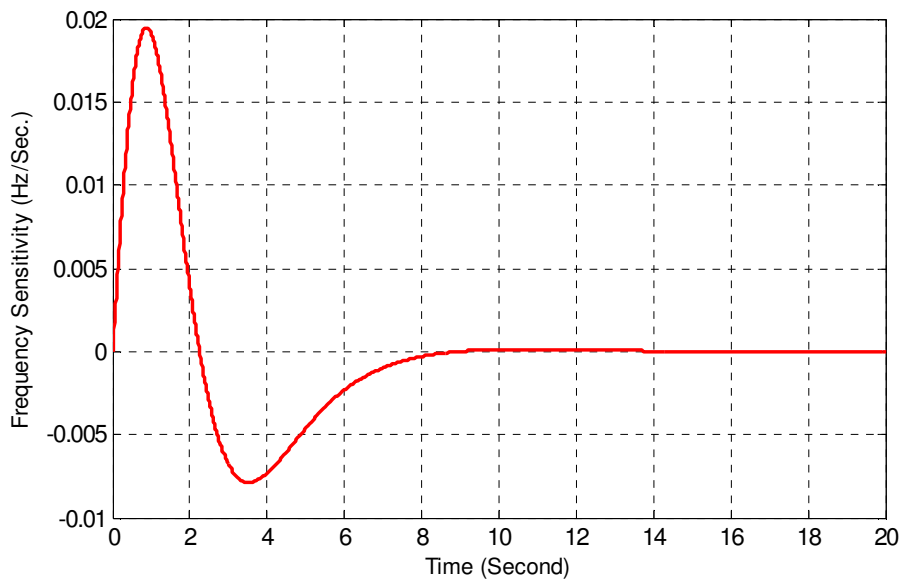


Figure B.4 $\partial \Delta f(t) / \partial H$ curve of a SISO system

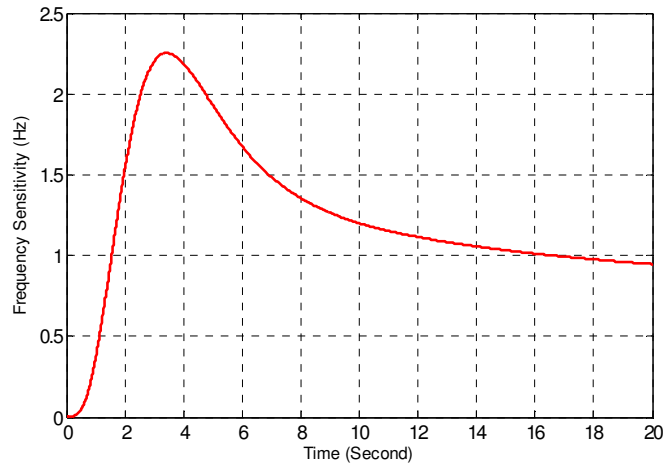


Figure B.5 $\partial\Delta f(t)/\partial R$ curve of a SISO system

B.4.1.2 Single Machine System – Unstable Case

In this case, we assume some disturbance happens to make the generation governor unstable at the time $t=0$ second. In this simulation, the parameter in the governor control is changed from $0.2s+1$ to $-0.2s+1$, for demonstration purpose, to produce a pole in the right half of the s plane. Here the simulation time period is 1 sec and 1.3 sec for the generator inertia coefficient H case and the governor speed coefficient R case respectively, because the system frequency is already close to the instability threshold (57Hz) at 1 sec for the generator inertia coefficient H case or 1.3 sec for the governor speed coefficient R case. After that, the system frequency will sharply deviate from 60 Hz.

The comparison results are shown in Figures B.6 and B.7 with different dH and dR values. The sensitivity of the frequency deviation Δf to the generator inertia coefficient H and the governor speed coefficient R are shown in Figures B.8 and B.9. These four figures indicate that the power system is unstable and has a trend to be even

worse than anticipated using the conventional model in (B.13), and the generator inertia coefficient H and the governor speed coefficient R can exert larger effect on SFR. So, they may accelerate the system frequency collapse in this case. Therefore, the effect of the generator inertia coefficient H and the governor speed coefficient R can be significant.

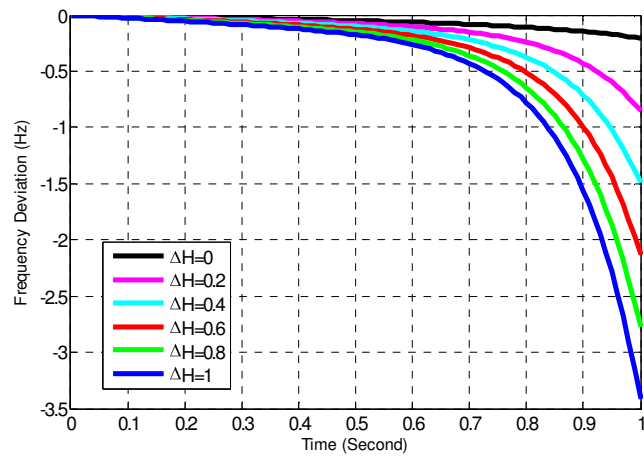


Figure B.6 $\Delta f(t)$ curves with H change of a SISO system in Case B.4.1.2

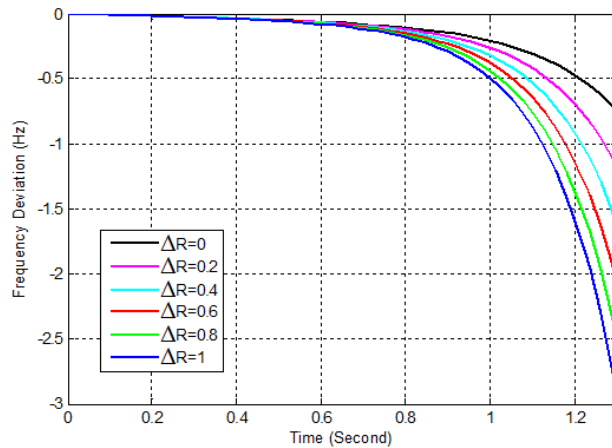


Figure B.7 $\Delta f(t)$ curves with R change of a SISO system in Case B.4.1.2

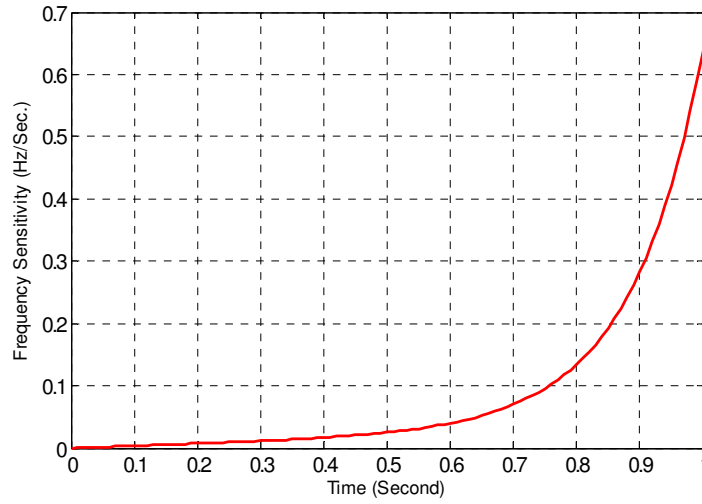


Figure B.8 $\partial\Delta f(t)/\partial H$ curve of a SISO system in Case B.4.1.2

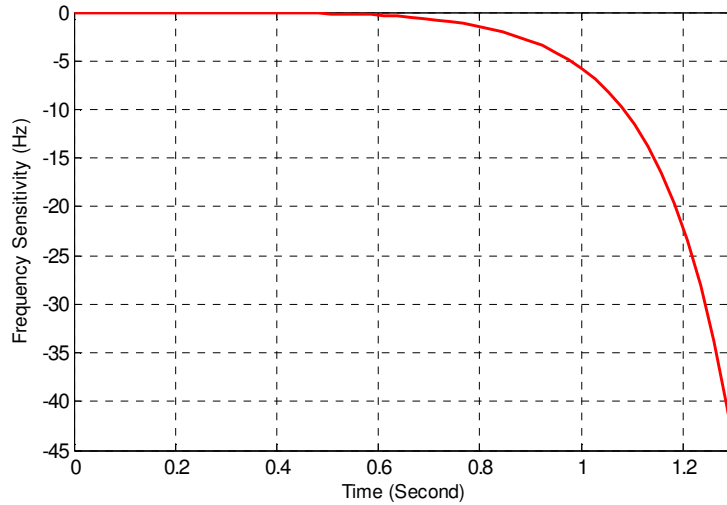


Figure B.9 $\partial\Delta f(t)/\partial R$ curve of a SISO system in Case B.4.1.2

B.4.2 Multi-machines System

In this subsection, a two-machine system is considered. Let $T_{RH1}=7$ sec, $T_{G1}=0.2$ sec, $T_{CH1}=0.3$ sec, $F_{HP1}=0.3$, $R_1=0.1$, $T_{RH2}=11$ sec, $T_{G2}=0.35$ sec, $T_{CH2}=0.25$ sec, $F_{HP2}=0.2$, $R_2=0.1$, $H=5$ sec, and $D=1$. Further, consider a 10% load increase on the first system

input, i.e., $\Delta P_{LI}=0.1$ p.u. Also consider the actual H or R is 20%, 40%, 60%, 80%, and 100%, respectively, higher than the expected value.

B.4.2.1 Multi-machines System – Stable Case

In this case the simulation time period is 20 *sec*. The six curves obtained from (B.13), (B.14) and (B.15) based on various dH and dR values are shown in Figures B.10 and B.11. If the six curves in Figure B.10 are compared, they are close but not similar; while in Figure B.11, they are similar and bounded but not close. The results of $\partial\Delta f(t)/\partial H$ and $\partial\Delta f(t)/\partial R$ are shown in Figures B.12 and B.13, respectively. Observations and conclusion are very similar to the ones in Case B.4.1.1. For example, the impact of the generator inertia coefficient H and the governor speed coefficient R on SFR is relatively small and bounded if compared with unstable cases. Note that the largest dips of the six curves in Figures B.10 and B.11 are not aligned at the same moment as in Chapter IV.

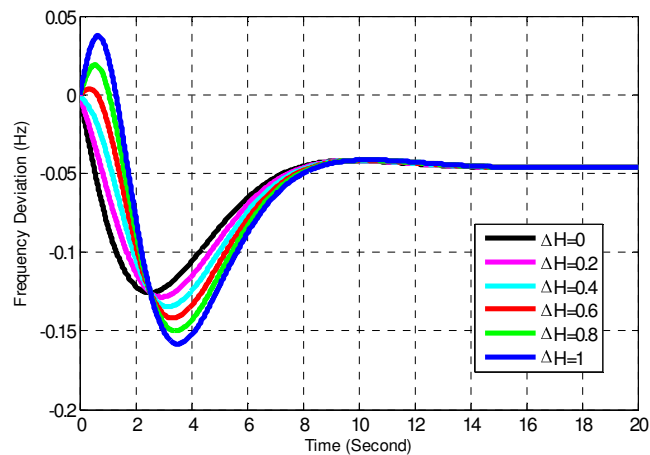


Figure B.10 $\Delta f(t)$ curves with H change of multi-machines system

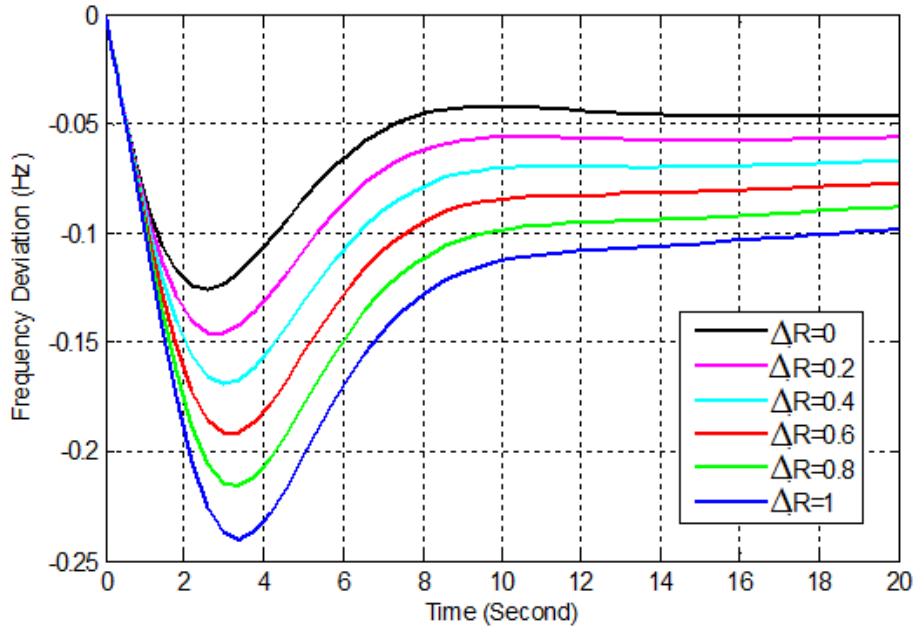


Figure B.11 $\Delta f(t)$ curves with R change of multi-machines system

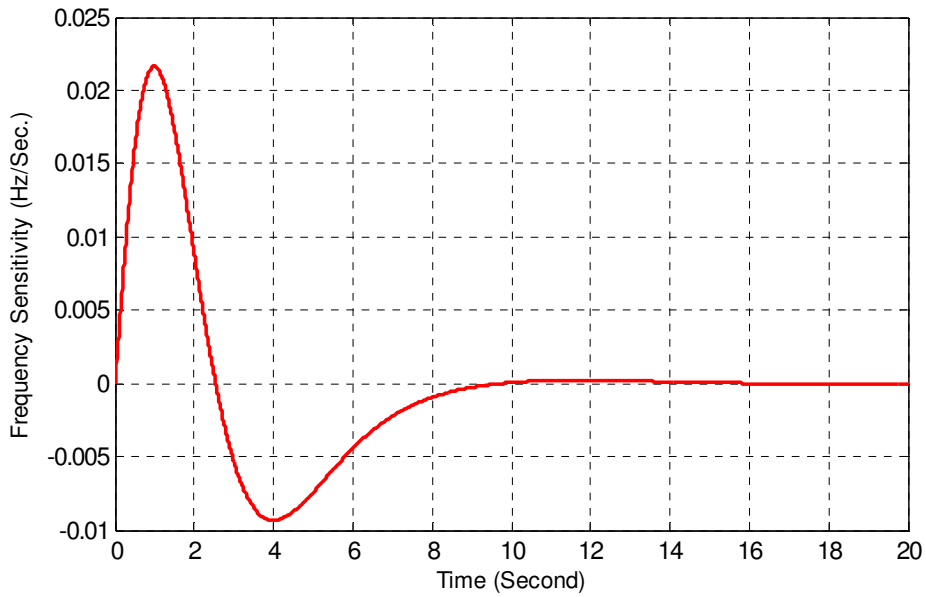


Figure B.12 $\partial \Delta f(t) / \partial H$ curve of multi-machines system

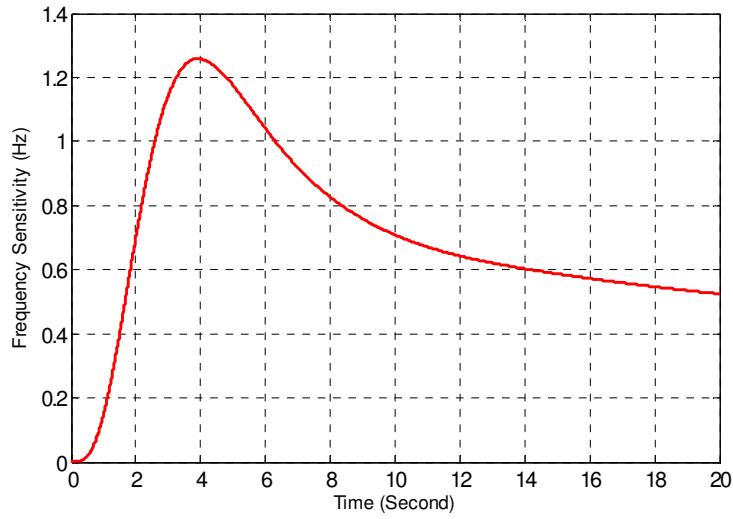


Figure B.13 Aggregated $\partial\Delta f(t)/\partial R$ curve of multi-machines system

B.4.2.2 Multi-machines System – Unstable Case

Similar to Case B.4.1.2, here we assume a fault on Governor 2 at $t=0$ causes the parameter to change from $0.35s+1$ to $-0.35s+1$ for demonstration purpose. This leads to a pole in the right half of the s plane. The simulation results are shown up to 1.7 sec for the generator inertia coefficient H or 2.2 sec for the governor speed coefficient R . After that, the system frequency will sharply deviate from 60 Hz. The comparison results are shown in Figures B.14 and B.15. The sensitivity $\partial\Delta f(t)/\partial H$ and $\partial\Delta f(t)/\partial R$ curves are shown in Figures B.16 and B. 17.

Similar to Case B.4.1.2, Figures B.14 and B.15 show that the frequency response using (B.14) and (B.15) is worse than the conventional model using (B.13). Thus, the consideration of H and R may lead to acceleration of frequency instability and less response time for corrective actions.

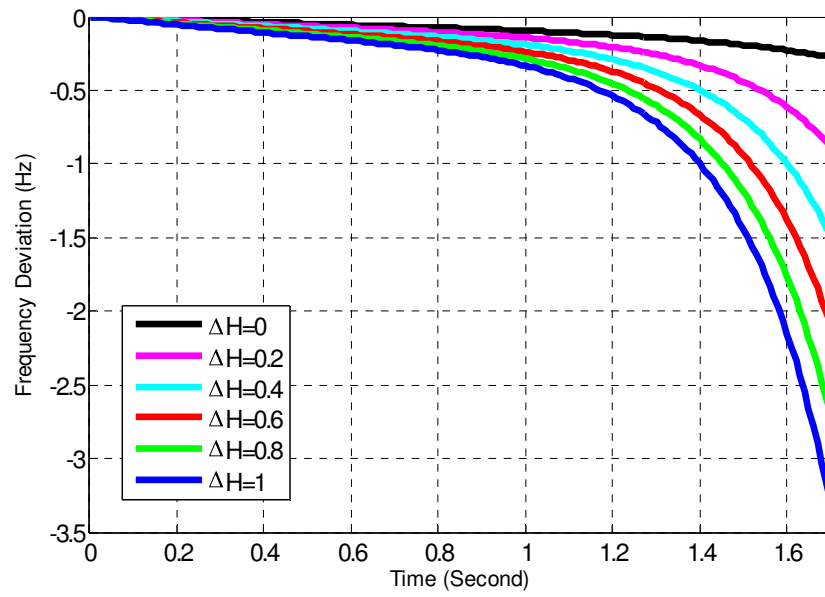


Figure B.14 $\Delta f(t)$ curves with H change of multi-machines system in Case B.4.2.2

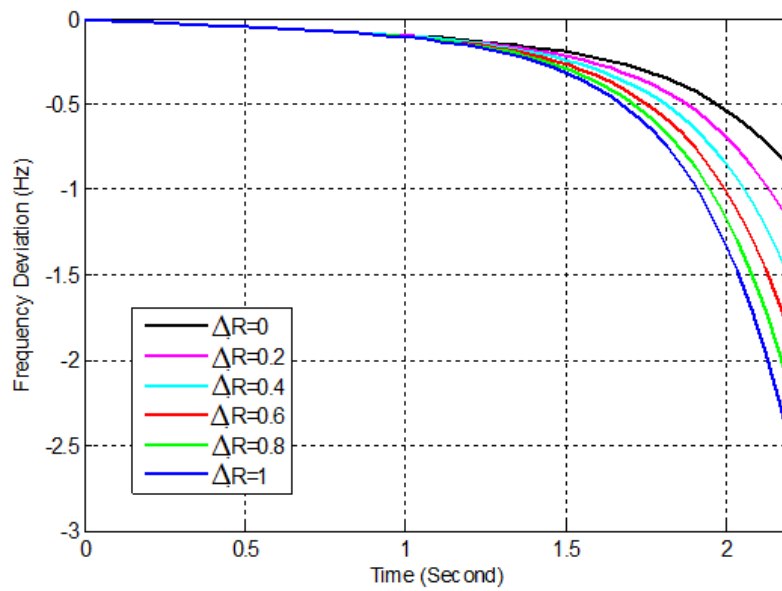


Figure B.15 $\Delta f(t)$ curves with R change of multi-machines system in Case B.4.2.2

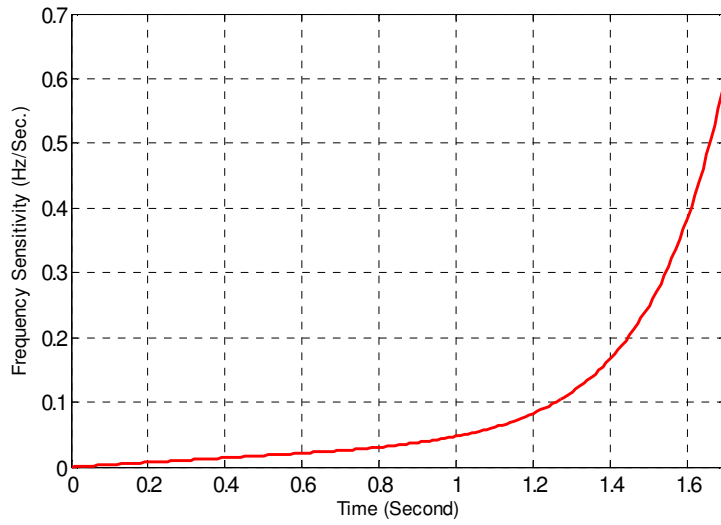


Figure B.16 $\partial\Delta f(t)/\partial H$ curve of multi-machines system in Case B.4.2.2

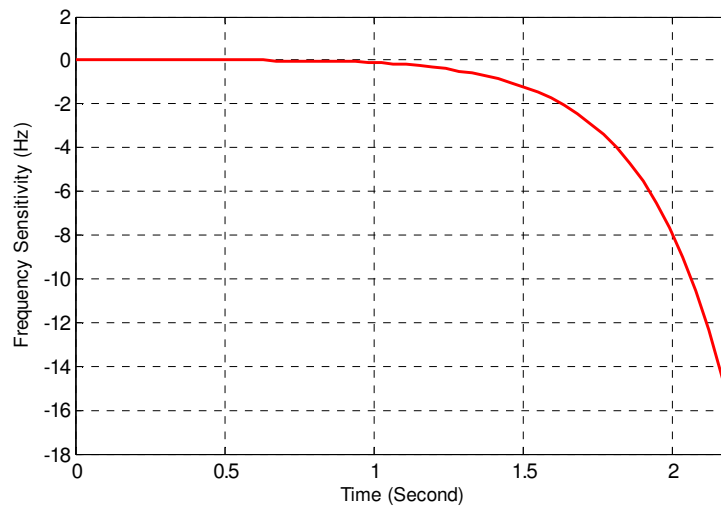


Figure B.17 Aggregated $\partial\Delta f(t)/\partial R$ curve of multi-machines system in Case B.4.2.2

B.5 Conclusions

With rapid development of intermittent renewable energy sources construction and integration of the power grid, renewable energy will take more responsibility on frequency regulation in the foreseeable future. Although the impact may not be clear, this

gives enough motivation to investigate the effect of the generator inertia coefficient H and the governor speed coefficient R change on the power system frequency regulation based on the typical SFR model. Theoretic analysis as well as simulation studies show that the impact of an inaccurate generator inertia coefficient H and governor speed coefficient R is relatively small and bounded when the power system is essentially stable; while the system frequency deviation may be accelerated when the power system is indeed unstable after disturbance.

The next step of research works may include: First, studying the effect of combining all frequency sensitivity functions including the load-damping coefficient D , the generator inertia coefficient H , and the governor speed coefficient R on regulation of power system frequency response and stability analysis based on the SFR model rather than considering them individually as in Chapter IV and Appendix B. Second, it is also worth mentioning that a strategically design of a robust load shedding scheme may be desired with the consideration of the variation of the load-damping coefficient D , the generator inertia coefficient H , and the governor speed coefficient R . At last, sensitivity study of other types of generator models such as hydraulic turbines, perhaps in a large-scale system, can be investigated.

APPENDIX C

PUBLICATIONS:

- [1] Hao Huang and Fangxing Li, “Sensitivity Analysis of Load-Damping Characteristic in Power System Frequency Regulation,” *IEEE Trans. on Power Syst.*, vol. 28, no. 2, pp. 1324-1335, May 2013.
- [2] Hao Huang and Fangxing Li, “Bidding Strategy for Intermittent Renewable Generation Considering Conventional Generation and Transmission Constraints,” submitted to *Electric Power System Research*.
- [3] Hao Huang and Fangxing Li, “Modeling Demand Response using Monte Carlo Simulation and Interval Mathematics for Boundary Estimation,” to be submitted to *IEEE Trans. on Power Syst.*
- [4] Hao Huang and Fangxing Li, “Sensitivity Analysis of Generator Inertia and Governor Speed Characteristics in Power System Frequency Regulation,” submitted to *IEEE PES General Meeting 2014*.

VITA

Hao Huang was born in Changsha, China in October 8th 1981. He received his B.S. and M.S. degrees in Electrical Engineering Department from Zhejiang University, Hangzhou, China in June 2003 and June 2006, respectively. He also received a M.S. degree in Electrical Engineering Department from Texas A & M University in December 2008. During this period, he worked with British Petroleum Alternative Energy, Electric Power Research Institute, and Entergy Service Inc. as interns. In fall 2009, he started the Ph.D. degree studies in Electrical Engineering and Computer Science Department of the University of Tennessee, Knoxville, TN, USA. His major research interest is in controllable load under power system operation and frequency regulation under local load shedding.